UNIVERSITAT POLITÈCNICA DE CATALUNYA
BARCELONATECH
Department of Signal Theory
and Communications

CLOSED FORM ANALYSIS OF POISSON CELLULAR NETWORKS: A STOCHASTIC GEOMETRY APPROACH

Ph.D. Dissertation

Author
Alexios Aravanis

Advisors
Dr. Olga Muñoz Medina
Dr. Antonio Pascual-Iserte

Barcelona, July 2019

This work was supported by the project ETN-5Gwireless (this project has received funding from the European Union's Horizon 2020 research and innovation programme under the Marie Skłodowska-Curie grant agreement No. 641985). Moreover, the work has been partially funded through the project DISNET (funding from the Spanish Ministerio de Economía y Competitividad, project code TEC2013-41315-R). Additional funding has been received from the grant 2017 SGR 578 (funded by the Catalan Government—Secretaria d'Universitats i Recerca, Departament d'Empresa i Coneixement, Generalitat de Catalunya, AGAUR) and the project TEC2016-77148-C2-1-R (AEI/FEDER, UE): 5G&B-RUNNER-UPC (funded by the Agencia Estatal de Investigación, AEI, and Fondo Europeo de Desarrollo Regional, FEDER).

Abstract

Ultra dense networks (UDNs) allow for efficient spatial reuse of the spectrum, giving rise to substantial capacity and power gains. In order to exploit those gains, tractable mathematical models need to be derived, allowing for the analysis and optimization of the network operation. In this course, stochastic geometry has emerged as a powerful tool for large-scale analysis and modeling of wireless cellular networks. In particular, the employment of stochastic geometry has been proven instrumental for the characterization of the network performance and for providing significant insights into network densification. Fundamental issues, however, remain open in order to use stochastic geometry tools for the optimization of wireless networks, with the biggest challenge being the lack of tractable closed form expressions for the derived figures of merit.

To this end, the present thesis revisits stochastic geometry and provides a novel stochastic geometry framework with a twofold contribution. The first part of the thesis focuses on the derivation of simple, albeit accurate closed form approximations for the ergodic rate of Poisson cellular networks under a noise limited, an interference limited and a general case scenario. The ergodic rate constitutes the most sensible figure of merit for characterizing the system performance, but due to the inherent intractability of the available stochastic geometry frameworks, had not been formulated in closed form hitherto. To demonstrate the potential of the aforementioned tractable expressions with respect to network optimization, the present thesis proposes a flexible connectivity paradigm and employs part of the developed expressions to optimize the network connectivity. The proposed flexible connectivity paradigm exploits the downlink uplink decoupling (DUDe) paradigm, which is a promising framework providing substantial capacity and outage gains in UDNs and introduces the DUDe connectivity gains into the 5G era and beyond.

Subsequently, the last part of the thesis provides an analytical formulation of the probability density function (PDF) of the aggregate inter-cell interference in Poisson cellular networks. The introduced PDF is an accurate approximation of the exact PDF that could not be analytically formulated hitherto, even though it constituted a crucial

tool for the analysis and optimization of cellular networks. The lack of an analytical expression for the PDF of the interference in Poisson cellular networks had imposed the use of intricate formulas, in order to derive sensible figures of merit by employing only the MGF. Hence, the present thesis introduces an innovative framework able to simplify the analysis of Poisson cellular networks to a great extent, while addressing fundamental issues related to network optimization and design.

Resume

Alexis I. Aravanis was born in Athens, Greece in 1988. He graduated from the German School of Athens and received the Dipl.-Ing. (MSc ECE) Degree in Electrical and Computer Engineering from the National Technical University of Athens (NTUA) in 2012. From 2011 to 2012, he completed his master's thesis and subsequently held a Junior Research Associate position with the SIGCOM group of Prof. Björn Ottersten in the Interdisciplinary Centre for Security, Reliability and Trust (SnT), University of Luxembourg. In 2013 he began his mandatory military service in the Research and Informatics Corps of the Hellenic Army. From 2014 to 2015, he was a Telecommunications Engineer at Synelixis Solutions Ltd., while being a Teaching Assistant with the Mobile Radiocommunications Laboratory of NTUA. During 2016 he was a Visiting Researcher at SnT and the SIGCOM group of Prof. Ottersten. Since May 2016 he holds a Marie Curie Early Stage Researcher (ESR) position in the 5Gwireless International Training Network (ITN) in the SPCOM research group at Universitat Politècnica de Catalunya (UPC), Barcelona, Spain. During 2018 he was a Visiting Researcher at the group of Prof. Marco Di Renzo in CNRS, CentraleSupèlec and University Paris-Sud (Paris 11) in Paris, France. Subsequently, he was a Visiting Researcher at the OTE Group of Companies, Deutsche Telekom AG in Athens, Greece. He has been involved in numerous ESA, FP7 and Horizon 2020 projects in the area of telecommunications and energy efficiency. His research interests include resource allocation, stochastic optimization, stochastic geometry, wireless and satellite communications. He is a member of the Technical Chamber of Greece (TEE).

Acknowledgements

The present Ph.D. thesis has been financially supported by a Marie Curie Early Stage Researcher (ESR) Fellowship, funded by the European Research Grant and the Marie Skłodowska Curie actions. Within the framework of this action, the present research material has been developed at the premises of three different European Research Partners. Namely, at the premises of Universitat Politècnica de Catalunya (UPC) in Barcelona, Spain, of CNRS and CentraleSupèlec in Paris, France, and of OTE Group of Companies of Deutsche Telekom AG in Athens, Greece. During that time, a number of people have contributed to the development of this material and I wish to particularly thank Prof. Olga Muñoz Medina and Prof. Antonio Pascual-Iserte from UPC, Prof. Marco Di Renzo and Dr. Thanh Tu Lam from CNRS/CentraleSupèlec, and Dr. George Agapiou and Panagiotis Matzoros from OTE. Without them this dissertation could not have been written.

Acronyms

ACK: acknowledgment;

AP: access point;

B5G: beyond 5G;

BS: base station;

CCDF: complementary cumulative distribution function;

CGF: cumulant generating function;

CF: characteristic function;

DL: downlink;

DUDe: Downlink Uplink Decoupling;

HARQ: hybrid automatic repeat request;

HetNet: heterogeneous network;

LOS: line of sight;

MC: macro cell;

MGF: moment generating function;

LBT: listen before transmitting;

LOS: line of sight;

PDF: probability density function;

PGFL: probability generating fuctional;

PPP: Poisson point process;

PUCCH: physical uplink control channel;

PUSCH: physical uplink shared channel;

QoS: quality of service;

RSRP: reference signals received power;

SAW: stop and wait;

SC: small cell;

SINR: signal to interference plus noise ratio;

SIR: signal to interference ratio;

TDD: time division duplex;

UDN: ultra dense network;

UE: user equipment;

UL: uplink;

URLLC: ultra-reliable low latency communications.

Contents

List of Figures

Chapter 1

Introduction

The advent of multimedia interactive services and the surge in the number of interconnected devices has imposed the investigation of new approaches able to enhance wireless capacity in 5G networks and beyond. In this course, three prime axes of network flexibility have been leveraged, namely the employment of wider spectrum, the enhancement of spectral efficiency and the employment of smaller cell sizes and, thus, of smaller transmit distances [1]. In retrospect over the evolution of wireless networks, the efficient spatial reuse of the spectrum, through the reduction of the inter-site distances, has provided, out of these three axes of flexibility, the most substantial capacity gains by a large margin [2]. Hence, the densification of networks arises as the most prominent candidate for achieving the envisaged capacity increase in the 5G era and beyond.

In the direction of densifying their networks, network operators employ system level simulations and network measurements. However, over the last decade, the seminal work of Baccelli et al. [3] gave rise to stochastic geometry as a tractable tool for the large-scale analysis and design of wireless networks. Indicatively, the formulation of mathematical expressions for the expectation of the aggregate interference in wireless networks [4] −which was not analytically formulated hitherto− paved the way for the theoretical analysis of the performance of wireless networks. Thenceforth, a multitude of research works have exploited these tools to provide significant insights into network densification. These insights are essential for understanding the innate features of dense networks and can be employed by network operators as densification road maps and guidelines for the use of system level simulators and of auxiliary network planning tools.

1.1 Stochastic Geometry Analysis of UDNs and State of the Art

The insights provided by such theoretical analyses brought significant changes in the understanding of wireless networks. In particular, for single-slope path loss models and

for networks comprising significantly more users than base stations (BSs), it has been demonstrated that the user signal quality is independent of the BS density [5]. Moreover, the probability of coverage (which constitutes the complementary cumulative distribution function (CCDF) of the signal to interference plus noise ratio (SINR)) is independent of the BS density and of the number of tiers [6]. Similar analysis for the uplink (UL) has demonstrated that the UL signal to interference ratio (SIR) is also invariant of the BS density [7]. As a result, it has been demonstrated that the network capacity increases linearly with the density of BSs and with the number of tiers [4].

These conclusions, however, which indeed hold for sparse wireless networks (e.g. tier of macro cells (MCs)), do not hold for extremely high BS densities. The reason for that is that after a BS densification threshold, the inter-site distances become so small that the proximity of the neighboring BSs allows them to create line of sight (LOS) interference to the intended user. As a result, after this densification threshold, the probability of coverage is diminished precipitately due to the presence of LOS interference [8, 9].

As opposed to this behavior of networks comprising much more users than BSs, the system performance is not bounded by the aforementioned threshold in the case of networks with more BSs than users; which is, in fact, the case of the envisaged UDNs [10]. The reason for that is that the excess BSs that do not serve any user can be switched off, thus, reducing the system energy consumption and interference. In this setup, densifying the network to the point that LOS interference arises, indeed diminishes the probability of coverage. However, the interference mitigation achieved by switching off excess BSs allows for the probability of coverage to increase again as the network becomes even denser, since the excess BSs in this dense setup remain idle [11].

An additional factor influencing the performance of UDNs has been proven to be the elevation of the BSs. In particular, in the presence of LOS interference, the densification of the network to the point where the inter-site distances become comparable to the elevation of the BS, has a severe detrimental effect on the network capacity, with the probability of coverage tending to zero [11]. This is due to the fact that as the network density increases, the LOS interferers approach the intended user at a faster rate than the rate in which the intended user can approach its serving BS, which is elevated.

In legacy systems, the sparsity of the involved macro cell BSs imposed their elevation in order to provide better coverage. However, the plethora and density of BSs in UDNs is expected to move BSs closer to the user level, thus, minimizing the elevation of BSs and implicitly the LOS interference to other users. This effect of densification can effectively counteract LOS interference in UDNs, allowing for the sought out linear capacity increase with the BS density. Moreover, intermediate densification steps have also been considered in the literature, following the heterogeneous network (HetNet) paradigm, with networks comprising elevated legacy macro cells (MCs) and dense mmWave small cells (SCs) closer to the user level [12]. However, mmWave SCs operate in a noise limited regime [12]

changing the analysis and the network behavior to a great extent.

1.2 Toward a Linear Increase of Capacity with Network Densification

Based on this comprehensive analysis, it has become evident that three key factors need to be taken into account by network operators in order to tap the capacity potential of UDNs. Firstly, the detrimental effect of LOS interference, secondly, the beneficial effect of idle (i.e. non transmitting) BSs and, thirdly the beneficial effect of mmWave SCs that can be overlaid over the existing infrastructure of MCs off-loading data without introducing additional interference due to blocking [19]. The incorporation of these three effects in the analysis and design of UDNs could engender extraordinary capacity gains, allowing for the envisaged linear increase of capacity with the densification of the network.

In order to achieve this goal, the effect of the three aforementioned key factors needs to be analyzed and taken into account in the design of UDNs. In this direction, standalone models need to be derived analyzing the effect of each of these factors on the network performance and allowing for the optimization of the network operation. The subsequent analysis will demonstrate that this imposes the derivation of standalone models for the noise limited, interference limited and general case (accounting for both noise and interference).

In particular, mmWave SCs operate in a noise limited regime due to blocking [12] and in a different frequency than the elevated MCs that operate in the sub 6GHz range to provide wide coverage. Hence, the analysis and optimization of this scenario mandates a dedicated noise limited analysis. A general analysis accounting for both noise and interference could be used as well, however a simpler and more tractable noise limited analysis is more sensible in this scenario allowing for the derivation of simple and tractable expressions. Such expressions would facilitate the resolution of complex optimization problems, pertaining to the operation of such HetNets, such as the operation of the network under a DUDe paradigm [13], [14], [15], which is tailored to ultra dense HetNets, providing substantial capacity, power and outage gains.

Similarly, in the case of UDNs operating in the sub 6GHz range, with BSs residing closer to the user level due to densification (i.e. in the absence of LOS interference), the employment of an interference limited analysis that would allow for the simple modeling and optimization of the network is preferable over a general but intractable analysis (accounting for both noise and interference). A closed-form tractable analysis could allow for network operators to leverage on the beneficial effect of the idle mode of not active BSs. In particular, in an UDN setup of idle and active BSs, users could be clustered dynamically under a single BS, not necessarily the one providing the best

service to each user. Thus, BSs that were acting as sources of principal interference to the network could be switched off. Given the high density of BSs, the connection to a neighboring BS after the best serving BS has been switched off would entail a minimal path loss increase, that would be outweighed by the interference mitigation gain achieved by strategically switching off BSs. Hence, the derivation of tractable models for UDNs in the interference limited case could be exploited for the resolution of complex problems that could engender substantial capacity gains.

In the two aforementioned setups, SC BSs are assumed to reside close to the user level as a result of densification, thus, counteracting LOS interference from BSs to surrounding users. However, given the extremely high capital expenditure (CAPEX) that is required by network operators in order to densify the network, this cannot happen overnight. Hence, in the pursuit of such dense deployments where BSs reside on the user level, an intermediate densification step will emerge where BSs are sparse enough that need to be elevated in order to provide consistent connectivity, but dense enough to give rise to LOS interference to surrounding users. In this setup, and in order to achieve the envisaged linear capacity increase with the density of BSs, interference mitigation techniques need to be considered to counteract the detrimental effect of LOS interference arising among adjacent cells.

In the direction of mitigating interference among immediate neighbors, BS coordination strategies were considered in early research works in the field. These approaches employed guard regions around fixed-size cells, which constituted interference free zones [16]. Similar strategies were also considered for D2D networks [17]. However, the coordination of all BSs residing within these guard regions, which is required by these techniques, is a highly involved task. Moreover, the coordination of all BSs within neighboring guard regions requires the coordination of the entire network as a whole.

As opposed to these techniques, a minimum coordination strategy technique involving a fixed number of coordinating BSs, (i.e. the ones residing closest to the selected BS), instead of a random number of BSs residing within a fixed zone, can be actually implemented in practice. That is since, (indicatively) in LTE systems BSs are aware of the topology of their immediate neighbors to facilitate the handover process. Moreover, the coordination of only LOS interferers, able to communicate and coordinate directly with the intended user, would not require intricate coordination schemes and could, indeed, allow for a linear capacity increase with the density of BSs. However, in this setup, the coordination of the immediate neighbors, which constitute the principal source of interference in UDNs, alters the analysis to a great extent and the interference limited approach considered above is not suitable for characterizing the network performance anymore. In other words, the interference mitigation achieved through the coordination accentuates the impact of noise on the analysis. This imposes the employment of a general framework for the analysis that could also be employed for quantifying the

performance of the system under different coordination strategies. Thus, allowing for optimizing the network performance and for selecting the optimum coordination strategy for the mitigation of LOS interference.

1.3 Addressing the Need for Tractable Closed-form Expressions

The development of mathematical frameworks for complex optimization problems, like the ones mentioned above, poses a great challenge. The reason for that is that the majority of the stochastic geometry approaches in the literature, including the references presented above, involve intractable integrations. Even though such integrals can be computed numerically, allowing for the analysis of the network behavior, they cannot be employed for the investigation of complex optimization problems. In these cases it is imperative that the considered objective functions, that evaluate the system performance, involve tractable closed form expressions. In this course, it is essential to exploit the available stochastic geometry tools to develop tractable and accurate approximations in addition to the available exact but cumbersome expressions.

In this direction, the first part of the present thesis (Chapters 2-4) focuses on the derivation of simple, albeit accurate approximations, that allow for defining the ergodic rate of Poisson cellular networks in closed form under a noise limited, an interference limited and a general case scenario. The ergodic rate constitutes the most sensible figure of merit for characterizing the system performance, but due to the inherent intractability of the available stochastic geometry frameworks, had not been formulated in closed form hitherto. To demonstrate the potential of the aforementioned tractable expressions with respect to network optimization, the present thesis proposes a flexible connectivity paradigm and employs part of the developed expressions to optimize the network connectivity. The proposed flexible connectivity paradigm builds upon the downlink uplink decoupling (DUDe) paradigm, which is a promising framework providing substantial capacity and outage gains in UDNs and introduces the DUDe connectivity gains into the 5G era and beyond.

Subsequently, the last part of the thesis (Chapter 5) provides an analytical formulation of the probability density function (PDF) of the aggregate inter-cell interference in Poisson cellular networks. The introduced PDF is an accurate approximation of the exact PDF that could not be analytically formulated hitherto, even though it constituted a crucial tool for the analysis and optimization of cellular networks. The lack of an analytical expression for the PDF of the interference in Poisson cellular networks had imposed the use of intricate formulas, in order to derive sensible figures of merit by employing only the MGF. Hence, the present thesis introduces an innovative framework able to simplify the analysis of Poisson cellular networks to a great extent, while

addressing fundamental issues related to network optimization and design.

The way the remainder of the thesis is organized is presented in the following section, along with a detailed presentation of the thesis' contributions.

1.4 Major Contributions

Chapter 2 provides the first contribution of the present thesis, which is the derivation of tractable approximations, in closed form, for the UL ergodic rate of Poisson cellular networks for the noise limited case. The analysis commences with the derivation of closed form bounds for the UL ergodic rate in the standalone cases where the network comprises only SCs or only MCs. Subsequently, the analysis is extended to the HetNet case where the network comprises both MSs and SCs. In the latter case users are expected to follow the traditional coupled connectivity (connecting to the same BS in the downlink (DL) and the UL) and the novel DUDe paradigm which can provide substantial capacity, power and outage gains. Hence, the derived closed-form expressions for the HetNet case account for both, the coupled and the DUDe connectivity paradigms. Since the coupled and the DUDe connectivity is only different in the UL, the analysis focused on the UL ergodic rate in order to differentiate the coupled and the DUDe cases. However, since the interference is not considered in this chapter the expressions developed for the UL ergodic rate can also be employed for the DL ergodic rate, by adjusting the SNR to account for the BS transmission power instead of the user power.

Subsequently, Chapter 2 exploits the closed form expressions developed for the UL ergodic rate, to solve an optimization problem pertaining to the optimal UL-DL connectivity frontiers in a flexible DUDe framework. The proposed flexible framework overcomes the constraints that were hampering the application of DUDe in 5G and introduces the DUDe connectivity benefits in the 5G era and beyond, while also demonstrating in a practical scenario the practicality of the closed-form expressions presented herein, for the resolution of complex optimization problems.

Chapter 3 focuses on the characterization of the performance of Poisson cellular networks in the interference limited case. The spatial distribution of the interferers in the DL follows a homogeneous Poisson point process (PPP), whereas in the UL it follows a non-homogeneous PPP [18]. Since the objective of the present thesis is the derivation of closed-form approximations that were not available hitherto, the analysis commences from the more tractable homogeneous PPPs and the extension to the non-homogeneous case remains to be addressed in future work. Hence, the present analysis focuses only on the DL and the third contribution of the thesis is the derivation of closed form expressions for the DL ergodic rate in the interference limited case. The derived expressions account for the fully loaded case and the non-fully loaded case where the network comprises more BSs than users. In the latter case the expressions depend on the density of users

and BSs, thus, setting out a densification road map for network operators and designers of significant value. Moreover, in Chapter 3 an additional contribution is presented, that is, the derivation of a very simple, albeit extremely accurate approximation for the moment generating function (MGF) of the aggregate other-cell interference in Poisson cellular networks. Given the pivotal role of the MGF of the aggregate interference in stochastic geometry and the tractability of the derived MGF, the latter is a valuable tool for researchers in the field that can simplify ensuing stochastic geometry analyses to a great extent.

Subsequently, in Chapter 4 the analysis is extended to the more complex general case scenario where both noise and interference are considered. This constitutes the sixth contribution of the thesis, that is, the derivation of closed form expressions for the DL ergodic rate of Poisson cellular networks in the general case under a minimum coordination scheme. In particular, a varying number of BSs is selected a priori to coordinate in order to counteract the line of sight (LOS) interference, which constitutes the main factor limiting the performance of UDNs. These expressions allow for the investigation of different coordination strategies and the resolution of complex optimization problems in the general case scenario where both noise and interference are considered.

Building upon the previously developed tools and approaches the seventh contribution of the present thesis is presented in Chapter 5. In particular, the proposed framework pertains to the analytical formulation of an approximation for the probability density function (PDF) of the aggregate inter-cell interference in Poisson cellular networks. To elaborate on the practicality of the latter, it should be noted that ever since the introduction of stochastic geometry for the analysis of cellular networks, more that ten years ago, the lack of an analytical expression for the PDF of the interference in Poisson cellular networks had imposed significant constraints on the tractability of all relevant analyses. In particular, it imposed the employment of intricate formulas involving the MGF, increasing the complexity and intractability of all stochastic geometry analyses. Hence, the present thesis introduces a framework able to simplify the analysis of Poisson cellular networks to a great extent, while addressing fundamental issues related to network optimization, that had remained open.

Finally, Chapter 6 concludes the present thesis and presents perspectives.

1.5 Publications

The publications developed from the present thesis are enumerated below:

1.5.1 Journals

- A. I. Aravanis, T. T. Lam, O. Muñoz, A. Pascual-Iserte and M. Di Renzo, "A Tractable Closed-Form Approximation of the Ergodic Rate in Poisson Cellular

Networks," EURASIP Journal on Wireless Communications and Networking, accepted for publication, 2019.

- A. I. Aravanis, A. Pascual-Iserte, O. Muñoz, P. Matzoros, G. Agapiou, and M. Dohler, "Downlink and Uplink Decoupling in 5G and Beyond: A Guide to Optimal Connectivity," IEEE Communications Magazine, submitted for publication, 2019.

- A. I. Aravanis, O. Muñoz, A. Pascual-Iserte and M. Di Renzo, "On the Probability Distribution of the Aggregate Interference in Poisson Cellular Networks," IEEE Transactions on Wireless Communications, to be submitted.

1.5.2 Conferences

- A. I. Aravanis, O. Munoz, A. Pascual-Iserte and M. Di Renzo, "On the Coordination of Base Stations in Ultra Dense Cellular Networks," 2019 IEEE 89th Vehicular Technology Conference (VTC2019-Spring), Kuala Lumpur, Malaysia, 2019, pp. 1-6.

- A. Aravanis, A. Pascual-Iserte and O. Muñoz-Medina, "Closed-Form Capacity Bounds for Downlink and Uplink Decoupling,"WSA 2018; 22nd IEEE International ITG Workshop on Smart Antennas, Bochum, Germany, Mar. 2018, pp. 1-5.

- A. I. Aravanis, O. Munoz, A. Pascual-Iserte, and J. Vidal, "Analysis of downlink and uplink decoupling in dense cellular networks," in 2016 IEEE 21st International Workshop on Computer Aided Modelling and Design of Communication Links and Networks (CAMAD), Oct. 2016, pp. 219–224.

Chapter 2

Noise-limited Analysis of Poisson Cellular Networks and the DUDe Paradigm

In order to characterize the performance of networks comprising mmWave SCs, we proceed with the derivation of closed-form expressions for the UL ergodic rate in the noise limited case, since mmWave SCs operate in a noise limited regime [12], due to the interference mitigating effect of blocking in mmWave bands [19]. In this direction, we will initially focus only on the derivation of approximations for the UL ergodic rate in a network comprising only mmWave SCs, that operate under a noise limited regime. However, mmWave SCs cannot provide wide coverage due to the blocking in mmWave frequencies and for that reason this analysis only makes sense in the framework of a HetNet comprising also sub 6GHz MCs. In this setup, MCs can provide the sought out wide coverage and consistent connectivity and the analysis is extended to the case of standalone MCs. Subsequently, we proceed with the examination of a HetNet comprising both SCs and MCs with respect to the UL ergodic rate.

In HetNets users are expected to follow the traditional coupled connectivity paradigms and novel decoupled paradigms (known as DUDe) where the user is not constrained to be associated to the same BS in the DL and the UL. In order to differentiate the coupled and the DUDe cases the developed expressions focus on the UL ergodic rate, but as already stressed in Section 1.4, since the interference is not considered in this chapter the same expressions can also be employed for the DL ergodic rate.

2.1 The Wireless Cellular Network Scenario

A wireless cellular system is considered, comprising a MC served by the access point AP_0. Moreover, a set of SCs are overlaid by means of low power and low complexity

access points AP_i, whose positions follow a homogeneous Poisson point process (PPP) of density λ (SCs/m^2) [20]. AP_0 transmits at a high power level. On the other hand, all AP_i transmit at a low power level. Furthermore, for the sake of simplicity in the notation, it is assumed that all user equipment (UE) and access points, both for the MC and the SCs, are equipped with one antenna. However, the extension to the multi-antenna case is straightforward and in this course, a relevant analysis is provided throughout the section when necessary. In particular, this analysis elaborates on how the expressions should be changed when considering M antennas in the macro access point and N antennas in the SCs access points. Intra cell users are assumed to be sharing orthogonal resources, as it is typically assumed in the literature [7], whereas adjacent mmWave SCs are assumed to not interfere due to the interference mitigating effect of blocking in mmWave bands [19]. Furthermore, MCs are assumed to operate in the sub 6GHz range, thus not interfering with the mmWave SCs. In addition, due to the limited transmit power of the UE in the UL, UE is assumed to not interfere with adjacent MCs.

2.2 UL Ergodic rate Bounds - Simplified Cases

This section focuses on the derivation of a lower bound of the ergodic UL rate for the most elementary network setups. That is a network comprising a single MC and a network comprising only SCs. Subsequently these elementary setups will be extended to the aforementioned HetNet case.

Ergodic rate for a Single MC Network

The ergodic rate of a user placed at distance d_0 from AP_0 resulting from averaging over fast fading, if no additional SC access points AP_i is overlaid, is given by

$$\mathbb{E}[R] = \mathbb{E}_{h_0}[\log(1 + d_0^{-\beta}|h_0|^2\gamma)], \tag{2.1}$$

where the expectation is with respect to the fading coefficient h_0, assuming a Rayleigh fading where h_0 follows a zero-mean circularly symmetric Gaussian distribution with variance equal to 1. $\log(\cdot)$ in all the expressions henceforth represents the natural logarithm, β is the path-loss exponent [21], and γ is the SNR given by:

$$\gamma = \frac{P_{UE}}{\sigma^2 L_{ref}}. \tag{2.2}$$

In (2.2) P_{UE} is the transmission power of the UE, σ^2 is the noise power, and L_{ref} is the equivalent path-loss at a reference distance of 1 meter, which includes also the effects of the transmit and receive antenna gains.

A lower, albeit very tight bound for the ergodic rate can be derived from [22] as

follows:

$$\begin{aligned}
&\mathbb{E}_{h_0}[\log(1 + d_0^{-\beta}|h_0|^2\gamma)] \\
&= \mathbb{E}_{h_0}[\log(1 + d_0^{-\beta}\gamma \exp(\log(|h_0|^2)))] \\
&\geq \log(1 + d_0^{-\beta}\gamma \exp(\mathbb{E}_{h_0}[\log(|h_0|^2)])) \\
&= \log(1 + d_0^{-\beta}\gamma\ \rho),
\end{aligned} \tag{2.3}$$

where the inequality in (2.3) arises from Jensen's inequality and the convexity of the $\log(1 + \exp(x))$ function [23]. For Rayleigh fading, ρ is the expectation of the logarithm of a Chi-square random variable which is equal to [24]:

$$\rho = \exp(\mathbb{E}_{h_0}[\log |h_0|^2]) = \exp(-\psi), \tag{2.4}$$

where $\psi \simeq 0.577$ is the Euler-Mascheroni constant [25].

In the case of a multi-antenna receiver, the preceding analysis holds with $|h_0|$ being replaced by $\|\mathbf{h_0}\|$. $\mathbf{h_0}$ is a vector composed by n i.i.d. elements, each one corresponding to the Rayleigh fading coefficient between the transmitter and the n^{th} antenna receiver with a variance equal to 1. Moreover, (2.4) needs to be revised accordingly, with ρ in the case of a multi-antenna receiver being equal to [24]:

$$\rho(n) = \exp\left(\mathbb{E}_{\mathbf{h_0}}[\log\|\mathbf{h_0}\|^2]\right) = \exp\left(-\psi + \sum_{j=1}^{n-1} \frac{1}{j}\right). \tag{2.5}$$

Hence, in case that the access point at the MC is equipped with M antennas, the above expression is calculated for $\rho(M)$, and in case the access points at the SCs employ N antennas, it has to be calculated for $\rho(N)$. However, for the present analysis assuming single-antenna access points and according to (2.4), ρ is employed, whereas brief guidelines are provided throughout the section toward adapting the expressions to the multi-antenna case whenever needed.

Ergodic rate for a Network of Small Cells

The ergodic rate of a user residing within a dense deployment of SCs served only by the access points AP_i can be considered to be independent of the position of the user within the coverage of the network. That is, due to the assumption that the access points AP_i are deployed according to a homogeneous PPP with spatial density λ. Assuming a distance d between a reference user and the AP of the closest SC, the probability density function (PDF) of the distance d between a reference user and its closest AP is given by [26]

$$f_d(d) = 2\pi d\lambda \exp(-\lambda\pi d^2), \tag{2.6}$$

where $d \geq 0$.

Thus, we can again calculate a lower bound of the ergodic rate for the case of a network consisting only of SCs. In this case, it is expected that the UE will connect to the closest SC and the expectation is with respect to both the fading and the distance d to the closest AP. Thus, proceeding as in (2.3) a bound of the ergodic rate is given by

$$\begin{aligned}
&\mathbb{E}_{h,d}[\log(1+d^{-\beta}|h|^2\gamma)] \\
&= \mathbb{E}_{h,d}[\log(1+\exp(\log(d^{-\beta}|h|^2\gamma)))] \\
&\geq \log(1+\gamma\exp(\mathbb{E}_{h,d}[\log(d^{-\beta}|h|^2)])) \\
&= \log(1+\gamma\exp(-\beta\mathbb{E}_d[\log(d)]+\mathbb{E}_h[\log(|h|^2)])). \qquad (2.7)
\end{aligned}$$

where, according to (2.4), $\exp(\mathbb{E}_h[\log(|h|^2)]) = \rho$ and, according to (2.6), the expected value $\mathbb{E}_d[\log(d)]$ can be computed as follows:

$$\begin{aligned}
\mathbb{E}_d[\log(d)] &= \int_0^\infty \log(r) 2\pi r\lambda \exp(-\lambda\pi r^2) dr \\
&= 2\int_0^\infty x\log(x)\exp(-x^2)dx - \log(\sqrt{\pi\lambda}) = -\frac{\psi}{2} - \log(\sqrt{\pi\lambda}). \qquad (2.8)
\end{aligned}$$

Thus, combining (2.7) and (2.8) a bound for the ergodic rate is obtained as follows:

$$\mathbb{E}_{h,d}[\log(1+d^{-\beta}|h|^2\gamma)] \geq \log\left(1+\gamma(\lambda\pi)^{\frac{\beta}{2}}\rho\exp(\beta\frac{\psi}{2})\right). \qquad (2.9)$$

Evidently, for a given setting of path loss exponent β and SNR γ, the above simple bound for the UL ergodic rate depends only on the density of the network, i.e. the value of λ. Hence, if this bound could be extended in the case of a complex network comprising both MCs and SCs, this could be proven a valuable tool for any network operator and designer toward meeting the QoS objectives based on the network densification. In this course, the UL ergodic rate analysis is extended in HetNets comprising both MCs and SCs hereafter.

2.3 The HetNet Case

Building upon expressions (2.3) and (2.9) we can combine them and derive closed form bounds for the UL ergodic rate in the case of HetNets, which encompass both MCs and SCs. In this direction, a common framework will be developed accounting for all types of networks and connectivity paradigms. In particular, the developed framework will account for the HetNet case, as well as the previously examined cases of only SCs or MCs, as particular cases of the framework.

Furthermore the proposed unified framework will account also for different connectivity paradigms where the serving BSs are selected by the user dynamically in order to maximize the achievable rate. The idea of the flexible selection of the serving BSs particularly with respect to the UL and DL emerged as a mechanism to exploit the density and

power disparity of network elements in HetNets. Hence, a unified framework quantifying the network performance of HetNets must also account for this flexible paradigm.

To this end, prior to the derivation of the aforementioned unified HetNet framework, it is considered wise to familiarize the reader with the concept of the flexible management of the UL and DL connectivity.

2.3.1 Downlink Uplink Decoupling

The advent of multimedia interactive services has induced a change in the entrenched perception of mobile networks, introducing a shift from asymmetric to symmetric traffic loads (i.e. symmetric with respect to the UL and DL traffic). Specifically, the rise of social media and online video gaming applications resulted in an unabated increase in the UL traffic, which in turn, mandated a dedicated optimization of the UL channel. In this direction, the need for an independent management of the UL and DL connectivity and of a dedicated optimization of the UL channel became more actual than ever. In classical schemes both the DL and the UL connectivity were driven by the DL conditions, which significantly deteriorated the UL performance. This realization gave rise to a disruptive approach where UE can be connected to a different serving node in the UL and the DL [27].

The feasibility of this approach relies on the density of BSs in current UDNs and on the disparity between the transmit power of the network elements. UDNs allow for a UE to have access to multiple BSs and to select the BS from which it receives the highest reference signals received power (RSRP) in the DL. As a result, a UE could connect to a distant MC BS, from which it receives a higher RSRP in the DL, as opposed to a small cell (SC) BS residing in its vicinity, but transmitting at a lower power level. However, this connectivity criterion disregards the performance of the UL, since the UE transmits at the same power level regardless of the BS that detects its signal. Hence, the connection to the distant MC instead of the adjacent small cell, has a detrimental effect on the system performance in the UL. Addressing this problem the independent management of the DL and UL connectivity, known as DUDe, allows for a user to connect to different BSs in the DL and the UL. Hence, DL and UL are no longer constrained to the same base station (BS) and the independent management and optimization of both links can provide substantial rate [7, 27] and power [28] gains. To elaborate on the connectivity of DUDe, an illustration is presented in Fig. 2.1 depicting a coupled connection versus a decoupled connection. In the decoupled connection the UE receives a higher RSRP from the MC BS in the DL but in the UL connects to the SC BS that resides closer.

Multitude of research works hitherto have documented the gains arising from the employment of DUDe in dense cellular networks [27] and have provided expressions for the evaluation of the UL performance [7]. However, in those expressions the performance of the UL channel is assumed to be independent of the density of the infrastructure,

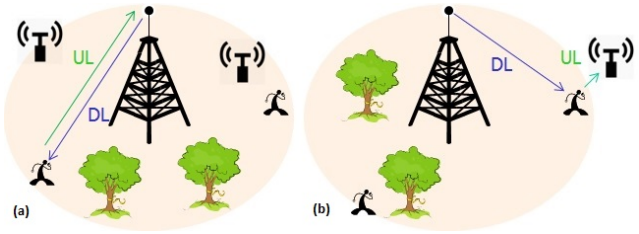

Figure 2.1: Indicative scenario under a coupled and a DUDe association policy.

which is not the case for systems operating in a noise limited regime. In fact, in those cases the performance of the channel depends heavily of the network density, as will be demonstrated in the ensuing analysis.

2.3.2 UL Ergodic Rate Bounds - HetNet Case

Having described the concept of DUDe and having derived the ergodic rate bounds of (2.3) for the case of a single MC and of (2.9) for the case of solely SCs, the analysis can now be extended to provide closed form simple expressions for the calculation of lower bounds for the UL ergodic rate in HetNets. In particular, the following HetNet analysis encompasses also, as particular cases, both the aforementioned approaches of only SCs and only a MC, as well as the DUDe and the coupled association policies.

In the coupled case the UE connects to the closest SC if the following holds for the distance d to the SC:

$$d \leq \left(\frac{P_{SC}}{P_{MC}}\right)^{\frac{1}{\beta}} d_0, \tag{2.10}$$

where P_{SC} is the transmit power of the SC and P_{MC} is the transmit power of the MC. That is, the connection criterion of the UE is the level of the received power from each AP[1].

In comparison, in the DUDe case the UE will connect to the closest AP and not to the AP from which it receives the highest power in the DL. Thus, the UE will connect to the closest SC instead of the MC if[2]

$$d \leq d_0. \tag{2.11}$$

[1]In the case of multi-antenna access points, the criterion in (2.10) should be rewritten as follows: $d \leq \left(\frac{M\rho(N)P_{SC}}{N\rho(M)P_{MC}}\right)^{1/\beta} d_0$. This criterion is equivalent to connecting in the UL to the access point from which the highest rate is obtained in the DL.

[2]In the case of multi-antenna access points, the criterion in (2.11) should be rewritten as follows: $d \leq \left(\frac{\rho(N)}{\rho(M)}\right)^{1/\beta} d_0$. This criterion is equivalent to connecting in the UL to the access point so that the maximum UL rate is achieved.

The previous two conditions can be unified under a single notation where the UE will connect to the closest SC if

$$d \leq \nu d_0, \tag{2.12}$$

where $\nu = (\frac{P_{SC}}{P_{MC}})^{\frac{1}{\beta}}$ in the coupled case and $\nu = 1$ in the DUDe case[3]. Moreover, the above notation is general enough to account also for the cases of only SCs and only a MC, since the case of a single MC corresponds to $\nu = 0$ and the case of solely SCs corresponds to $\nu = \infty$. Therefore, the selection criterion for the UL connectivity defined in (2.12) takes all examined cases into account according to an *a priori* defined value of ν.

Ergodic rate for the HetNet Case

In order to calculate the ergodic rate for a generic network, encompassing both MC and SCs and supporting both DUDe and coupled transmission policies, a generic approach must be adopted taking into account the selection criterion described in (2.12). In particular, the ergodic rate can be calculated as the sum of the conditioned ergodic capacities in the case of the UE being connected to the MC and to the closest SC weighted by the probability of each of the two contingencies happening. Specifically, the average ergodic rate is calculated as follows:

$$\mathbb{E}[R] = \mathbb{E}_{h_0}[R|MC]P(MC) + \mathbb{E}_{h,d|SC}[R|SC]P(SC), \tag{2.13}$$

where $\mathbb{E}_{h_0}[R|MC]$ is the ergodic rate conditioned to the fact that the reference user has connected to the MC for a given d_0, $P(MC)$ is the probability of the user to connect to the MC, $\mathbb{E}_{h,d|SC}[R|SC]$ is the ergodic rate conditioned to the fact that the user has connected to the closest SC. $d|SC$ denotes that the expectation is with respect to the distance d, conditioned to the fact that this distance has imposed the connection to the SC. Then, $P(SC)$ denotes the probability of the user to connect to the closest SC.

According to the selection criterion defined in (2.12), the probability $P(SC)$ is equal to the probability $P(d \leq \nu d_0)$, which after employing (2.6) can be calculated by:

$$P(SC) = P(d \leq \nu d_0) = \int_0^{\nu d_0} 2\pi x \lambda \exp(-\lambda \pi x^2) dx = 1 - \exp(-\lambda \pi \nu^2 d_0^2), \tag{2.14}$$

and $P(MC)$ is calculated by:

$$P(MC) = 1 - P(SC) = \exp(-\lambda \pi \nu^2 d_0^2). \tag{2.15}$$

Furthermore, in case $d > \nu d_0$, a lower bound can be defined by (2.3) and (2.4) for $\mathbb{E}_{h_0}[R|MC]$ as:

$$\mathbb{E}_{h_0}[R|MC] \geq \log(1 + d_0^{-\beta} \gamma \rho). \tag{2.16}$$

[3]Assuming that the antenna gains of the MC and the SCs are equal, whereas the ν factor should be weighted accordingly if the antenna gains are different.

However, in order to compute lower bounds for $\mathbb{E}_{h,d|SC}[R|SC]$ a different approach than the one followed in (2.8) needs to be considered, since the distance to the closest SC d is conditioned by the fact that $d \leq \nu d_0$ (i.e. it is conditioned by the fact that the UE has decided to connect to the SC). Therefore, the PDF defined in (2.6) needs to be revised accordingly and the following truncated version of the PDF needs to be employed for the conditioned random variable $d|SC$ [31]:

$$f_{d|SC}(d|SC) = \begin{cases} 0, & d < 0 \\ \frac{1}{k}\ 2\pi d\lambda \exp(-\lambda\pi d^2), & 0 \leq d < \nu d_0 \\ 0, & \nu d_0 \leq d \end{cases} \tag{2.17}$$

where k is a constant selected appropriately so that the area of $f_{d|SC}(d|SC)$ is equal to 1. That is,

$$k = \int_0^{\nu d_0} 2\pi x\lambda \exp(-\lambda\pi x^2)dx = P(SC). \tag{2.18}$$

Hence, similarly to (2.8) the expected value $\mathbb{E}_{d|SC}[\log(d)]$ for the new PDF defined in (2.17) can be calculated by

$$\begin{aligned} \mathbb{E}_{d|SC}[\log(d)] &= \frac{\int_0^{\nu d_0} \log(d) 2\pi d\lambda \exp(-\lambda\pi d^2)dd}{P(SC)} \\ &= \frac{2\int_0^{\nu d_0\sqrt{\lambda\pi}} x\log(x)\exp(-x^2)dx}{P(SC)} - \log(\sqrt{\pi\lambda}). \end{aligned} \tag{2.19}$$

Thus, after combining (2.13), (2.14), (2.15), (2.16), and (2.19) the bound for the ergodic rate in the HetNet case is given by:

$$\begin{aligned} \mathbb{E}[R] \geq\ & \log(1+\gamma d_0^{-\beta}\rho)\exp(-\lambda\pi\nu^2 d_0^2) \\ & + \log\left(1+\gamma(\lambda\pi)^{\beta/2}\rho\exp\left(-\frac{2\beta}{1-\exp(-\lambda\pi\nu^2 d_0^2)}\int_0^{\nu d_0\sqrt{\lambda\pi}} x\log(x)\exp(-x^2)dx\right)\right) \\ & \cdot (1-\exp(-\lambda\pi\nu^2 d_0^2)). \end{aligned} \tag{2.20}$$

It is evident from the expressions obtained from the preceding analysis, that the ergodic rate in the UL depends only on the values of λ and the distance d_0 from the MC access point, for a given UL association policy given by the decision factor ν.

Corollary 1. *For $\nu d_0\sqrt{\lambda\pi} \geq 4$, (2.20) can be approximated by (2.21). Thus, if the above criterion is met a simpler bound for the ergodic rate in the UL can be employed. This approximation arises from the behavior of the integral: $\int_0^{\nu d_0\sqrt{\lambda\pi}} x\log(x)\exp(-x^2)dx$, the value of which is approximately constant for any upper limit greater than 4. This can be further verified by the visual representation of the function that is being integrated depicted in Fig. (2.2).*

$$\mathbb{E}[R] \geq \log(1+\gamma d_0^{-\beta}\rho)\exp(-\lambda\pi\nu^2 d_0^2) + \log\left(1+\gamma(\lambda\pi)^{\beta/2}\rho\exp\left(\frac{\beta\psi/2}{1-\exp(-\lambda\pi\nu^2 d_0^2)}\right)\right)(1-\exp(-\lambda\pi\nu^2 d_0^2)),$$
$$\nu d_0\sqrt{\lambda\pi} \geq 4 \tag{2.21}$$

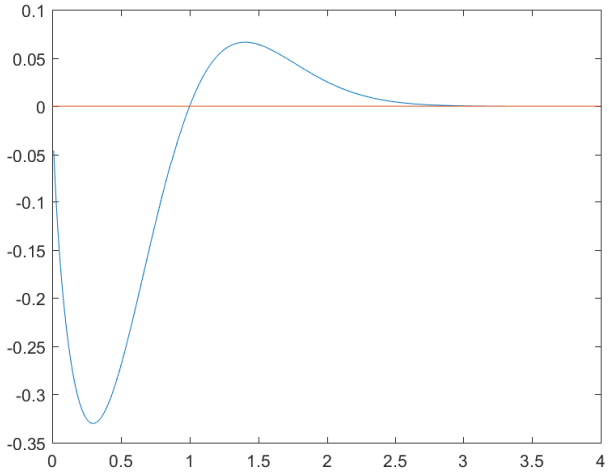

Figure 2.2: Visual representation of function $x\log(x)\exp(-x^2)$.

The simplicity of the derived analytical bounds as well as their dependency solely upon the values of λ and d_0 is of paramount importance for the network operator. In particular, these bounds provide complete information regarding the QoS and the densification of the network, enabling the network operator to adjust the network to the emerging traffic requirements. However, in order for these bounds to be of actual merit and to provide an accurate picture of the network performance to the operator, they have to be tight. In the direction of corroborating how tight the obtained bounds are, the performance of a network comprising MC as well as SCs is simulated for all different settings defined above. The simulation results are compared in the next section against the analytical results obtained from the introduced bounds, verifying the tight relationship of both results.

2.3.3 Simulations

In order to demonstrate the tight performance of the devised analytical bounds, a HetNet has been simulated encompassing a MC, SCs positioned according to a homogeneous PPP of spatial density λ and a reference user. The SCs are located also beyond the coverage area of the MC. In addition, the simulations have been repeated for all four of

the considered scenarios, i.e. for only a MC, for only SCs, for a HetNet under DUDe (i.e. $\nu = 1$), and for a HetNet under a coupled association with $\nu = 0.3$.

The basic parameters required for the link budget are tabulated in Table 2.1. According to these values, the factor $\nu = (0.01)^{0.25} = 0.3$ for coupled UL-DL association corresponds to a 20dB difference between the MC power and SC power, whereas $\nu = 1$ corresponds to DUDe association policy and, for both cases, γ is calculated based on the tabulated UE power. In the simulations, a density $\lambda = 6.25\ 10^{-06} SC/m^2$ is defined *a priori* and the expected rate has been compared against the distance d_0 from the MC access point with the performance of the simulated network and the analytical bounds being depicted in Fig. 2.3. Subsequently, the simulations have been repeated for an *a priori* defined distance $d_0 = 250m$ and the expected rate has been compared against the network density λ in Fig. 2.4. Thus, the performance of the reference user is analyzed for a given distance from the single MC access point which is considered in the simulations.

Table 2.1: Link Budget Parameters

Parameter	**Value**
UE Transmit Power P_{UE}	33 dBm
SC Transmit Power P_{SC}	33 dBm
MC Transmit Power P_{MC}	53 dBm
Bandwidth	10 MHz
Noise Power Spectral Density	-174 dBm/Hz
Noise Power	-104 dBm
Path Loss at Reference Distance L_{ref} (Including Antenna Gains)	25.6 dB
Path Loss Exponent	4
ν (UL-DL coupling)	$(0.01)^{0.25} = 0.3$
ν (UL-DL decoupling)	1

The tight relationship between the obtained analytical bounds and the simulated results is manifested in both figures verifying the reliability of the preceding analysis and its utility in network management and design. In addition, another pivotal conclusion drawn from the presented simulations is the validity of the approximation result presented in (2.21), since the performance of the decoupled network converges to that of the network employing only SCs as the values of λ and d_0 increase. The reason for that is that as the density of the SCs increases the probability of a SC residing closer to the UE than a MC increases as well. Hence, since the user connects to the closest BS in the decoupled case the probability of connecting to a SC increases and the performance of the decoupled system converges to that of the system comprising only SCs. The previous work has

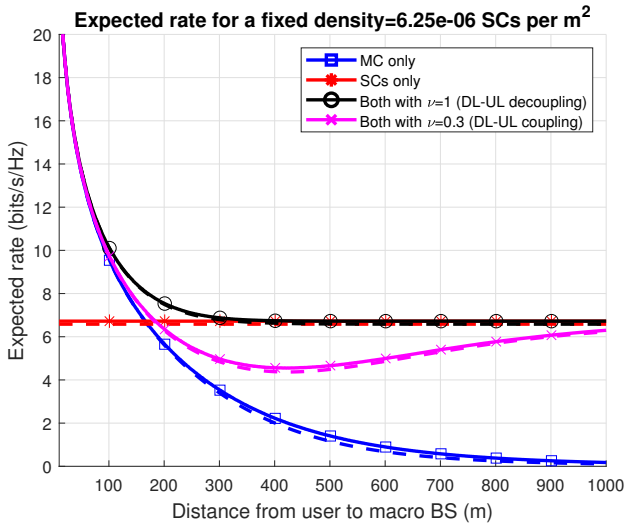

Figure 2.3: Expected UL rate vs distance to the MC access point.

been published in [32].

2.4 Averaging over the MC coverage / Synchronization Aware Analysis

In the previous section simple analytical expressions were provided for quantifying the performance of dense wireless networks in 4 different cases, that is for networks comprising SCs only, a MC only, a coupled HetNet and a decoupled HetNet. Enhancing these results, the present section proposes even simpler bounds that do not depend on the distance of the UE to the MC BS like the previously defined expressions, but depend solely on the density of the infrastructure.

Moreover, the present analysis shifts from the binary analyses employed in the literature hitherto, which focused only on the UE connection to the MC or to the SC in the UL, and neglected the DL connectivity. The following analysis takes also the DL connectivity into account, thus, distinguishing the coupled connection to the SC from the decoupled connection to the SC. Hence, the decoupled connection in the UL arises as a standalone case, allowing for addressing inherent drawbacks of DUDe pertaining to this case. Thus, the present approach accommodates a holistic analysis of DUDe, while specifically accounts for the standalone decoupled case allowing for addressing salient drawbacks of DUDe related to the decoupled operation.

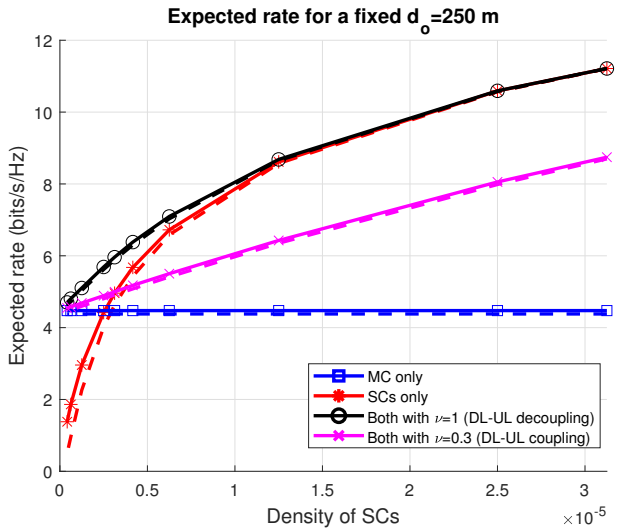

Figure 2.4: Expected UL rate vs density of SCs.

2.4.1 DUDe Connectivity Regions

In order to distinguish the coupled connection to the SC from the decoupled connection to the SC in the UL, and examine them as standalone cases we need to focus on a holistic connectivity mapping accounting for both the DL and the UL. This will allows us to examine the emerging connectivity regions and policies in DUDe enabled systems. In this course, the connectivity regions of DUDe in the DL and UL are examined hereafter.

Assuming that d_{SC} denotes the distance from the UE to its closest SC BS, and d_{MC} the distance to its closest MC BS, the UE connects in the UL to the SC if $d_{SC} < d_{MC}$ and to the MC if $d_{MC} < d_{SC}$. On the other hand, the UE connects in the DL to the SC if $d_{SC} < \mu d_{MC}$ and to the MC if $\mu d_{MC} < d_{SC}$. The constant factor μ denotes the ratio of the SC transmit power over the MC transmit power, adjusted by the pathloss exponent. This gives rise to an UL and a DL connectivity frontier at $d_{MC} = d_{SC}$ and at $d_{SC} = \mu d_{MC}$ respectively, that partition the MC coverage area in three distinct connectivity regions, A, B and C as depicted in detail in Fig. 2.5.

These connectivity regions determine the connectivity policy of the UE they comprise. Specifically, a UE positioned in region A follows a coupled connection to the MC, whereas a UE positioned in region C employs a coupled connection to the SC. A UE located in region B follows a decoupled connection, connecting to the MC in the DL and to the SC in the UL. The path loss benefits arising for a UE residing in region B, through the connection to the closest BS in the UL, provide commensurable rate, power and outage gains. However, this comes at the expense of increased network complexity since the acknowledgments (ACK/NAK) and the related control messages of the decoupled

links need to be routed through the backhaul [33] as depicted in Fig. 2.5. The latency introduced by the decoupling of the acknowledgements may have a detrimental effect on the network performance. Hence, this trade off needs to be effectively managed when selecting the optimal connectivity policy.

In order to select the optimal connectivity policy, additional connectivity criteria may need to be taken also into account. Indicatively, in the case of high-mobility users, the need for consistent connectivity could motivate the connection to a MC, instead of a SC, as the optimal anchor point to minimize the handover signaling overhead. Hence, in order to devise an optimal connectivity policy, the system must be able to account for all these factors, including its ability to implement each policy in practice.

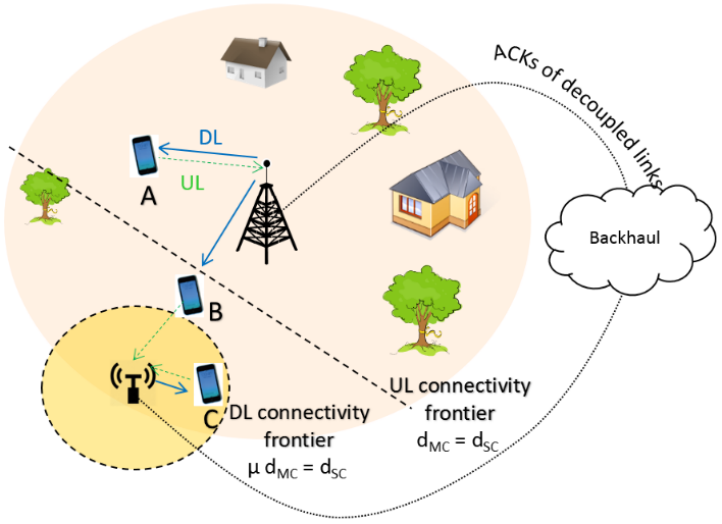

Figure 2.5: DUDe association policy defined by the UL and DL connectivity frontiers. User in region A connects to the MC in the DL and the UL, user in region B connects to the MC in the DL and to the SC in the UL, and user in region C connects to the SC in the DL and the UL. The ACKs of the decoupled links are routed through the backhaul.

Having described the DUDe connectivity regions we can proceed with examining individually each of the emerging connectivity policies hereafter. The DUDe approach depicted in Fig. 2.5 gives birth to 3 distinct association cases depending on the distance of the UE to the surrounding BSs. These cases are:

1) DL-UL connected to a MC,

2) DL-UL connected to a SC,

3) DL connected to a MC and UL connected to a SC.

In the previous section a unified selection criterion was defined in (2.12), with the value of ν changing to indicate a SC only, a MC only, a coupled or decoupled HetNet. However, the introduction of the 3 aforementioned standalone cases imposes the revision

of the selection criterion, in order to distinguish between them. Hence, instead of a parameter ν taking different values, the dedicated parameters α and μ are employed to indicate the limits of each connectivity region. Hence, the selection criterion for each of the above association cases is based on the distance d_{MC}, which is henceforth denoted by d_0 for brevity in the notation and d_{SC} which is denoted by d. Employing the new notation, the UE connects to the closest SC in the DL if the following condition holds:

$$d \leq \mu d_0, \tag{2.22}$$

where $\mu = \left(\frac{P_{SC}}{P_{MC}}\right)^{\frac{1}{\beta}} < 1$. That is, the connection criterion for the UE is the level of the received power from each BS.

On the other hand, the UE connects to the closest SC in the UL if the SC BS is closer than the MC BS, namely if $d \leq d_0$. However, to fully exploit the leeway provided by DUDe in selecting the optimum connectivity, a decision parameter α is introduced in the notation and the criterion for connecting to the closest SC in the UL is redefined as follows:

$$d \leq \alpha d_0. \tag{2.23}$$

The decision parameter α ($\mu \leq \alpha \leq 1$) allows for the extension of the analysis, toward optimizing the overall system connectivity and for this reason it has been introduced in the present analysis. In conventional DUDe and in the present section α is equal to 1. However, in the next section the expressions derived herein will be employed to optimize the value of α with respect to the optimization of the system connectivity.

The combination of (2.22) and (2.23), leads to 3 association intervals for the respective association cases described above:

$$\text{1) DL-UL connected to a MC:} \quad \mathcal{I}_1(d_0) = \{d : \alpha d_0 \leq d\}, \tag{2.24}$$

$$\text{2) DL-UL connected to a SC:} \quad \mathcal{I}_2(d_0) = \{d : d \leq \mu d_0\}, \tag{2.25}$$

$$\text{3) DL to MC, UL to SC:} \quad \mathcal{I}_3(d_0) = \{d : \mu d_0 < d < \alpha d_0\}. \tag{2.26}$$

The probability of a random reference user to reside within the association interval defined in (2.24)-(2.26) can be calculated based on the probability density function (PDF) of the distance d to the closest SC, which for a homogeneous PPP deployment of SCs is given by (2.6). Thus, the probability P_1 corresponding to the selection criterion (2.24) is given by:

$$P_1(d_0) = P(\alpha d_0 \leq d) = \int_{\alpha d_0}^{\infty} f_d(x)dx = \exp(-\lambda \pi \alpha^2 d_0^2), \tag{2.27}$$

Respectively, P_2 corresponds to the selection criterion (2.25) is given by:

$$P_2(d_0) = 1 - \exp(-\lambda \pi \mu^2 d_0^2), \tag{2.28}$$

and P_3 of criterion (2.26) is given by:

$$P_3(d_0) = \exp(-\lambda\pi\mu^2 d_0^2) - \exp(-\lambda\pi\alpha^2 d_0^2). \tag{2.29}$$

2.4.2 Synchronization Aware Analysis

As already mentioned, the applicability of DUDe from a network design perspective, depends on the network's ability to provide strong synchronization of the acknowledgments (ACK/NAK) of the decoupled links and strong data connectivity (e.g. via fiber) between the involved BSs [33]. Therefore, the feasibility of DUDe relies heavily on the status of the backbone network and its capability to provide strong synchronization and data connectivity, as well as the application requirements in higher layers with respect to latency, mobility, etc., as will be demonstrated in the following section.

However, this aspect has generally been disregarded in the literature. In this course, we introduce the probability p of having packet losses in the backbone network, since the acknowledgments of the UL and the DL are routed through the backbone when the channels are decoupled. The introduction of p into the devised bounds allows for characterizing the performance of the UL channel more accurately while accounting for the network implementation aspects of DUDe.

The connectivity region subjected to the aforementioned synchronization issue is that corresponding to the interval (2.26). Hence, in the ensuing analysis the UL rate of UE residing in this interval is weighted by the probability $(1-p)$. Namely, the probability of a successful acknowledgment synchronization of the decoupled links via the network backbone.

2.4.3 The UL Rate Bounds

UL Ergodic Rate vs Distance to MC BS

Having described the network architecture and the methodology for accounting for the synchronization of the decoupled acknowledgments, the analytical bounds for the UL rate are derived hereafter. The average UL ergodic rate is obtained by the sum of the conditioned UL ergodic capacities $\mathbb{E}_h[R|1], \mathbb{E}_h[R|2], \mathbb{E}_h[R|3]$ in the case that each of the 3 association cases are selected, weighted by the probabilities P_1, P_2, P_3 of each of these contingencies happening. The expectation of the ergodic capacities is with respect to the fading coefficient h, assuming a Rayleigh fading with $\mathbb{E}[|h|^2] = 1$.

Moreover, to obtain the average UL ergodic rate, the expectation with respect to the distance d needs to be calculated. Hence, the instantaneous average UL ergodic rate is given by:

$$\bar{\mathbf{R}}(d_0) = \mathbb{E}_h[R|1]P_1 + \mathbb{E}_{h,d|2}[R|2]P_2 + \mathbb{E}_{h,d|3}[R|3]P_3(1-p). \tag{2.30}$$

In the above expression, the first term corresponds to the coupled connection to the MC and, therefore, it is independent of the distance d to the closest SC. As opposed to that, the second and third terms are averaged over the distance d, conditioned to the fact that d falls within the association interval imposing the selection of the respective association.

Employing expression (2.3) the following bounds hold:

$$\mathbb{E}[\log(1+g(x))] \overset{(\cdot)=\exp(\log(\cdot))}{\geq} \log(1+\exp(\mathbb{E}[\log(g(x))])), \tag{2.31}$$

and

$$\mathbb{E}_h[R|1] = \mathbb{E}_h[\log(1+d_0^{-\beta}h^2\gamma)] \overset{(2.31)}{\geq} \log(1+d_0^{-\beta}\gamma\rho). \tag{2.32}$$

Since the the random variables h and $d|i$ are independent, the following bound can be derived for $\mathbb{E}_{h,d|i}[R|i]$, $i=2,3$ (i.e. for the second and third terms of (2.30)):

$$\mathbb{E}_{h,d|i}[\log(1+d^{-\beta}h^2\gamma)] \overset{(2.3)}{\geq} \log(1+\gamma\exp(-\beta\mathbb{E}_{d|i}[\log(d)]+\mathbb{E}_h[\log(h^2)])). \tag{2.33}$$

In order to calculate $\mathbb{E}_{d|i}[\log(d)]$, the PDFs $f_{d|i}(d|i)$, $i=\{2,3\}$ need to be employed, which are the truncated PDFs for the condition that the distance d falls within the association interval $\mathcal{I}_2$ or $\mathcal{I}_3$. Hence, the two PDFs are defined as follows:

$$f_{d|i}(d|i) = \begin{cases} \frac{1}{k_i}\ 2\pi d\lambda\exp(-\lambda\pi d^2), d\in\mathcal{I}_i(d_0), \\ 0, \qquad\qquad\qquad\qquad \text{elsewhere}, \end{cases} \tag{2.34}$$

where k_i is a constant selected appropriately so that the area of $f_{d|i}(d|i)$ is equal to 1. Accordingly, $k_2 = P_2(d_0)$ and $k_3 = P_3(d_0)$, whereas the term $\mathbb{E}_{d|i}[\log(d)]$ of (2.33) is given by:

$$\mathbb{E}_{d|i}[\log(d)] = \int_{\mathcal{I}_i(d_0)} \frac{\log(d)2\pi d\lambda\exp(-\lambda\pi d^2)}{P_i(d_0)} dd. \tag{2.35}$$

UL Ergodic rate vs MC Radius

It is readily deduced that the above bounds still depend on d_0. Specifically the dependence is manifested in the probabilities $P_i(d_0)$, in (2.32), and in the integration limits of (2.35). In order to provide a comprehensive characterization of the UL channel over the whole MC coverage (which is defined by a disk of radius R_0), (2.30) needs to be averaged over d_0 and, thus, the UL ergodic rate is given by:

$$\begin{aligned} \bar{\bar{\mathbf{R}}}(R_0) =& \mathbb{E}_{d_0}[\bar{\mathbf{R}}(d_0)] \overset{(2.30),(2.32),(2.4),(2.33)}{\geq} \\ & \mathbb{E}_{d_0}\Big[\log(1+d_0^{-\beta}\gamma\rho)P_1(d_0)\Big] + \mathbb{E}_{d_0}\Big[\mathbb{E}_{d|2}\left[\log(1+d^{-\beta}\gamma\rho)\right]P_2(d_0)\Big] + \\ & \mathbb{E}_{d_0}\left[\mathbb{E}_{d|3}\left[\log(1+d^{-\beta}\gamma\rho)\right]P_3(d_0)\right](1-p), \end{aligned} \tag{2.36}$$

where (2.4) has already been substituted in (2.33) before the latter is applied. Assuming that the users are uniformly distributed over the MC coverage, the PDF of the distance d_0 is given by $f_{d_0}(d_0) = \frac{2d_0}{{R_0}^2}$ $(0 \leq d_0 \leq R_0)$ and the 3 terms of (2.36) need to be calculated employing $f_{d_0}(d_0)$.

In order to apply the bound of (2.3) to (2.36), each individual term of (2.36) is expanded as follows:

$$\begin{aligned}
&\mathbb{E}_{d_0}\left[\mathbb{E}_{d|i}\left[\log(1+d^{-\beta}\gamma\ \rho)\right] P_i(d_0)\right] \\
&= \int_0^{R_0}\int_{\mathcal{I}_i(d_0)} \log(1+d^{-\beta}\gamma\ \rho) f_{d|i}(d|i) f_{d_0}(d_0) P_i(d_0) dddd_0 \\
&= m_i \int_0^{R_0}\int_{\mathcal{I}_i(d_0)} \log(1+d^{-\beta}\gamma\ \rho)\epsilon_i(d,d_0) dddd_0 \overset{(2.3)}{} \\
&\geq m_i \log\left(1+\gamma\ \rho \exp(-\beta \mathbb{E}_{\epsilon_i(d,d_0)}[\log(d)])\right). \qquad (2.37)
\end{aligned}$$

In (2.37), $\epsilon_i(d, d_0)$ is a pseudo PDF, over which an auxiliary expectation $\mathbb{E}_{\epsilon_i(d,d_0)}$ is applied to allow for the employment of (2.3). Thus, for the three terms of (2.36) three pseudo PDFs emerge: ϵ_i, $i = \{1, 2, 3\}$ which are valid for $0 \leq d_0 \leq R_0$ and $d \in \mathcal{I}_i(d_0)$. For each of the pseudo PDFs ϵ_i the constants m_i, $i = \{1, 2, 3\}$ are computed for the volume of each PDF to be equal to 1. Thus, ϵ_i and m_i are given by:

$$\epsilon_1(d_0) = \frac{P_1(d_0) f_{d_0}(d_0)}{m_1}, \qquad (2.38)$$

$$\epsilon_i(d, d_0) = \frac{f_d(d) f_{d_0}(d_0)}{m_i}, i = \{2, 3\}, \qquad (2.39)$$

$$m_1 = \left(1 - \exp(-(\alpha x)^2)\right)/(\alpha x)^2, \qquad (2.40)$$

$$m_2 = 1 - \frac{1 - \exp(-(\mu x)^2)}{(\mu x)^2}, \qquad (2.41)$$

$$m_3 = \frac{1}{x^2}\left(\frac{1 - \exp(-(\mu x)^2)}{\mu^2} - \frac{1 - \exp(-(\alpha x)^2)}{\alpha^2}\right), \qquad (2.42)$$

where $x = R_0\sqrt{\lambda\pi}$, for brevity in the notation. Expanding (2.36) as in (2.37) and applying the bound of (2.3), we obtain in (2.44) the bound for the UL ergodic rate[4].

[4] After employing the following expressions obtained through integration by parts:

$$\int_0^{\omega} \phi \log(\phi) \exp(-\phi^2) d\phi = \frac{1}{4}\left(\mathrm{Ei}(-\omega^2) - \psi - \frac{\log(\omega^2)}{\exp(\omega^2)}\right). \qquad (2.43)$$

$$\int_0^{\omega} \phi \left(\mathrm{Ei}(-\phi^2) - \frac{\log(\phi^2)}{\exp(\phi^2)}\right) d\omega = \frac{(\omega^2 - 1)\,\mathrm{Ei}(-\omega^2) - 1 + \psi}{2} + \frac{1 + \log(\omega^2)}{2\exp(\omega^2)},$$

where $\mathrm{Ei}(\phi) = \int_{\phi}^{\infty} \frac{e^{-t}}{t} dt$ is the exponential integral.

$$\begin{aligned}\bar{\bar{\mathbf{R}}}(R_0) \geq\, & m_1 \log\left(1+\gamma\rho\exp(-\beta\mathbb{E}_{\epsilon_1(d_0)}[\log(d_0)])\right)\\ & + m_2 \log\left(1+\gamma\rho\exp(-\beta\mathbb{E}_{\epsilon_2(d,d_0)}[\log(d)])\right)\\ & + m_3 \log\left(1+\gamma\rho\exp(-\beta\mathbb{E}_{\epsilon_3(d,d_0)}[\log(d)])\right)(1-p),\end{aligned} \tag{2.44}$$

$$\mathbb{E}_{\epsilon_1(d_0)}[\log(d_0)] = \frac{\left(\mathrm{Ei}(-(\alpha x)^2) - \psi - \frac{\log((\alpha x)^2)}{\exp((\alpha x)^2)}\right)}{2-2\exp(-(\alpha x)^2)} - \log(\alpha\sqrt{\lambda\pi}), \tag{2.45}$$

$$\begin{aligned}\mathbb{E}_{\epsilon_2(d,d_0)}[\log(d)] = \frac{1}{m_2}\Bigg(& -\frac{\psi}{2} + \frac{1}{2(\mu x)^2}\left(((\mu x)^2-1)\,\mathrm{Ei}(-(\mu x)^2) - 1 + \psi + \frac{1+\log((\mu x)^2)}{\exp((\mu x)^2)}\right)\\ & - \log(\sqrt{\lambda\pi}) + \frac{\log(\sqrt{\lambda\pi})(1-\exp(-(\mu x)^2))}{(\mu x)^2}\Bigg),\end{aligned} \tag{2.46}$$

$$\begin{aligned}\mathbb{E}_{\epsilon_3(d,d_0)}[\log(d)] = & \frac{1}{m_3}\left(\frac{1}{2(\alpha x)^2}\left(((\alpha x)^2-1)\,\mathrm{Ei}(-(\alpha x)^2) - 1 + \psi + \frac{1+\log((\alpha x)^2)}{\exp((\alpha x)^2)}\right)\right)\\ & + \frac{1}{m_3}\Bigg(-\frac{1}{2(\mu x)^2}\left(((\mu x)^2-1)\,\mathrm{Ei}(-(\mu x)^2) - 1 + \psi + \frac{1+\log((\mu x)^2)}{\exp((\mu x)^2)}\right)\\ & + \log(\sqrt{\lambda\pi})\left(\frac{(1-\exp(-(\alpha x)^2))}{(\alpha x)^2} - \frac{(1-\exp(-(\mu x)^2))}{(\mu x)^2}\right)\Bigg)\end{aligned} \tag{2.47}$$

Corollary 2. *The previous analysis and the employment of (2.3) and (2.4) can give rise to a remarkably simple bound for the case of a standalone MC. The average MC ergodic UL rate is given by:*

$$\bar{\bar{\mathbf{R}}}_{MC}(R_0) = \mathbb{E}_{h,d_0}[\log(1+d_0^{-\beta}|h|^2\gamma)] \geq \log\left(1+\gamma\rho R_0^{-\beta}\exp(\frac{\beta}{2})\right), \tag{2.48}$$

whereas (2.48) can also be employed for the DL rate, if γ is adjusted to account for the MC BS transmission power.

2.4.4 Simulations

In order to demonstrate the accuracy of the devised bounds, the performance of (2.44) is compared against extensive Monte Carlo simulations for the link budget parameters tabulated in Table 2.2. The comparison of the analytical bound against the simulation results is depicted in Fig. 2.6, while the bound of (2.48) is plotted as well in Fig.2.6 for the sake of completeness.

Table 2.2: Link Budget Parameters

Parameter	**Value**	**Parameter**	**Value**
Noise Spect. Dens.	-174 dBm/Hz	P_{UE}	33 dBm
Noise Power	-104 dBm	P_{SC}	33 dBm
Path Loss at L_{ref}	25.6 dB	P_{MC}	53 dBm
α	1	BW	10 MHz
μ	$(0.01)^{0.25} = 0.3$	Path Loss Exp.	4

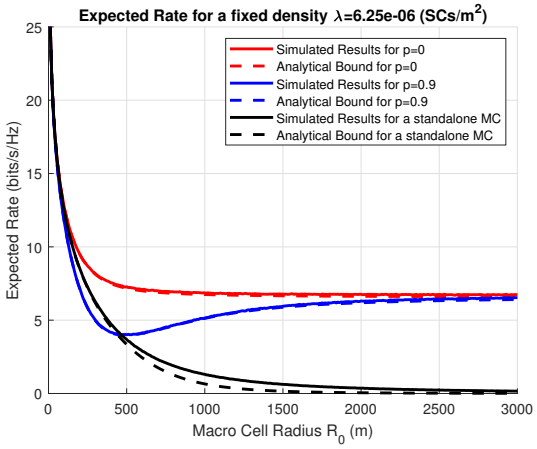

Figure 2.6: Expected UL rate vs macro cell radius.

For low values of R_0 (which correspond to a small MC coverage) the probability of a coupled association to the MC is high. Conversely, for high values of R_0 (which correspond to a large MC coverage) the probability of a coupled association to the SC is high. In those two cases the performance of a network able to support the decoupling ($p = 0$) and of a network that is unable to support it ($p = 0.9$) is identical. However, for the intermediate values of R_0 where the probability of a decoupled connection is high, the effect of the packet losses due to the synchronization of the acknowledgments becomes evident. Hence, the proposed bounds capture accurately the detrimental effect of synchronization in DUDe, while providing an extremely tight performance.

Summing up, we have provided tight and closed form rate bounds, which capture accurately both the performance of the system in terms of the instantaneous average UL ergodic rate, as well as the detrimental effect of the ACK synchronization in DUDe. This allows for quantifying the effect of the decoupling on the throughput and therefore on the the network performance in general. Moreover, the devised bounds provide an insight into the minimum degree of densification that guarantees meeting the QoS objectives.

The work presented above has been published in [34].

2.5 Downlink and Uplink Decoupling in 5G and Beyond: A Guide to Optimal Connectivity

Having defined the previous expressions for the noise limited operation of decoupled HetNets the present section focuses on DUDe and its applicability in 5G and beyond, employing the developed expressions for analyzing the performance of DUDe systems and optimizing their connectivity in the framework of a newly proposed flexible DUDe paradigm.

To elaborate, the framework proposed hereafter, attempts to facilitate the seamless integration of DUDe into 5G networks, which for the moment is hampered due to the increased network and architecture complexity of DUDe systems. To address this problem the present section performs a systematic study of the factors influencing the applicability of DUDe in 5G and proposes a flexible DUDe framework which allows for the application of DUDe to 5G and beyond. The proposed framework can adapt to the diverse requirements of 5G as well as the requirements of the software-controlled and software defined logical networks beyond 5G. The flexibility of the framework paves also the way for the introduction of hybrid cellular/WiFi DUDe schemes, able to exploit the unlicensed spectrum without degrading the performance of the incumbent Wi-Fi and cellular networks. This flexibility can also allow for the dynamic management of the UL connectivity toward macro cell (MC) off-loading and load balancing, exploiting the strong backhaul support that can be provided by the network's dark fiber.

In the direction of proposing the aforementioned flexible DUDe framework we commence the analysis by examining the 5G and beyond 5G ecosystems with respect to the applicability of DUDe in this newly shaped environment.

2.5.1 DUDe in 5G and Beyond

The advent of 5G networks has provided an extraordinary rate increase, through the employment of denser infrastructures, cooperating antenna elements and frequency bands in the mmWave range [1]. As 5G networks evolve, the achieved rate is expected to increase further, with the focus, however, being on high data rates for everyone, rather than providing extremely high data rates only to specific users under specific conditions [53]. The consistent connectivity for everyone constitutes one of the key challenges of 5G and beyond 5G (B5G) networks, in the pursuit of improved QoS. The impact of the latter on the QoS is demonstrated by the fact that even consumers, that seem unwilling to pay for higher data rates are interested in upgraded services with respect to improved coverage [53]. In the direction of obtaining the sought out ubiquitous connectivity, DUDe emerged, exploiting the ultra-dense network (UDN) architectures of 5G. DUDe can lead

to significant rate, power and particularly, outage gains, providing the desired improved connectivity [33].

Building upon the benefits arising from DUDe, the 3GPP initiative has already been engaged with the standardization of the decoupling of the UL and DL frequency bands. However, the actual implementation of DUDe through the connection to different BSs in the UL and the DL poses a great challenge, given the need for strong synchronization between the decoupled links [33]. In particular, the following sections will demonstrate that even though 5G can support this synchronization in the physical layer, the requirements of some of the 5G applications in higher layers (with respect to latency, mobility, etc.) cannot be supported by DUDe in practice. Hence, the application of DUDe to 5G networks cannot be achieved through a monolithic DUDe framework.

Moreover, a monolithic DUDe framework that cannot adapt dynamically to the network requirements would impose constraints on the flexible operation of the emerging software-controlled networks that employ software defined logical architectures [54]. In particular, the advent of networks, such as the envisaged B5G and 6G networks [55], is revolutionizing the entrenched network operation, providing additional pillars of flexibility that have already been manifested by the current networks that rely heavily on network softwarization.

To elaborate, current networks employ software defined networking for controlling the separated control and data planes. In addition, the advancements in edge computing have led to the employment of software defined infrastructure for the connection of low-cost hardware with distributed processing units through the fronthaul [56]. Such processing units allow for network operators to process the traffic information that has been aggregated, through data capture, at the core and at the access network segments in order to adjust the network operation.

Thus, networks can operate in a proactive and flexible manner with BSs that do not serve users entering into idle mode, minimizing energy consumption [57] and with excess resources being dedicated to different network slices [54]. Thus, resources are reallocated dynamically, reducing network CAPEX and OPEX by a factor of 5 compared to the 2010 levels, with a commensurable increase of the network efficiency [58]. This software-controlled operation paves also the way for the advent of the envisaged 6G smart radio ecosystems where even the propagation environments become software-reconfigurable entities, customizing the propagation of the radio waves [55].

In order to introduce the DUDe connectivity benefits into this new era a flexible DUDe framework needs to be devised. To this end, the present analysis surveys the factors hindering the application of DUDe to 5G and proposes a flexible DUDe framework that allows the application of DUDe to 5G and beyond. The proposed framework is application-centric and can, therefore, adjust to the diverse requirements of the 5G applications, while it can also be extended to the notion of sliced networks, adjusting to

the requirements of different software defined logical networks (i.e. network slices) [54]. Moreover, the proposed DUDe framework can improve the indoor connectivity and allow for efficient load balancing. In particular, the present analysis addresses the following questions:

- Can DUDe be seamlessly integrated into 5G and B5G networks supporting diverse services and accommodating different network slices?
- Can DUDe strategies be employed by hybrid cellular/Wi-Fi schemes towards improving indoor connectivity and exploiting the unlicensed spectrum?
- Can flexible DUDe schemes be employed to optimize the DL and UL connectivity with respect to load balancing, utilizing underused network resources?

DUDe and 5G architecture

The DUDe operation along with the benefits and disadvantages of the scheme have been discussed in detail in section 2.4.1 and presented graphically in Fig. 2.5. Building upon this detailed description we can proceed with examining the applicability of DUDe to 5G architectures.

The easiest way to implement a DUDe connectivity policy in 5G systems is through the separation of the control and data planes in the UL. Thus, in the case of a UE residing in region B of Fig. 2.5, the physical uplink shared channel (PUSCH), i.e. the channel carrying the data, is configured towards the SC, whereas the physical uplink control channel (PUCCH) is configured towards the MC. In this case the PUCCH provides also the hybrid automatic repeat request (HARQ) feedback (i.e. the ACK/NACK) to the MC and, thus, the acknowledgments do not need to travel through the backhaul.

This approach is similar to the dual connectivity scheme, since in both cases the MC serves as the anchor point. However, in DUDe the data is transmitted to the SC, whereas in the dual connectivity case, the data is received from the SC (after arriving there from the MC through a logical interface, i.e. X2 in LTE and Xn in 5G). Dual connectivity is already implemented in LTE advanced and, therefore, the proposed approach can be easily supported without additional standardization support. However, this approach practically negates the two strongest advantages of DUDe, i.e. the outage reduction and the interference mitigation. That is, since, due to the PUCCH, the UE still needs to transmit to the MC with its limited power even under unfavorable channel conditions, thus, diminishing the outage gain of DUDe. Moreover, due to the PUSCH, the streams of data transmitted simultaneously by different UE toward the SC create interference in the SC.

The aforementioned separation of the control and data plane, however, is not the only way to implement DUDe in 5G systems. In particular, given the increased flexibility of the HARQ timing in 5G, the system can tolerate higher HARQ latencies compared to

LTE. To elaborate, the HARQ process is a stop and wait (SAW) process that has to receive an ACK/NACK in order to be resumed. To minimize the effect of this inactive time on the throughput, sequential processes commence. Thus, while each process waits for an ACK/NACK, all other processes transmit also their requests. In LTE FDD the maximum number of processes is 8, however, the maximum number of HARQ processes in 5G is 16, allowing for a higher latency tolerance without HARQ stalling [59]. Moreover, as opposed to the synchronous UL HARQ of LTE, 5G employs an asynchronous HARQ both in the DL and the UL, allowing for HARQ processes to commence in a non-sequential order, and, therefore, manage their inactive time more efficiently. In addition, the HARQ latency depends also on the load (and time sharing between users), the time division duplex (TDD) scheme employed (if any) and the 5G numerology (defining the slot length within each subframe). The first two factors are not system specific, however, the flexibility of the numerology in 5G provides additional leeway compared to LTE [59]. All of the above factors give rise to an extremely adaptable environment able to accommodate the latency introduced by the decoupling of the ACKs in the physical layer.

However, the "bottleneck" of the performance of DUDe does not lie in the physical layer, but in higher layers. In legacy systems, each application, operating on top of the network infrastructure, sets its own timeout requirements. With the advent of network slicing, these requirements have been formalized in the form of vertical services (i.e. network slices) [54]. 5G has introduced services, such as the ultra-reliable low latency communications (URLLC) of 1ms end-to-end latency and 99.999% reliability, which DUDe cannot support easily in practice. The general framework shaped by the 5G vertical services with respect to their requirements is outlined hereafter. In this course, three real-life use cases are presented, which are characterized by numerous and disparate requirements, demonstrating the multidimensionality of the emerging architectures to which DUDe needs to adapt.

2.5.2 Software-controlled networks & 5G vertical services

In order to demonstrate the disparity of the 5G vertical services that a DUDe enabled network needs to support, three real 5G use cases, developed within the framework of the 5G-PPP infrastructure project, 5G EVE [60], are presented. Each use case is described by the respective radar chart in order to highlight the requirements of each service.

The first use case, implemented in practice by Ericsson, pertains to the centralized wireless control of automated guided vehicles in manufacturing environments by an artificial intelligence entity. The second use case, implemented in practice by Wind, focuses on the wireless ultra-fast and ultra-reliable fault management of distributed electricity generation (e.g. renewable sources) in smart grids. The third use case, implemented in practice by Trenitalia, focuses on smart railways, adapting to train and passenger

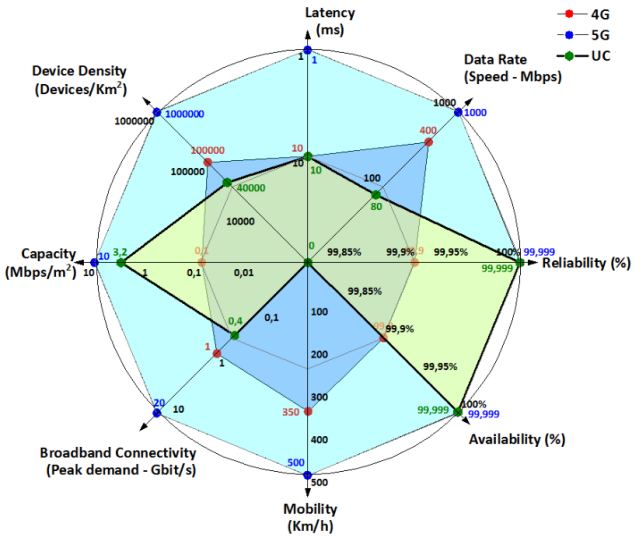

Figure 2.7: 4G(red) / 5G(blue) capabilities versus Use Case requirements (green) for the Ericsson use case.

mobility patterns while providing high quality video streaming to high speed trains. The respective radar charts of each of the three cases are presented in Fig. 2.7-2.9.

These use cases are not hypothetical, but genuine use cases, implemented and validated within the framework of a European platform comprising numerous vertical industries. Hence, the requirements specified by the radar charts of Fig. 2.7-2.9 constitute the actual 5G requirements that DUDe needs to support. The support of requirements, such as the 1ms latency and the 300km/h mobility of Fig. 2.7-2.9, poses a great technological challenge even without the application of DUDe, which, as already mentioned in the previous section, affects decisively the latency and the mobility capabilities of the network. Moreover, aspects such as the reliability and availability could also be influenced by the ability of DUDe to provide strong synchronization through the backhaul.

It can, therefore, be deduced that a monolithic application of DUDe to 5G cannot support all of the above vertical services. However, the wide range of the requirements of Fig. 2.7-2.9, (e.g. mobility of 0-300km/h and latency of 1-10ms) demonstrates that DUDe can support some of these 5G services. Hence, the application of DUDe in 5G is preconditioned on the existence of a criterion evaluating the applicability of DUDe to each service and on a framework allowing its flexible application thereafter.

2.5.3 DUDe & 5G vertical services

As already stressed, the effect of DUDe on the performance of the 5G vertical services (i.e. network slices) is multidimensional. However, if the application of DUDe to a slice

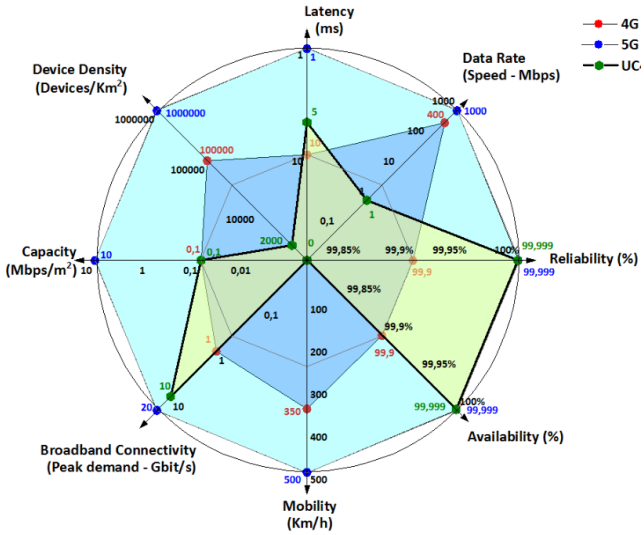

Figure 2.8: 4G(red) / 5G(blue) capabilities versus Use Case requirements (green) for the Wind use case.

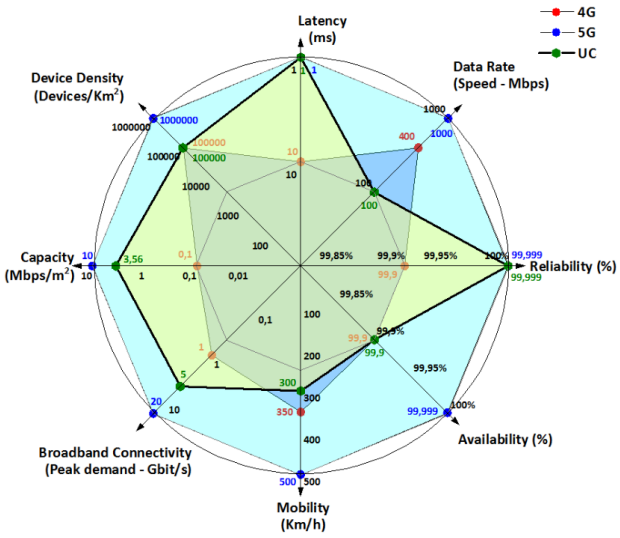

Figure 2.9: 4G(red) / 5G(blue) capabilities versus Use Case requirements (green) for the Trenitalia use case.

results in the loss of a packet, the network is agnostic to the reason why the packet is lost. Regardless of the reason, the detrimental effect of the decoupled acknowledgements on each slice can be quantified by the ACK failure probability p of section 2.4.2. This probability can be measured by the network and provided as an intrinsic feature of each slice.

Employing p, the performance of a DUDe enabled system can be quantified by means of the UL ergodic rate. Thus, the UL rate of a UE residing in region B of Fig. 2.5 is scaled down by p and, implicitly, the average UL rate of the whole coverage of Fig. 2.5 is also affected by p. In order to quantify the effect of p on the network UL rate, the closed form expressions for the UL ergodic rate developed in section 2.4.3 are employed. In particular, expressions (2.44)-(2.47) quantify the UL ergodic rate in a DUDe enabled system, as a function of p.

Employing these expressions developed above and presented in Fig. 2.6, we quantify the performances of a DUDe enabled system for different values of p and compare them against the performance of a coupled system in Fig. 2.10. The comparison is made with respect to the expected UL rate with the latter depending on the radius of the MC coverage, as already explained in the previous section. In particular, we remind the reader, that the low values of the MC radius indicate a high chance for a coupled association to the MC and the high values of the MC radius indicate a high chance for a coupled association to the SC. This is why the DUDe enabled system converges to the coupled system for low and high values of the MC radius. The intermediate values, on the other hand, correspond to a configuration where decoupled connections are more likely to be established. In this intermediate interval, a network not losing decoupled ACKs ($p = 0$), due to the slice requirements, can support successfully a decoupled connection, whereas a network unable to meet the requirements ($p = 0.9$) performs even worse than the conventional coupled system. This means that, for p=0.9, the loss of packets in higher layers outweighs the gain emerging in the physical layer from the reduced pathloss.

Evidently, a DUDe connectivity approach, performing worse than a conventional coupled system, needs to be revisited in order to give rise to a flexible DUDe connectivity able to adapt to the diverse service requirements of 5G.

2.5.4 Flexible DUDe Connectivity

The previous analysis demonstrated that, as p increases, the loss of packets in higher layers gradually outweighs the DUDe path-loss gain in the physical layer. Hence, the successful application of DUDe depends on the efficient management of this trade-off. To this end, as p increases the number of decoupled connections should decrease and this can be achieved in practice if the UL connectivity frontier of Fig. 2.5 starts contracting inwards (towards the DL connectivity frontier) monotonically with the increase of p. This dynamic expansion and contraction of the UL connectivity frontier within the range of

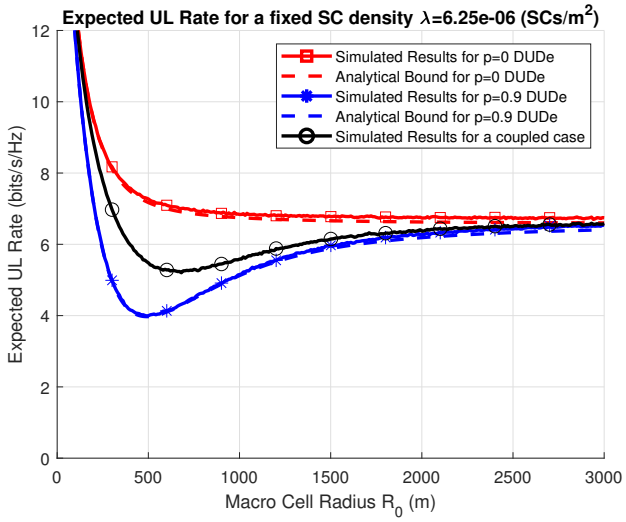

Figure 2.10: Expected UL rate for a coupled system and for a DUDe enabled system, losing packets due to the requirements of the slice ($p = 0.9$) and not losing packets due to the requirements of the slice ($p = 0$). The rate depends on the MC radius.

connectivity region B can be achieved by the introduction of an appropriate weighting factor α ($\mu \leq \alpha \leq 1$), as described in the previous section. Thus, the UL connectivity frontier of Fig. 2.5 is defined at $d_{SC} = \alpha d_{MC}$ and the adjustment factor α can be dynamically optimized in response to p. This allows for a flexible DUDe connection that for $\alpha = 1$ coincides with the standard DUDe of Fig. 2.5 and for $\alpha = \mu$ coincides with the coupled case, thus canceling the application of DUDe if the service requirements cannot be supported.

Even after the introduction of the adjustment factor α, the decision concerning the UL connectivity is still made based on the distances d_{SC} and d_{MC}. Thus, if a system entity can provide an optimized value of α based on p, the optimization of the UL connectivity can be provided as an intrinsic feature of the DUDe scheme without any additional standardization support.

The effect of this dynamic adjustment of α on DUDe operation and connectivity becomes evident in Fig. 2.11-2.13, where the DL and UL connectivity regions of a MC and three SCs are depicted for a coupled, a DUDe and an optimized DUDe system. The depiction of the DL and UL connectivity regions demonstrate vividly the potential benefits arising from the application of DUDe over conventional coupled systems, and the adding up benefits arising from the application of an optimized DUDe over DUDe.

Specifically, Fig. 2.11 depicts the DL connectivity regions, which are the same in all three systems (i.e. coupled, DUDe and optimized DUDe). The DL connectivity regions of Fig. 2.11 constitute also the UL connectivity regions of a coupled system. These

regions are defined by the level of the received power from each BS. Fig. 2.12 depicts the UL connectivity regions of a DUDe enabled system, defined by the distance to the closest BS. Hence, Fig. 2.12 constitutes a Voronoi diagram partitioning the plane into regions based on the distance to the closest BS.

These first two plots provide significant insight into the benefits of DUDe over a coupled association policy. Indicatively, user O(650,650) connects in Fig. 2.11 to the MC in the UL, experiencing a significant path-loss, while acting as a source of principal interference to SC1. As opposed to this connectivity policy, a more sensible approach is followed in the DUDe system of Fig. 2.12, where the user connects to the neighboring SC, thus mitigating the adverse effects of the coupled connectivity.

This favorable connectivity policy of user O is retained in Fig.2.13, where the UL connectivity regions of an optimized DUDe system are depicted for an optimized weighting factor $\alpha = 0.8$. Hence, the benefits of DUDe over a coupled system are retained, while the additional benefits of this approach over DUDe are highlighted by the connectivity policy of user X(-700,400). User X employs a decoupled policy in Fig. 2.12, whereas he employs a coupled policy in the MC in the optimized DUDe system of Fig. 2.13. The reason for that is that the user's position, close to the UL connectivity frontier in Fig. 2.12, entails only a minimal path loss gain from the decoupling. However, if the packet loss from the decoupling is substantial in higher layers, user X does not follow a decoupled connection in the optimized DUDe system of Fig. 2.13.

The feasibility of this approach relies heavily on the optimization of the weighting factor α. In the case of a DUDe deployment with multiple radio units with a different cell-ID connected to a centralized node (as in the case of a cloud RAN, C-RAN) [33], α can be optimized at the centralized node and broadcasted to all connected radio units without the need for any additional standardization support. The optimization of α can be performed by the network at each slice and for each value of p.

As a proof of concept, the optimization of p with respect to the UL rate has been performed based on the expressions (2.44)-(2.47) and presented in Fig. 2.14. Fig. 2.14 demonstrates the performance of DUDe and of an optimized DUDe system for p=0.1, p=0.5 and p=0.9. Evidently, the optimized system (dashed lines) always outperforms the non-optimized DUDe system (solid lines). The performance gain of the optimized DUDe over DUDe increases with p, since for small values of p the system is not in need of optimization. More importantly, the optimized system performs at least as good as the coupled system even under a severe ACK failure regime, rendering the performance of the optimized DUDe system superior to that of a coupled system in every setting. Thus, the proposed scheme gives rise to a flexible DUDe framework that can be applied to all emerging 5G slices, without any negative, but with only positive, impact on the system performance.

Furthermore, from an implementation perspective, the proposed scheme is not dis-

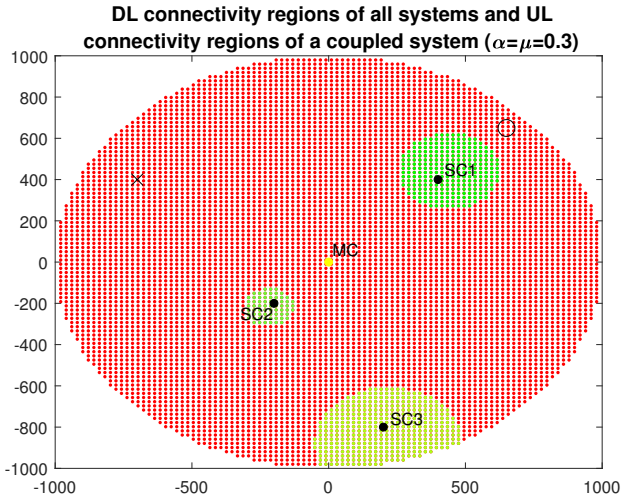

Figure 2.11: DL connectivity regions of all systems, UL connectivity regions of a coupled system. The red area indicates the connectivity region of the MC BS which is positioned in the middle of the figure, whereas the green areas represent the connectivity regions of the SC BSs. The difference between the transmit power of the assumed MC and the SCs is 20dB and the path loss exponent is equal to 4 (i.e. $\mu = 0.01^{0.25} = 0.3$). Users X(-700,400) and O(650,650) are indicatively selected.

ruptive to the entrenched DUDe and network slicing architectures. Each slice must just be aware of its ACK failure probability p and the respective optimized weighting factor α. Then, every slice follows the optimized DUDe connection of Fig. 2.11-2.13 for the respective value of α.

2.5.5 Flexible DUDe and unlicensed spectrum

The rate and broadband connectivity requirements of 5G, presented in Fig. 2.7-2.9, and the scarcity of the available spectrum has pushed operators in the direction of exploiting the potential of the unlicensed spectrum. In this direction, technologies such as LTE-U, 5G New Radio-U and MulteFire have emerged, allowing operators to use the unlicensed spectrum. However, the key technology in the unlicensed spectrum is Wi-Fi, which continues to evolve through the new 802.11ax and 802.11ay standards.

The dominant role of Wi-Fi has motivated operators to exploit the operator-owned and installed Wi-Fi access points (APs) to aggregate licensed and unlicensed spectrum, while the cellular APs act as the anchor point for seamless mobility. In addition, attempts such as Fon [61] provide a global Wi-Fi network allowing users to register and share their Wi-Fi APs with other registered users across the globe. In this setup, Wi-Fi plays an

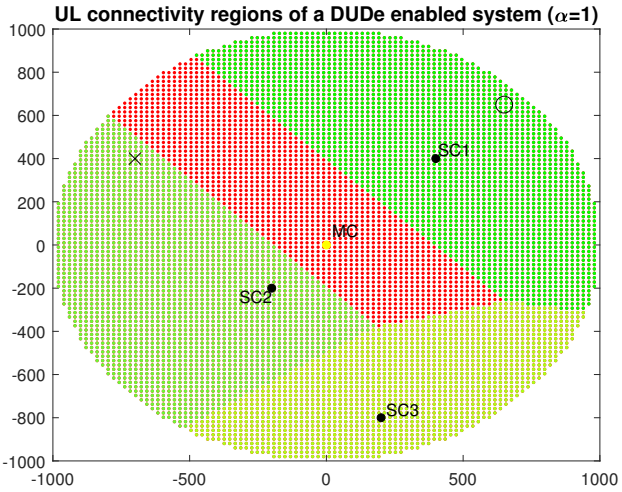

Figure 2.12: UL connectivity regions of a DUDe enabled system.

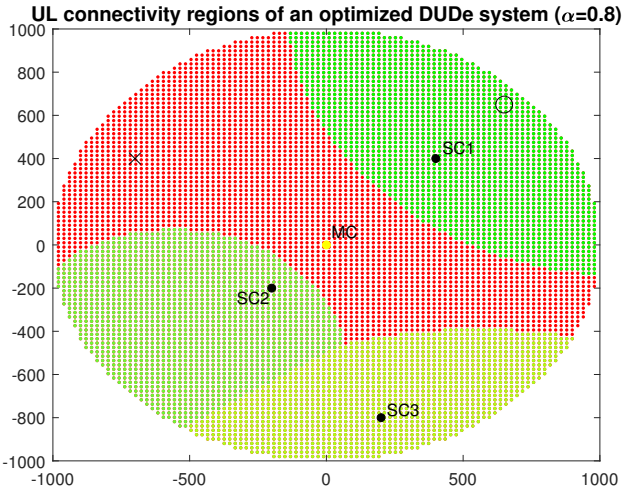

Figure 2.13: UL connectivity regions of an optimized DUDe system (bottom).

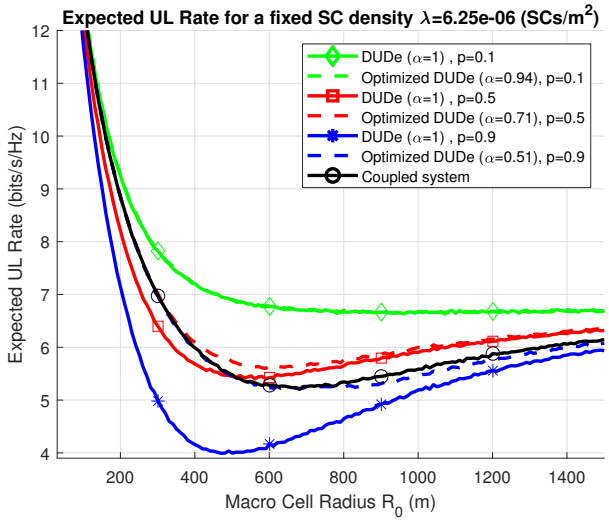

Figure 2.14: Expected UL rate after optimizing the weighting factor α with respect to the ACK failure probability. The weighting factor α has been optimized for MCs of different MC radius for p=0.1, p=0.5 and p=0.9.

auxiliary role to LTE with users connecting to adjacent Fon APs to offload traffic or boost connectivity (particularly, in indoor environments) and return to the LTE network after leaving the Wi-Fi coverage. Such commensal approaches increasingly attract the interest of consumers, with traffic through Fon APs in OTE's network increasing by 40% per year.

The advent of DUDe, however, gives rise to more disruptive hybrid cellular/Wi-Fi approaches that can upgrade the joint performance of the network without degrading the performance of the incumbent Wi-Fi and cellular networks. In particular, focusing on the performance of Wi-Fi, it can be noted that its "bottleneck", in the fully loaded case, lies in the UL due to the contention of users that have to listen before transmitting (LBT). In this setup, DUDe allows the connection to the Wi-Fi AP in the DL to exploit the Wi-Fi bandwidth and to the LTE AP in the UL to exploit the scheduler of LTE. This technique engenders substantial rate gains for Wi-Fi [62] and has already been included in the 3GPP LWIP Release 13.

Similar approaches could also be employed to upgrade the performance of cellular networks with UE connecting to LTE in the DL and to Wi-Fi AP in the UL. Given the ubiquity of Wi-Fi, this can enhance the outdoor and, particularly, the indoor connectivity substantially. Moreover, the flexible DUDe framework presented above guarantees that the employment of such DUDe hybrid schemes will not degrade the cellular performance even in 5G architectures, allowing for the formation of hybrid 5G/Wi-Fi paradigms able to integrate Wi-Fi into the 5G ecosystem.

2.5.6 Load balancing, capitalizing on dark fiber

DUDe and the connection to adjacent SCs rather than the MC in the UL can allow for effective load balancing and MC offloading. This effect of DUDe becomes evident by the connectivity regions of Fig. 2.11-2.13. Given the expected volume of data in 5G, the offloading of MCs can be proven instrumental for the operation of 5G networks. In this course, the flexible DUDe approach can be employed to provide strong backhaul support by steering the offloaded MC traffic to fiber connected SCs.

In particular, all operators own a high percentage of dark (i.e. unused) fiber, with a rough estimate in OTE's network giving a percentage of 75%, which is expected to be reduced to 65% as more customers request fiber to the home services. In order to exploit this unused infrastructure, low-cost APs can be installed at the end points of the deployed dark fiber. In particular, multiple APs can be installed within a radius or elevation of 250m around the end point of the fiber by exploiting G.fast [63]. G.fast provides aggregate (upstream and downstream) data rates of up to 1 Gb/s over copper, over distances of up to 250m. Moreover, the upstream and downstream spectrum can be allotted at will, allowing for fully supporting the UL traffic offloaded through the SCs.

In this setup, SCs of strong backhaul support can emerge and the aforementioned flexible DUDe can steer UL traffic in their direction through the dynamic adjustment of the UL connectivity frontier.

2.6 Conclusions

The present analysis has performed a systematic study of the factors influencing the applicability of DUDe in 5G architectures. This gave rise to a flexible DUDe framework allowing for the application of DUDe in 5G and B5G software-controlled networks supporting different vertical services. Moreover, the proposed framework allows for the integration of Wi-Fi into the 5G ecosystem through DUDe connectivity schemes and for strong backhaul support through the exploitation of dark fiber.

Chapter 3

Interference-limited Analysis of Poisson Cellular Networks

Having derived simple expressions for the ergodic rate under a noise limited regime and having built upon them to propose a flexible DUDe framework, we can proceed with the analysis of UDNs taking also the network interference into account. The spatial distribution of the interferers in the DL follows a homogeneous Poisson point process (PPP), whereas in the UL it follows a non-homogeneous PPP [18]. Since the objective of the present thesis is the derivation of closed-form approximations that were not available hitherto, the analysis commences from the more tractable homogeneous PPPs and the extension to the non-homogeneous case remains to be addressed in future work. Hence, the present chapter provides closed form expressions for the DL ergodic rate.

The network is assumed to be ultra dense and, therefore, operating under an interference limited regime. Moreover, as explained in section 1.1 the density of the network is assumed to have moved BSs on the user level, thus counteracting LOS-interference. The expressions account for networks comprising more users than BSs, as well as networks comprising more BSs than users. In the latter case, the DL rate is associated by a closed form expression to the density of BSs and of users allowing for the investigation of complex optimization problems like the one mentioned in Section 1.2, on the dynamic clustering of users under active BSs. Last but not least, in the direction of obtaining the aforementioned expressions, an extremely accurate and simple approximation of the MGF of the aggregate other-cell interference in the DL is provided. In the existing literature, the complexity of the exact MGF imposed inherent limitations on the extension of the stochastic geometry analysis to complex optimization problems. However, the present chapter lifts these inherent limitations by introducing a simple, albeit extremely accurate expression for the MGF of the other cell interference.

3.1 The Wireless Cellular Network

The previous chapter focused on the noise-limited operation of mmWave SCs which cannot provide wide coverage due to the effect of blocking in this frequency. This imposed the employment of a HetNet with sub 6GHz MCs providing the coverage the mmWave SCs could not provide. However, the present analysis assumes only one tier of sub 6GHz SCs that can provide consistent connectivity over the whole network coverage.

The wireless cellular system considered, comprises a set of BSs, denoted by BS_i, whose positions $x_i \in \mathbb{R}^2$ follow a spatial distribution given by a homogeneous PPP Ψ of density λ (BSs/m^2). Moreover, the positions of the overlaid user equipment (UE) follow also a spatial distribution given by a homogeneous PPP Φ of density λ_{UE} (UE/m^2). The reference UE, denoted by UE_0, is located at the origin and is served by its closest BS, denoted by BS_0. The UE adjoined at the origin can be singled out and the location of the other UE follows the reduced Palm distribution of Φ, which is the same as the original distribution Φ (as stated by Slivnyaks theorem [35]). Hence, adjoining UE_0 at the origin does not change the distribution of Φ.

For the sake of simplicity in the notation, it is assumed that all UE and BSs are equipped with one antenna and all BSs transmit at the same power level. Intra cell users are assumed to be sharing orthogonal resources, as it is typically the case in the literature [7], whereas all BSs use the same frequency band. If not explicitly mentioned otherwise (as will be done in the following sections), it is assumed that the network comprises significantly more users than BSs (i.e. $\lambda_{UE} \gg \lambda$). As a result, every BS is active and transmitting, acting as an interferer in the DL. The other-cell interference in the DL is mathematically defined as the interference coming from all BSs residing at a distance $||x_i||$ from the origin greater than the distance $||x_0||$ of BS_0 from the origin, where $||\cdot||$ denotes the l^2-norm. Note that the origin is where the reference UE UE_0 is located. Last but not least, a single-slope unbounded path-loss model is assumed in the analysis.

The considered scenario is depicted in Figure 3.1. UE_0 is marked by the magenta diamond, BS_0 by the magenta circle and the intra cell users are depicted in red. The interfering BSs are depicted in black and reside in distances ($||x_i|| > ||x_0||$), where the circle of radius $||x_0||$ around UE_0 is depicted in green. Every BS residing in the region outside this circle is acting as an interferer in the DL.

3.2 MGF of the Aggregate Other-cell Interference

Having presented the considered network scenario and having defined the set of interfering BSs by means of their distance to the origin, we can proceed with the mathematical formulation of the aggregate other-cell interference and the MGF of the latter.

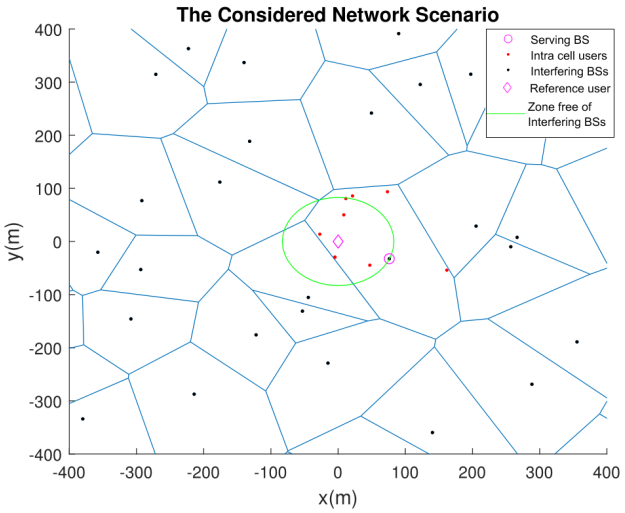

Figure 3.1: The considered network scenario.

3.2.1 Derivation of the MGF

The aggregate other-cell interference in the DL is mathematically formulated as follows:

$$g = \sum_{\substack{x \in \Psi, \\ x \neq x_0}} \frac{P_{tx}}{\kappa \left\| x \right\|^{\beta}}, \tag{3.1}$$

where P_{tx} denotes the transmit power of the BSs, β the path-loss exponent, $\|x\|$ the distance of the interferer to the origin and κ the path-loss at a reference distance of 1 meter.

Although a term of fast fading, denoted by $\left|h^{(x)}\right|^2$, is present at the propagation, it has not been introduced in the previous expression (3.1). The reason for that is that taking into account the fast fading of the interferers during the computation of the UE rate would implicitly mean that the UE has perfect knowledge of the channel of all interferers. However, since this is not the case in practice, averaging over this fading would provide an upper bound for the rate. As opposed to that, the omission of the fast fading $\left|h^{(x)}\right|^2$ provides a lower bound for the rate [17]. Since a worst case scenario analysis is more sensible than an overoptimistic calculation of the achievable rate, the fast fading of the interferers is not introduced. However, if accounting for the fast fading is of interest, this can be done without increasing significantly the complexity of the presented analysis as will be demonstrated in Section 3.2.3.

The set of interfering BSs in (3.1) has been defined by means of their distances to the origin, i.e. $\|x_i\| > \|x_0\|$. Equivalently, by defining the path-loss as follows:

$$L^{(x)} = \kappa \left\| x \right\|^{\beta}, \tag{3.2}$$

the set of interfering BSs can be defined by means of their path-loss to the origin (i.e. $L^{(x)} > L^{(0)}$, where $L^{(0)} = L^{(x_0)}$ for brevity in the notation). Having defined mathematically the set of interfering BSs, the MGF of g can be obtained by employing the probability generating fuctional (PGFL) theorem according to which [4]:

$$\begin{aligned}\mathbb{E}\left\{\prod_{x\in\Psi} f(x)\right\} &\overset{(a)}{=} \exp\left(-\lambda\int_{\mathbb{R}^2}(1-f(x))\,dx\right)\\ &\overset{(b)}{=} \exp\left(\int_{\mathbb{R}}(f(r)-1)\,2\pi\lambda r dr\right)\\ &\overset{(c)}{=} \exp\left(\int_{\mathbb{R}}(f(r)-1)\,\frac{2\pi\lambda}{\beta}\left(\frac{1}{\kappa}\right)^{\frac{2}{\beta}} y^{\frac{2}{\beta}-1}dy\right),\end{aligned} \tag{3.3}$$

where (3.3b) is obtained by computing the double integral of (3.3a) in polar coordinates for $0 \le \theta \le 2\pi$ and for $r = \|x\|$, and (3.3c) is obtained by changing the variable of the integration to the path-loss according to (3.2). Hence, employing (3.3c) the MGF of g is given by [36]:

$$\begin{aligned}M_g\left(s; L^{(0)}\right) &= \mathbb{E}_\Psi\left\{\exp\left(-sg\right)\right\}\\ &= \mathbb{E}_\Psi\left\{\exp\left(-s\sum_{x\in\Psi}\frac{P_{\text{tx}}}{L^{(x)}}\,\mathbf{1}\left(L^{(x)} > L^{(0)}\right)\right)\right\}\\ &= \mathbb{E}_\Psi\left\{\prod_{x\in\Psi}\exp\left(-s\frac{P_{\text{tx}}}{L^{(x)}}\,\mathbf{1}\left(L^{(x)} > L^{(0)}\right)\right)\right\}\\ &\overset{(a)}{=} \exp\left(\int_{L^{(0)}}^{\infty}\left(\exp\left(-s\frac{P_{\text{tx}}}{y}\right)-1\right)\frac{2\pi\lambda}{\beta}\left(\frac{1}{\kappa}\right)^{\frac{2}{\beta}} y^{\frac{2}{\beta}-1}dy\right)\\ &\overset{(b)}{=} \exp\left(\pi\lambda\left(\frac{L^{(0)}}{\kappa}\right)^{\frac{2}{\beta}}\left(1-{}_1F_1\left(-\frac{2}{\beta},1-\frac{2}{\beta},\frac{-sP_{\text{tx}}}{L^{(0)}}\right)\right)\right),\\ &s\in\mathbb{R},\end{aligned} \tag{3.4}$$

where the second argument of $M_g\left(s; L^{(0)}\right)$ denotes the dependence of the MGF on the random variable $L^{(0)}$ and $\mathbf{1}(\cdot)$ is the indicator function. (a) holds by employing (3.3c), and (b) is attained by using the result of [37] according to which:

$$I = \int_a^{\infty}\left(\exp\left(\frac{b}{z}\right)-1\right)z^{v-1}dz = \frac{1}{v}a^v\left(1-{}_1F_1\left(-v,1-v,\frac{b}{a}\right)\right), \tag{3.5}$$

with ${}_1F_1(a,b,z)$ being the Kummer confluent hypergeometric function given by:

$${}_1F_1(a,b,z) = \sum_{k=0}^{\infty}\frac{(a)_k z^k}{(b)_k k!}, \tag{3.6}$$

where $(\cdot)_k$ denotes the Pochhammer function given by:

$$(x)_k = \prod_{n=0}^{k-1}(x+n). \tag{3.7}$$

The definitions of (3.6) and (3.7) demonstrate the intractability of (3.4b). Since the derivation of the MGF of the aggregate interference is one of the fundamental tools of stochastic geometry, the intractability of (3.4b) propagates to every analysis employing the MGF, hindering the derivation of closed form figures of merit.

3.2.2 MGF Approximation

In order to overcome the limitations imposed by (3.4b), the present analysis introduces a simple, albeit extremely accurate, approximation of the MGF by introducing an alternative calculation of (3.4a). In this course, the MGF is derived as follows:

$$\begin{aligned}
M_g\left(s; L^{(0)}\right) &\overset{(a)}{=} \exp\left(\int_{L^{(0)}}^{\infty}\left(\exp\left(-s\frac{P_{\text{tx}}}{y}\right)-1\right)\frac{2\pi\lambda}{\beta}\left(\frac{1}{\kappa}\right)^{\frac{2}{\beta}} y^{\frac{2}{\beta}-1}dy\right)\\
&\overset{(b)}{=} \exp\left(\int_{L^{(0)}}^{\infty}\left(\sum_{n=1}^{\infty}\frac{1}{n!}\left(-s\frac{P_{\text{tx}}}{y}\right)^n\right)\frac{2\pi\lambda}{\beta}\left(\frac{1}{\kappa}\right)^{\frac{2}{\beta}} y^{\frac{2}{\beta}-1}dy\right)\\
&\overset{(c)}{=} \exp\left(\frac{2\pi\lambda}{\beta}\left(\frac{L^{(0)}}{\kappa}\right)^{\frac{2}{\beta}}\left(\sum_{n=1}^{\infty}\frac{(-1)^{n+1}(sP_{\text{tx}})^n}{\left(L^{(0)}\right)^n n!(\frac{2}{\beta}-n)}\right)\right)\\
&\overset{(d)}{=} \exp\left(-\pi\lambda\left(\tfrac{L^{(0)}}{\kappa}\right)^{\frac{2}{\beta}}\left(\exp\left(\tfrac{-sP_{\text{tx}}}{L^{(0)}}\right)-1+\left(\tfrac{sP_{\text{tx}}}{L^{(0)}}\right)^{\frac{2}{\beta}}\Gamma\left(1-\tfrac{2}{\beta},0,\tfrac{sP_{\text{tx}}}{L^{(0)}}\right)\right)\right)\\
&\overset{(e)}{=} \exp\left(-\pi\lambda\left(\tfrac{L^{(0)}}{\kappa}\right)^{\frac{2}{\beta}}\left(\exp\left(\tfrac{-sP_{\text{tx}}}{L^{(0)}}\right)-1+\left(\tfrac{sP_{\text{tx}}}{L^{(0)}}\right)^{\frac{2}{\beta}}\int_0^{\frac{sP_{\text{tx}}}{L^{(0)}}} t^{-\frac{2}{\beta}}\exp(-t)dt\right)\right),
\end{aligned} \tag{3.8}$$

where (b) holds by employing the Taylor expansion of the exponential term, (c) holds by a simple calculation of the integral, and (d) and (e) are obtained from the definition of the generalized incomplete gamma function $\Gamma(\cdot,\cdot,\cdot)$.

Having defined (3.8e), it can be noted that the term within the integral of (3.8e) eventually tends to 0. When this happens, namely when $\exp\left(\frac{-sP_{\text{tx}}}{L^{(0)}}\right) \approx 0$, the integral converges to a constant value. Hence, (3.8e) can be approximated by a piecewise function, involving a constant value when $\exp\left(\frac{-sP_{\text{tx}}}{L^{(0)}}\right) \approx 0$ and a varying function when $\exp\left(\frac{-sP_{\text{tx}}}{L^{(0)}}\right) \neq 0$.

In particular, by employing the constant value to which the integral converges when $\exp\left(\frac{-sP_{\text{tx}}}{L^{(0)}}\right) \approx 0$, it holds that:

$$\exp\left(\frac{-sP_{\text{tx}}}{L^{(0)}}\right)-1+\left(\frac{sP_{\text{tx}}}{L^{(0)}}\right)^{\frac{2}{\beta}}\int_0^{\frac{sP_{\text{tx}}}{L^{(0)}}} t^{-\frac{2}{\beta}}\exp(-t)dt \overset{\left(\exp\left(\frac{-sP_{\text{tx}}}{L^{(0)}}\right)\approx 0\right)}{\approx} \left(\frac{sP_{\text{tx}}}{L^{(0)}}\right)^{\frac{2}{\beta}}\Gamma\left(1-\frac{2}{\beta}\right)-1 \tag{3.9}$$

and when $\exp\left(\frac{-sP_{\text{tx}}}{L^{(0)}}\right)\neq 0$, (3.8e) can be approximated by the Taylor expansion around 0 as follows:

$$\exp\left(\frac{-sP_{\text{tx}}}{L^{(0)}}\right)-1+\left(\frac{sP_{\text{tx}}}{L^{(0)}}\right)^{\frac{2}{\beta}}\int_0^{\frac{sP_{\text{tx}}}{L^{(0)}}} t^{-\frac{2}{\beta}}\exp(-t)dt=\sum_{n=1}^{\infty}\frac{-2(-sP_{\text{tx}})^n}{\left(L^{(0)}\right)^n n!(n\beta-2)}. \tag{3.10}$$

Thus, by combining (3.9) and (3.10), (3.8e) can be approximated as follows:

$$M_g\left(s;L^{(0)}\right)\approx \begin{cases}\exp\left(\pi\lambda\left(\frac{L^{(0)}}{\kappa}\right)^{\frac{2}{\beta}}\sum_{n=1}^{\infty}\frac{2(-sP_{\text{tx}})^n}{\left(L^{(0)}\right)^n n!(n\beta-2)}\right), & \frac{sP_{\text{tx}}}{L^{(0)}}\leq c,\\ \exp\left(\pi\lambda\left(\frac{L^{(0)}}{\kappa}\right)^{\frac{2}{\beta}}\left(-\left(\frac{sP_{\text{tx}}}{L^{(0)}}\right)^{\frac{2}{\beta}}\Gamma\left(1-\frac{2}{\beta}\right)+1\right)\right), & \frac{sP_{\text{tx}}}{L^{(0)}}>c\end{cases} \tag{3.11}$$

and by employing only the first two terms of the Taylor expansion, (3.11) can be approximated by:

$$M_g\left(s;L^{(0)}\right)\approx \begin{cases}\exp\left(\pi\lambda\left(\frac{L^{(0)}}{\kappa}\right)^{\frac{2}{\beta}}\left(\frac{-2}{(\beta-2)}\frac{sP_{\text{tx}}}{L^{(0)}}+\frac{1}{2\beta-2}\left(\frac{sP_{\text{tx}}}{L^{(0)}}\right)^2\right)\right), & \frac{sP_{\text{tx}}}{L^{(0)}}\leq c\\ \exp\left(\pi\lambda\left(\frac{L^{(0)}}{\kappa}\right)^{\frac{2}{\beta}}\left(-\left(\frac{sP_{\text{tx}}}{L^{(0)}}\right)^{\frac{2}{\beta}}\Gamma\left(1-\frac{2}{\beta}\right)+1\right)\right), & \frac{sP_{\text{tx}}}{L^{(0)}}>c\end{cases} \tag{3.12}$$

where c is a constant indicating the point after which the integral of (3.8e) converges to a constant value. c can be computed as the point of intersection of the two functions of (3.12) and can be obtained by solving the following equation:

$$\frac{-2c}{\beta-2}+\frac{c^2}{2\beta-2}=-c^{\frac{2}{\beta}}\Gamma\left(1-\frac{2}{\beta}\right)+1. \tag{3.13}$$

Although, (3.13) cannot be solved analytically, for the limited range of the path loss exponent β (i.e. $\beta\in[2,5]$) it can be computed numerically and the value of c for any value of $\beta\in[2,5]$ can be approximated by:

$$c\approx 0.06662\log(\beta-1.528)+1.227. \tag{3.14}$$

The employment of the Taylor expansion and of the exact value of the generalized incomplete function $\Gamma(\cdot,\cdot,\cdot)$ at the extreme cases guarantees the tightness of the approximation far from the intersection point c. However, the tightness of the proposed approximation still needs to be verified close to c. In this course, relevant figures will be provided in the following sections validating the tightness of the approximation close

to c against the exact result of (3.4b). Given the dependence of c on β, the provided figures will demonstrate the tightness of the proposed approximation in the whole range of $\beta \in [2, 5]$, which is also the range of interest in wireless networks. It should also be noted that the value of λ does not have any impact on the tightness of the approximation since the term of (3.8e) that has been approximated by (3.9) and (3.10) does not involve λ. Therefore, the proposed approximation of (3.12) is far more tractable and simple than (3.4b), but also accurate over the whole range of values that are of interest in wireless networks.

3.2.3 Fast Fading of Interferers

The aforementioned analysis can be easily extended to account also for the fast fading of the interferers, if the latter is of interest. In this course, an independently marked point process can be employed, that is, a point process where a random variable, known as mark and denoted by M_x, is randomly assigned to each random point of the point process x [4]. The marks are mutually independent and the conditional distribution of mark $M_x \in \mathbb{R}^l$ of a point $x \in \Psi$ depends only on the location of x. For an independently marked homogeneous PPP with density λ on $\mathbb{R}^2$ and marks with distribution $F_x(dM)$ on $\mathbb{R}^l$, the Laplace transform of a function $f(x, M_x)$ is given by [38]:

$$\begin{aligned}\mathcal{L}_\Psi(f) &= \mathbb{E}\left\{\exp(-\sum_{x\in\Psi} f(x, M_x))\right\} \\ &= \exp\left(-\lambda\int_{\mathbb{R}^2}\left(1 - \int_{\mathbb{R}^l}\exp\left(-f(x, M_x)\right) F_x(dM)\right)\right). \end{aligned} \tag{3.15}$$

Hence, if the fast fading of the interferes needs be introduced in (3.1), (3.15) can be applied directly to (3.4), with $M_x = \left|h^{(x)}\right| \in \mathbb{R}$, in order to compute the expectation with respect to the path-loss and to the fading of the interferers. That is, by setting:

$$f(x, h) = s\frac{P_{\text{tx}}\left|h^{(x)}\right|^2}{L^{(x)}}\ \mathbf{1}\left(L^{(x)} > L^{(0)}\right) \tag{3.16}$$

and $l = 1$ and by employing the distribution $F_H(h)$ for the respective type of fading, the MGF of (3.4a) is revised as follows:

$$M_g\left(s; L^{(0)}\right) = \exp\left(\int_{h=0}^{\infty}\left[\int_{L^{(0)}}^{\infty}\left(\exp\left(-s\frac{P_{\text{tx}}|h|^2}{y}\right) - 1\right)\frac{2\pi\lambda}{\beta}\left(\frac{1}{\kappa}\right)^{\frac{2}{\beta}} y^{\frac{2}{\beta}-1}dy\right] F_H(h)\right),$$

$$s \in \mathbb{R}. \tag{3.17}$$

The employment of (3.15) allowed for moving the expectation over the fading within the exponential term of (3.17), thus, simplifying the analysis to a great extent. As a result, the expectation over the fading of the interferes can also be moved within

the exponential term of (3.12). Given the tractability of (3.12), the introduction of an additional integral within the exponential term has a minor effect on the complexity of the derived expressions and the analysis can be easily extended accordingly.

However, as already mentioned, the present analysis does not account for the fading of the interferers focusing on a realistic scenario where the UE does not have perfect knowledge of the channel of all interferers.

3.3 Ergodic Rate in the DL

Having defined a simple approximation of the MGF, the latter can be employed to provide closed form expressions for the DL ergodic rate for the interference limited case. In this course, the analysis will commence by employing the MGF of (3.4b) and (3.12) to derive the coverage probability for the interference limited case. The latter can be derived by both expressions, i.e. (3.4b) and (3.12), in spite of the intractability of the former, allowing for the comparison of the two results and thus demonstrating the accuracy of the introduced approximation. Subsequently, capitalizing on the accuracy of the introduced approximation, the DL ergodic rate will be derived in closed form by employing the introduced approximate expression for the coverage probability.

The analysis which will initially account only for networks comprising much more users than BSs will then be extended to networks comprising more BSs than users.

3.3.1 Probability of Coverage

The probability of coverage (i.e. the probability of the SINR exceeding the value γ) is defined as follows:

$$P_{cov} = \mathbb{P}\left(\frac{P_{\text{tx}}\left|h^{(0)}\right|^2 / L^{(0)}}{\sum\limits_{x\in\Psi, x\neq x_0} P_{\text{tx}}/L^{(i)} + \sigma_N^2} \geq \gamma\right) = \mathbb{P}\left(\left|h^{(0)}\right|^2 \geq \frac{\gamma L^{(0)}\left(g+\sigma_N^2\right)}{P_{\text{tx}}}\right), \tag{3.18}$$

where σ_N^2 denotes the noise power and $h^{(0)}$ the fast fading of the intended user. As opposed to the fast fading of the interferers, the fast fading of the intended user is estimated and known in practice.

Assuming Rayleigh fading, then the random variable $\left|h^{(0)}\right|^2$ follows an exponential distribution with unit mean and the P_{cov} is given by:

$$\begin{aligned} P_{cov} &\overset{(a)}{=} \mathbb{E}_{g,L^{(0)}}\left\{\exp\left(-\frac{\gamma L^{(0)}(g+\sigma_N^2)}{P_{\text{tx}}}\right)\right\} \\ &\overset{(b)}{=} \mathbb{E}_{L^{(0)}}\left\{\exp\left(-\frac{\gamma L^{(0)}\sigma_N^2}{P_{\text{tx}}}\right) M_g\left(\frac{\gamma L^{(0)}}{P_{\text{tx}}}; L^{(0)}\right)\right\} \\ &\overset{(c)}{=} \int_{y=0}^{\infty} \exp\left(-\frac{\gamma y \sigma_N^2}{P_{\text{tx}}}\right) M_g\left(\frac{\gamma y}{P_{\text{tx}}}; y\right) f_{L^{(0)}}(y) dy, \end{aligned} \tag{3.19}$$

where (a) is obtained by the CCDF of the exponential distribution, (b) is obtained based on the definition of the MGF in (3.4), and (c) from computing the expectation with respect to the path-loss $L^{(0)}$ to the serving BS BS_0.

The probability density function (PDF) of the distance between a reference user and its closest BS for a PPP is given in [26]. By employing this PDF and the definition of (3.2), the PDF of the path-loss between a reference user and its closest BS $f_{L^{(0)}}(y)$ is given by:

$$f_{L^{(0)}}(y) = \frac{2\pi\lambda}{\beta}\left(\frac{1}{\kappa}\right)^{\frac{2}{\beta}} y^{\frac{2}{\beta}-1} \exp\left(-\pi\lambda\left(\frac{y}{\kappa}\right)^{\frac{2}{\beta}}\right). \tag{3.20}$$

In the interference limited case, the exponential term of (3.19c) is equal to 1 and, by employing (3.20), the coverage probability can be calculated as follows:

$$\begin{aligned} P_{cov} &= \int_0^\infty M_g\left(\frac{y\gamma}{P_{\text{tx}}}; y\right)\frac{2\pi\lambda}{\beta}\left(\frac{1}{\kappa}\right)^{\frac{2}{\beta}} y^{\frac{2}{\beta}-1}\exp\left(-\pi\lambda\left(\frac{y}{\kappa}\right)^{\frac{2}{\beta}}\right)dy \\ &\overset{(a)}{=} \frac{1}{{}_1F_1\left(-\frac{2}{\beta}, 1-\frac{2}{\beta}, -\gamma\right)} \\ &\overset{(b)}{\approx} \frac{\mathbf{1}\left(\gamma \le c\right)}{\left(-\frac{\gamma^2}{2\beta-2}+\frac{2\gamma}{\beta-2}+1\right)} + \frac{\mathbf{1}\left(\gamma > c\right)}{\gamma^{\frac{2}{\beta}}\Gamma(1-\frac{2}{\beta})}, \end{aligned} \tag{3.21}$$

where (a) is obtained by employing (3.4b) and (b) by employing the approximate MGF of (3.12).

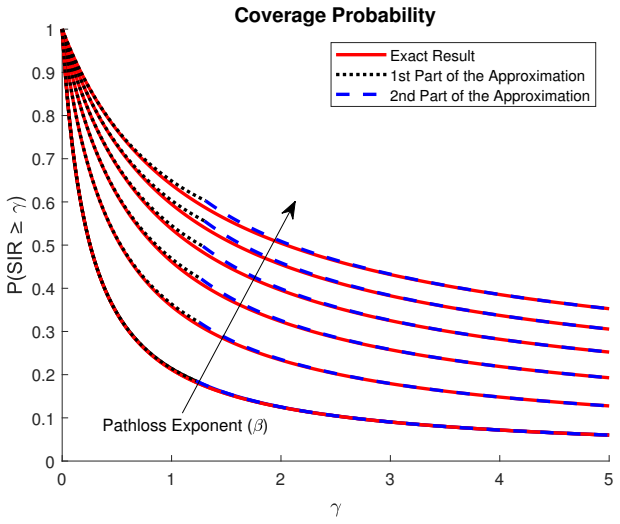

Figure 3.2: Probability of coverage for different path loss exponent values $2.5 \le \beta \le 5$. β increases in the direction of the arrow with a step of 0.5.

The results of (3.21) verify the theoretical results presented in Section 1.1, since for a single-slope path loss model and for more users than BSs, the coverage probability of (3.21) does not depend on the density of BSs λ, but only on the path loss exponent β and the SIR value γ (c is also a function of β given by (3.14)). The accuracy of (3.21b) and, implicitly, the accuracy of the MGF of (3.12), is demonstrated in Fig. 3.2 where the approximate coverage probability of (3.21b) is compared against the exact result of (3.21a). Apart from extremely accurate, the approximate coverage probability of (3.21b) is also significantly more tractable than the exact result of (3.21a).

3.3.2 Approximations of the Ergodic Rate

Having defined the tractable and accurate approximation of (3.21b) for the probability of coverage, this can be employed to compute the DL ergodic rate. In particular, the probability of coverage given by (3.21b) constitutes the CCDF of the SIR (i.e. for $SIR = w$, $P_{cov} = 1 - F_W(w)$). Hence, the derived tractable expression of the CCDF of the SIR allows for the computation of the DL ergodic rate by averaging over the SIR as follows:

$$\begin{aligned} R &= \mathbb{E}_w\{\log(1+w)\} = \int_0^\infty \log(1+w) F'_W(w) dw \\ &\overset{(a)}{=} \int_0^\infty \frac{P_{cov}}{1+w} dw \\ &\overset{(b)}{\approx} \int_0^c \frac{1}{\left(-\frac{w^2}{2\beta-2} + \frac{2w}{\beta-2} + 1\right)(1+w)} dw + \int_c^\infty \frac{1}{\left(w^{\frac{2}{\beta}}\Gamma\left(1-\frac{2}{\beta}\right)\right)(1+w)} dw, \end{aligned} \tag{3.22}$$

where (a) is obtained by integrating by parts and (b) is obtained by employing (3.21b). The employment of (3.21a) in (3.22a) would not allow the analytical computation of the above integral. However, (3.22b) can be computed in closed form and the rate is given by:

$$\begin{aligned} R =& (2\beta-2)\left(\frac{4+2\alpha-3\beta-\alpha\beta}{2\alpha(10-11\beta+2\beta^2)}\left(\log\left(\frac{c+\alpha-\frac{2\beta-2}{\beta-2}}{\alpha-\frac{2\beta-2}{\beta-2}}\right)\right)\right. \\ &+ \frac{-4+2\alpha+3\beta-\alpha\beta}{2\alpha(10-11\beta+2\beta^2)}\left(\log\left(\frac{c-\alpha-\frac{2\beta-2}{\beta-2}}{-\alpha-\frac{2\beta-2}{\beta-2}}\right)\right) + \frac{-2+\beta}{(10-11\beta+2\beta^2)}\left(\log(c+1)\right)\Bigg) \\ &+ \frac{\beta c^{-\frac{2}{\beta}}}{2\Gamma\left(1-\frac{2}{\beta}\right)} {}_2F_1\left(1, \frac{2}{\beta}, \frac{2+\beta}{\beta}, -\frac{1}{c}\right), \end{aligned} \tag{3.23}$$

where the first three terms of (3.23) are obtained by the calculation of the first term of (3.22b) and the last term of (3.23) is obtained by the calculation of the last term of (3.22b). ${}_2F_1(a,b,c,z)$ denotes the Gaussian hypergeometric function, c is given by (3.14)

and depends on β and $\alpha = \sqrt{\left(\frac{2\beta-2}{\beta-2}\right)^2 + 2\beta - 2}$. Again, as in the case of (3.21), (3.23) depends only on the path loss exponent β.

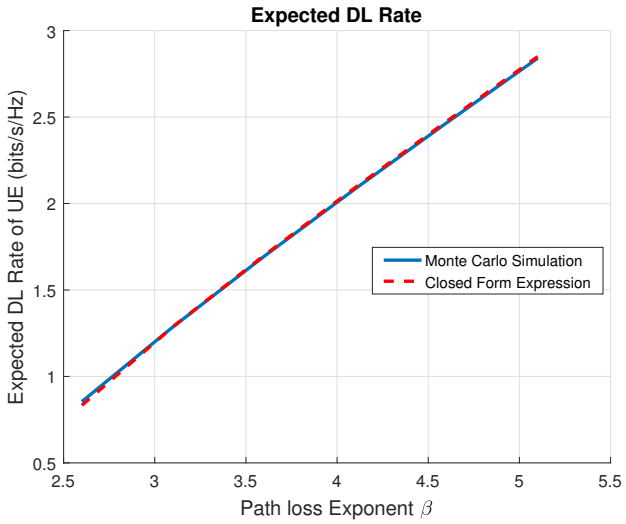

Figure 3.3: DL ergodic rate vs path loss exponent for the interference limited case.

The employment of (3.23) allows the computation of the rate for the interference limited case in closed form. The tight performance of (3.23) for the calculation of the ergodic rate is demonstrated in Fig. 3.3, where (3.23) is compared against the results obtained by Monte Carlo simulations. Even though the rate does not depend on the density of the BSs, the density employed for generating the simulation of Fig. 3.3 was $\lambda = 1.27e-06$.

Several research works have focused on deriving expressions for the DL ergodic rate, since the latter constitutes the most sensible figure of merit for evaluating the performance of UDNs. Indicatively, in [39] the authors have provided expressions for the DL ergodic rate in heterogeneous cellular networks for all different types of fading. However, in all of these works, including the latter, the calculation of the DL ergodic rate involved at least one integration that had to be computed numerically. This imposed inherent limitations to the applicability of those expressions to complex optimization problems. In order to overcome this problem the authors of [40] provided expressions for the DL ergodic rate in the interference limited case, for a fully loaded scenario (i.e. for $\lambda_{UE} \gg \lambda$) that did not involve any numerical integration. In this direction, the authors of [40] provided lookup tables and employed the Meijer-G function to provide a tight approximation of the DL ergodic rate in the fully loaded case. In particular, the approximate ergodic rate of [40] is given by:

$$C = \frac{-s^* \log_2 e}{1+s^*} \left(\mathrm{E}_1 \left(\frac{-s^*}{D_\delta} \right) - \exp\left(\frac{1+s^*}{D_\delta} \right) \mathrm{E}_1 \left(\frac{1}{D_\delta} \right) \right) + \frac{\sin(\pi\delta) \log_2 e}{\pi} G_{2,3}^{2,2} \left(\begin{matrix} 0,\ 1-\delta \\ 0,0,-\delta \end{matrix} \middle| z \right), \tag{3.24}$$

where s^* is the solution to the equation ${s^*}^\delta \Gamma(-\delta, s^*) = 0$, given by lookup tables that are computed a priori for all relevant values of β. Furthermore, $\delta = \frac{2}{\beta}$, $D_\delta = \frac{s^*}{\log(1-\mathrm{sinc}(\delta))}$, $\mathrm{E_n}(x) = \int_1^\infty t^{-n} e^{-xt} dt$ is the exponential integral and

$$G_{p,q}^{m,n} \left(\begin{matrix} a_1,\ldots,a_n,a_{n+1},\ldots,a_p \\ b_1,\ldots,b_m,b_{m+1},\ldots,b_q \end{matrix} \middle| z \right) =$$

$$\frac{1}{2\pi i} \int_{\mathcal{L}} \frac{\prod_{k=1}^{m} \Gamma(s+b_k) \prod_{k=1}^{n} \Gamma(1-a_k-s)}{\prod_{k=n+1}^{p} \Gamma(s+a_k) \prod_{k=m+1}^{q} \Gamma(1-b_k-s)} z^{-s} ds, \tag{3.25}$$

is the Meijer-G function. Improving the result of (3.24), the present analysis introduces a closed form approximation for the ergodic rate in (3.23), without the need for an a priori computed lookup table. Furthermore, the result of (3.23) is significantly more tractable than the result of (3.24), and Fig. 3.4 demonstrates the superior performance of (3.23) over (3.24) with respect to the tightness of the approximation, where in Fig. 3.4 the range of β is defined by the range of the respective lookup table provided in [40]. The accuracy and, more importantly, the tractability of the above expressions, allow for the extension of the analysis to even more complex scenarios, as will be demonstrated in the following sections.

3.3.3 Ergodic Rate over Density of Users and BSs

As already mentioned, the previous analysis corresponds to a scenario where the density of users is much greater than the density of BSs (i.e. $\lambda_{UE} \gg \lambda$) and, therefore, every BS is in transmission mode. However, since in the envisaged UDNs the number of BSs is expected to be higher than the number of UE [10], the analysis needs to be extended accordingly, taking into account the non transmitting mode of the excess BSs that do not have any UE in their coverage. In this course, the proposed tractable MGF is revised to account for the probability of the excess BSs to remain idle. This probability is defined by the density of UE λ_{UE} and the density of BSs λ. Thus, following a similar approach as before, we derive closed form expressions for the DL ergodic rate (i.e. peak and divided among intra-cell users) which depend on the density of UE λ_{UE} and the density of BSs λ.

The probability that a randomly chosen BS does not have any UE in its Voronoi cell and, therefore, goes into idle mode is given by [41]:

$$P_{inactive} = \left(1 + \frac{\lambda_{UE}}{3.5\lambda} \right)^{-3.5} \tag{3.26}$$

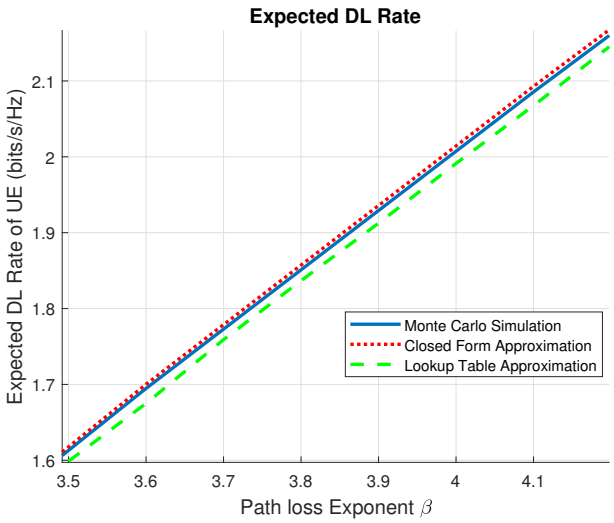

Figure 3.4: DL ergodic rate vs path loss exponent for the interference limited case. Tightness of closed form approximation compared to the lookup table approximation employing the Meijer-G function.

and the probability of a BS being in transmission mode and, thus, acting as an interferer in the DL, is denoted by:

$$P_{active} = 1 - P_{inactive}. \tag{3.27}$$

Since only a subset of the BSs create interference in the DL, the density of the BSs λ must be thinned out by the probability P_{active}. By introducing the thinned out density λP_{active} into (3.4) an (3.12), the MGF is revised as follows:

$$\begin{aligned} M_g\left(s; L^{(0)}\right) &= \exp\left(\int_{L^{(0)}}^{\infty}\left(\exp\left(-s\frac{P_{\text{tx}}}{y}\right)-1\right)\frac{2\pi\lambda P_{active}}{\beta}\left(\frac{1}{\kappa}\right)^{\frac{2}{\beta}} y^{\frac{2}{\beta}-1}dx\right) \\ &\overset{(a)}{=} \exp\left(\pi\lambda\left(\frac{L^{(0)}}{\kappa}\right)^{\frac{2}{\beta}}\left(1-{}_1F_1\left(-\frac{2}{\beta}, 1-\frac{2}{\beta}, \frac{-sP_{\text{tx}}}{L^{(0)}}\right)\right)P_{active}\right) \\ &\overset{(b)}{\approx} \begin{cases} \exp\left(\pi\lambda\left(\frac{L^{(0)}}{\kappa}\right)^{\frac{2}{\beta}}\left(\frac{-2sP_{\text{tx}}}{(\beta-2)L^{(0)}}+\frac{(sP_{\text{tx}})^2}{(2\beta-2)(L^{(0)})^2}\right)P_{active}\right), & \frac{sP_{\text{tx}}}{L^{(0)}} \leq c \\ \exp\left(\pi\lambda\left(\frac{L^{(0)}}{\kappa}\right)^{\frac{2}{\beta}}\left(-\left(\frac{sP_{\text{tx}}}{L^{(0)}}\right)^{\frac{2}{\beta}}\Gamma\left(1-\frac{2}{\beta}\right)+1\right)P_{active}\right), & \frac{sP_{\text{tx}}}{L^{(0)}} > c \end{cases} \\ & s \in \mathbb{R}, \end{aligned} \tag{3.28}$$

and, following the approach of (3.21) for the MGF of (3.28), the coverage probability is

now given by:

$$P_{cov/active} \overset{(a)}{=} \frac{1}{1+\left({}_1F_1\left(-\frac{2}{\beta},1-\frac{2}{\beta},-\gamma\right)-1\right)P_{active}}$$
$$\overset{(b)}{\approx} \frac{\mathbf{1}\left(\gamma \le c\right)}{1+\left(-\frac{\gamma^2}{2\beta-2}+\frac{2\gamma}{\beta-2}\right)P_{active}} + \frac{\mathbf{1}\left(\gamma > c\right)}{1+\left(\gamma^{\frac{2}{\beta}}\Gamma(1-\frac{2}{\beta})-1\right)P_{active}}. \tag{3.29}$$

The probability of coverage defined by the exact result of (3.29a) and by the approximation of (3.29b) is plotted in Fig. 3.5 for a path loss exponent $\beta = 4$ and for density ratios $\lambda_{UE}/\lambda = 0.1, 0.4, 0.7, 1$, demonstrating, once again, the accuracy of the derived approximation.

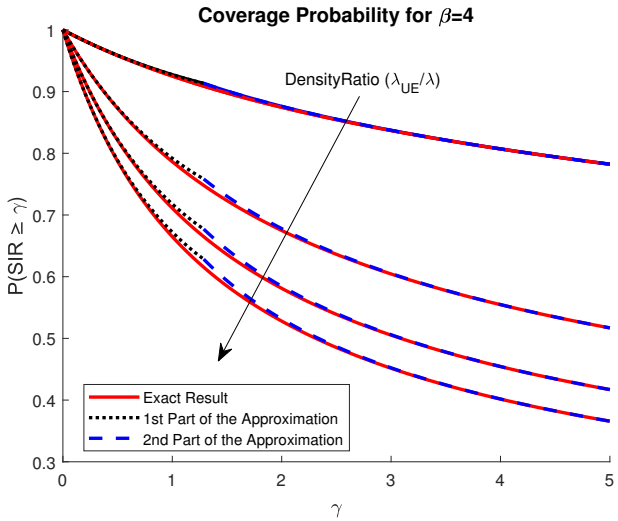

Figure 3.5: Probability of coverage for different density ratios ($0.1 \le \lambda_{UE}/\lambda \le 1$). The density ratio increases in the direction of the arrow with a step of 0.3.

Following the same approach as in (3.22) for the results of (3.29b), the DL ergodic peak rate can be computed in closed form as follows:

$$R_{peak} = \int_0^c \frac{1}{\left(1+\left(-\frac{w^2}{2\beta-2}+\frac{2w}{\beta-2}\right)P_{active}\right)(1+w)}dw$$
$$+ \int_c^\infty \frac{1}{\left(1+\left(w^{\frac{2}{\beta}}\Gamma\left(1-\frac{2}{\beta}\right)-1\right)P_{active}\right)(1+w)}dw. \tag{3.30}$$

For path loss exponent values of $\beta = 3, 4, 5$ the closed form expressions for the peak rate are given in Table 3.2. The expressions (3.33)-(3.35) provide a closed form representation of the peak DL ergodic rate over the probability P_{active} and, implicitly through (3.27), over the density of BSs λ and of UE λ_{UE}.

The probability that a randomly chosen UE is assigned a resource block at a given time and is served by its nearest BS is given by [41]:

$$P_{selection} = \frac{\lambda}{\lambda_{UE}} \left(1 - (1 + \frac{\lambda_{UE}}{3.5\lambda})^{-3.5} \right). \tag{3.31}$$

Employing this probability, a more sensible figure of merit than the peak rate can be derived. This figure of merit is the actual DL ergodic rate of the reference UE, i.e., the rate of the reference UE after dividing the available resources and, thus, the peak rate among all intra-cell UE. The latter is given by:

$$R = R_{peak} P_{selection}. \tag{3.32}$$

The accuracy of expressions (3.32)-(3.35) is demonstrated in Fig. 3.6 and 3.7 where the peak and the actual DL ergodic rates are plotted over the ratio of the densities λ_{UE}/λ and compared against Monte Carlo simulations.

In the Monte Carlo simulations, the BSs are deployed following the PPP Ψ of density λ and the users are deployed following the PPP Φ of density λ_{UE}, whereas the reference UE resides at the origin. BSs with no UE in their coverage (i.e. within their Voronoi cell) do not create any interference. To compute the actual rate, the number of users residing within the Voronoi cell of BS_0 are counted in each realization and the peak rate is divided among these users and the reference UE. The number of simulated BSs is fixed and the simulation area expands or contracts as the BS density λ changes, in order to accommodate the predefined number of BSs, while the density of users λ_{UE} remains fixed.

The closed form expressions derived in (3.32)-(3.35) provide, among others, a substantial computational gain when compared to the computational time of the respective Monte Carlo simulations. Especially, since the simulation of a wireless network, that comprises both users and BSs of different spatial distributions, and the calculation of their relative distances is computationally expensive. In order to demonstrate the gain arising by the employment of the closed form expressions of (3.32)-(3.35), the computational time of the derived closed form expressions is tabulated in Table 3.1. Since this time is not an absolute metric, but depends on the hardware employed, Table 3.1 presents the computational time of the expressions as a percentage of the computational time required for simulating the respective wireless networks of Fig. 3.7 using the same hardware.

Table 3.1 demonstrates that the computational gain arising by the derived expressions is immense. The time required for the analytical computation of the rate is practically zero compared to the time required for simulating the respective scenario. At this point it should also be noted that the variations in the values of the computational time arise due to the variations in the time required for the respective simulations. That is since the simulation area has to expand and contract as λ changes in order to accommodate

Table 3.1: Computational time of expressions (3.32)-(3.35) as a percentage of the respective computational time for simulating the scenarios of Fig. 3.7.

Path-loss (β)	**Density Ratio λ_{UE}/λ**			
	0.17	4.34	8.51	11.11
3	$6.9\ 10^{-4}$ %	$6.7\ 10^{-4}$ %	$3.4\ 10^{-7}$ %	$2.7\ 10^{-7}$ %
4	$6.9\ 10^{-4}$ %	$6.8\ 10^{-4}$ %	$1.8\ 10^{-7}$ %	$1.3\ 10^{-7}$ %
5	$2.2\ 10^{-3}$ %	$4.6\ 10^{-3}$ %	$2.3\ 10^{-6}$ %	$1.6\ 10^{-6}$ %

a fixed number of BSs. The variations with respect to β emerge due to the different complexity of the analytical expressions of (3.33)-(3.35) with respect to β.

Apart from the computational gain that has been demonstrated by Table 3.1, the closed form expressions of (3.32)-(3.35) and the respective figures, i.e. Fig. 3.6 and 3.7 provide a deep understanding of the behavior of UDNs as the density of users λ_{UE} and BSs λ changes. First of all, expressions (3.33)-(3.35) and Fig. 3.6 verify one of the fundamental findings of stochastic geometry, already explained in Section 1.1, that in the fully loaded case (i.e. for $\lambda_{UE} \gg \lambda$) the ergodic rate remains invariant while the BS density changes. However, Fig. 3.7 demonstrates that even if the peak rate remains invariant, the rate of the users that have to share this peak rate tends to zero as the density ratio (i.e. the expected number of users per typical cell) increases. This behavior demonstrates why the envisaged UDNs are expected to comprise more BSs than users, highlighting the importance of the non-fully loaded case. Given the importance of the non-fully loaded case, expressions (3.33)-(3.35) and Fig. 3.6 allow to quantify the threshold between the non-fully and the fully loaded case. In particular, in all three expressions for the different values of β, the network exhibits the behavior of a fully loaded network for $\lambda_{UE}/\lambda > 4$, way earlier than implied by the notation $\lambda_{UE} \gg \lambda$.

Another interesting finding can be derived from the behavior of the network in the non-fully loaded case when the BSs that do not comprise any user in their coverage do not create any interference. In this setup, Fig. 3.6 demonstrates that the densification of the network can provide substantial rate gains since the achieved DL ergodic rate in this range is significantly higher than the rate achieved at the fully loaded case. Thus, Fig. 3.6 demonstrates that just by switching off the BSs that do not comprise users in their coverage, substantial rate gains can be engendered for the network. This motivates the use of even more intricate schemes where BSs can be switched off strategically to mitigate interference. This optimization problem is only one of the problems that the derived expressions can be applied to, with additional applications being presented in the following section.

Moreover, expressions (3.33)-(3.35) and the respective figures verify the results of the

expressions (3.23) and (3.24), and of the figures 3.3 and 3.4, according to which the DL ergodic rate increases monotonically with the path-loss exponent β. In particular, since the distance from the UE to the serving BS is always smaller than the distance to the interfering BSs, i.e. since $\|x_i\| > \|x_0\|$, each term of the sum $\sum_{\substack{x\in\Psi,\\ x\neq x_0}} \left(\frac{\|x_0\|}{\|x_i\|}\right)^{\beta}$ decreases with β. Consequently, the SIR and the DL ergodic rate increase monotonically with β.

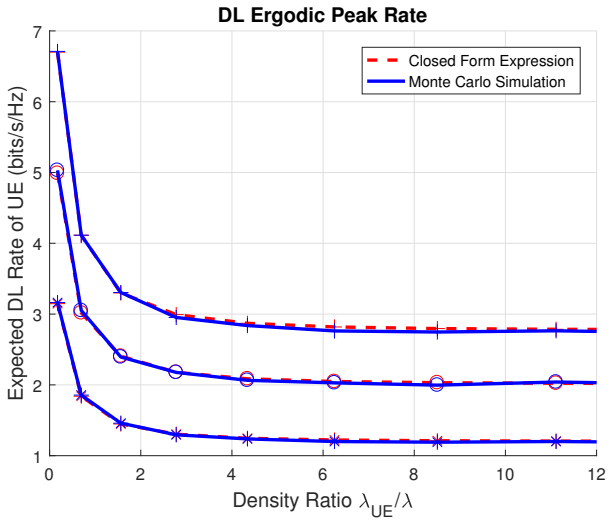

Figure 3.6: DL ergodic peak rate vs ratio of densities λ_{UE}/λ for a path loss exponent β =3(∗), 4(o) and 5(+).

3.3.4 Applications of the Derived Expressions

Figures 3.6 and 3.7 corroborate the accuracy of the derived expressions while providing a deeper understanding of the network performance as a function of the user and BS densities. Hence, these expressions, that for the first time associate the DL ergodic rate with the densities of the UE and of the BSs is a closed form, pave the way for the investigation of complex optimization problems, toward improving UDN operation and offered QoS.

In particular, given the maximum density of UE λ_{UE} during the operation of the network and the minimum rate requirement per user (imposed by the QoS constraints), Fig. 3.7 and (3.32) can be employed by network operators to define the minimum BS density λ that guarantees this rate. Hence, (3.32) can be employed as a rule of thumb for the lower limit of the densification of BSs that guarantees the QoS objectives, implicitly quantifying the minimum capital expenditure required by network operators.

In addition to that, given the aforementioned minimum rate requirement per user

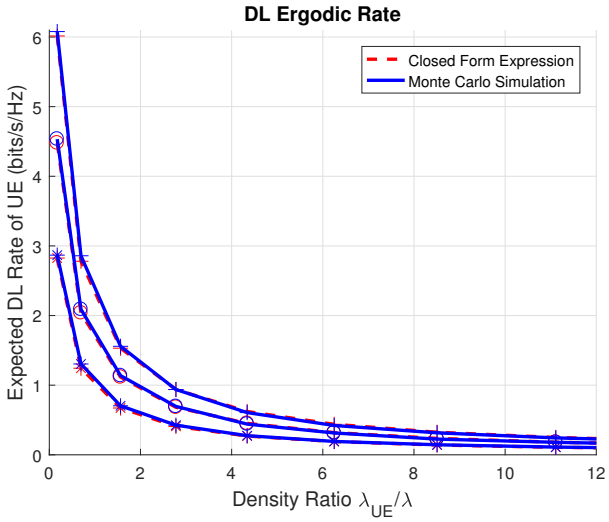

Figure 3.7: DL ergodic rate vs ratio of densities λ_{UE}/λ for a path loss exponent β =3(∗), 4(o) and 5(+).

and a network of BS density λ, comprising UE whose density λ_{UE} varies during the operation of the network, Fig. 3.7 and (3.32) can be employed to dynamically define the probability of transmission P_{active} that achieves the predefined rate requirement as λ_{UE} changes. This probability can indicate the density of transmitting BSs λP_{active}, i.e. the density of the BSs comprising at least one UE in their coverage. The latter density can be input into optimization modules to be used as a starting point for the search aiming at pinpointing the optimum set of BSs to be switched off, additionally to those that do not comprise any UE in their coverage. Given the high density of the BSs, strategically switching off the best serving BSs of a UE for the latter to be served by a neighboring BS has a only minimal impact on the path-loss, while it can provide substantial rate gains through the mitigation of the interference.

Table 3.2: Closed Form expressions for the DL ergodic peak rate for different path loss exponents

β	**DL Ergodic Peak Rate:**
3	$R_{peak} =$ $\frac{-4}{P_{active}}\left(\frac{\log\left(\frac{c-4+b}{-4+b}\right)}{2b(-5+b)}+\frac{\log\left(\frac{c-4-b}{-4-b}\right)}{2b(5+b)}-\frac{\log(c+1)}{(-5+b)(5+b)}\right)-\frac{\sqrt{3}P_{active}\arctan\left(\frac{-1+2c^{1/3}}{\sqrt{3}}\right)\Gamma(\frac{1}{3})}{1+P_{active}(-2+P_{active}+(P_{active}-1)\Gamma(\frac{1}{3})+P_{active}\left(\Gamma(\frac{1}{3})\right)^2)}$ $+\Bigg[-(1-P_{active})^{3/2}P_{active}\,\pi\left(-\sqrt{3}+3\sqrt{-\frac{P_{active}\Gamma(\frac{1}{3})}{P_{active}-1}}\right)\Gamma\left(\frac{1}{3}\right)-6\left(P_{active}-1\right)\left(P_{active}\Gamma\left(\frac{1}{3}\right)\right)^{3/2}$ $\arctan\left(\sqrt{\frac{P_{active}\Gamma\left(\frac{1}{3}\right)}{1-P_{active}}}c^{1/3}\right)+\sqrt{1-P_{active}}\Bigg[\sqrt{3}\left(P_{active}\Gamma\left(\frac{1}{3}\right)\right)^2\pi-2P_{active}\Gamma\left(\frac{1}{3}\right)\left(-1+P_{active}\left(1+\Gamma\left(\frac{1}{3}\right)\right)\right)$ $\log\left(1+c^{1/3}\right)+P_{active}\Gamma\left(\frac{1}{3}\right)\left(-1+P_{active}\left(1+\Gamma\left(\frac{1}{3}\right)\right)\right)\log\left(1-c^{1/3}+c^{2/3}\right)+(-1+P_{active})^2\Big[-2\log(1+c)$ $-3\log\left(P_{active}\Gamma\left(\frac{1}{3}\right)\right)+3\log\left(1-P_{active}\left(-1+c^{2/3}\Gamma\left(\frac{1}{3}\right)\right)\right)\Big]\Bigg]\Bigg]/$ $\left[2\sqrt{1-P_{active}}\left(-(-1+P_{active})^3+\left(P_{active}\Gamma\left(\frac{1}{3}\right)\right)^3\right)\right],\ where\ b=2\sqrt{4+\frac{1}{P_{active}}},\ c=1.2528$ (3.33)
4	$R_{peak} =$ $\frac{-6}{P_{active}}\left(\frac{\log\left(\frac{c-3+b}{-3+b}\right)}{2b(-4+b)}+\frac{\log\left(\frac{c-3-b}{-3-b}\right)}{2b(4+b)}-\frac{\log(c+1)}{(-4+b)(4+b)}\right)+\frac{-2\log(P_{active})(1+P_{active})+(P_{active}-1)\log((1+c)\pi)}{1+P_{active}(-2+P_{active}(1+\pi))}$ $+\frac{\pi^{1.5}P_{active}-2\sqrt{\pi}P_{active}\arctan\sqrt{c}-2(P_{active}-1)\log\left(1-P_{active}+\sqrt{\pi c}P_{active}\right)}{1+P_{active}(-2+P_{active}(1+\pi))},\ where\ b=\sqrt{9+\frac{6}{P_{active}}},\ c=1.2873$ (3.34)
5	$R_{peak} =$ $\frac{-8}{P_{active}}\left(\frac{3\log\left(\frac{c-8/3+b}{-8/3+b}\right)}{2b(-11+3b)}+\frac{3\log\left(\frac{c-8/3-b}{-8/3-b}\right)}{2b(11+3b)}-\frac{9\log(c+1)}{(-11+3b)(11+3b)}\right)+\Bigg[10\sqrt{\frac{1}{1-P_{active}}}\left(-1+P_{active}\right)^2$ $\pi\left(P_{active}\Gamma\left(\frac{3}{5}\right)\right)^{5/2}-20\left(1-P_{active}\right)^{3/2}\left(P_{active}\Gamma\left(\frac{3}{5}\right)\right)^{5/2}\arctan\left(\frac{\left(P_{active}\Gamma\left(\frac{3}{5}\right)\right)^{1/2}c^{1/5}}{\sqrt{1-P_{active}}}\right)+2\sqrt{2}\left(P_{active}\Gamma\left(\frac{3}{5}\right)\right)$ $\arctan\left(\frac{1+\sqrt{5}-4c^{1/5}}{\sqrt{10-2\sqrt{5}}}\right)\left(1+P_{active}\left(-1+\Gamma\left(\frac{3}{5}\right)\right)\right)\left(\sqrt{5+\sqrt{5}}+P_{active}\left(\left(-2+P_{active}\left(1+\left(\Gamma\left(\frac{3}{5}\right)\right)^2\right)\right)\right.\right.$ $\left.\left.\sqrt{5+\sqrt{5}}+\sqrt{10+4\sqrt{5}}\left(-1+P_{active}\right)\Gamma\left(\frac{3}{5}\right)\right)\right)+\left(-1+P_{active}\right)\left(P_{active}\Gamma\left(\frac{3}{5}\right)\right)^3\left(\sqrt{10-2\sqrt{5}}\pi-\log(4)\right)$ $+\left(P_{active}\Gamma\left(\frac{3}{5}\right)\right)^4\left(\sqrt{2\left(5+\sqrt{5}\right)}\pi-\log(4)\right)$ $-\left(P_{active}\Gamma\left(\frac{3}{5}\right)\right)^2\left(\sqrt{10-2\sqrt{5}}\left(-1+P_{active}\right)^2\pi+\log(4)\left(1+\left(P_{active}\right)^2\right)-P_{active}\log(16)\right)$ $-\left(P_{active}-1\right)\left(P_{active}\Gamma\left(\frac{3}{5}\right)\right)\left(\sqrt{2(5+\sqrt{5})}\left(P_{active}-1\right)^2\pi+\log(4)\left(1+\left(P_{active}\right)^2\right)-P_{active}\log(16)\right)$

$$
\begin{aligned}
&-4\log(1+c)-10\log\left(P_{active}\Gamma\left(\frac{3}{5}\right)\right)+P_{active}\Big[\mathrm{i}\left(1+\mathrm{P_{active}}\left(-1+\Gamma\left(\frac{3}{5}\right)\right)\right)\Gamma\left(\frac{3}{5}\right)\\
&\left(\sqrt{10-2\sqrt{5}}+P_{active}\Big(-2\sqrt{10-2\sqrt{5}}+\sqrt{10-2\sqrt{5}}P_{active}-2\sqrt{5-2\sqrt{5}}\,(-1+P_{active})\,\Gamma\left(\frac{3}{5}\right)\right.\right.\\
&\left.\left.+\sqrt{10-2\sqrt{5}}P_{active}\Gamma\left(\frac{3}{5}\right)^2\Big)\right)\log\left(-1+\frac{\mathrm{i}\left(-1+\sqrt{5}+4\mathrm{c}^{1/5}\right)}{\sqrt{2\left(5+\sqrt{5}\right)}}\right)+P_{active}\Gamma\left(\frac{3}{5}\right)^4\Big(-\mathrm{i}\sqrt{10-2\sqrt{5}}\\
&\log\left(1+\frac{\mathrm{i}(-1+\sqrt{5}+4\mathrm{c}^{1/5})}{\sqrt{2(5+\sqrt{5})}}\right)-4\log\left(1+c^{1/5}\right)+(1+\sqrt{5})\log\left(2+(-1+\sqrt{5})c^{1/5}+2c^{2/5}\right)\\
&-(-1+\sqrt{5})\log\left(2-(1+\sqrt{5})c^{1/5}+2c^{2/5}\right)\Big)+(-1+P_{active})^3\,\Gamma\left(\frac{3}{5}\right)\Big(\mathrm{i}\sqrt{10-2\sqrt{5}}\\
&\log\left(1+\frac{\mathrm{i}(-1+\sqrt{5}+4\mathrm{c}^{1/5})}{\sqrt{2(5+\sqrt{5})}}\right)-4\log\left(1+c^{1/5}\right)+(1+\sqrt{5})\log\left(2+(-1+\sqrt{5})c^{1/5}+2c^{2/5}\right)\\
&-(-1+\sqrt{5})\log\left(2-(1+\sqrt{5})c^{1/5}+2c^{2/5}\right)\Big)+\left((1+P_{active})\,\Gamma\left(\frac{3}{5}\right)\right)^2P_{active}\Big(-\mathrm{i}\sqrt{2(5+\sqrt{5})}\\
&\log\left(1+\frac{\mathrm{i}(-1+\sqrt{5}+4\mathrm{c}^{1/5})}{\sqrt{2(5+\sqrt{5})}}\right)-4\log\left(1+c^{1/5}\right)-(-1+\sqrt{5})\log\left(2+(-1+\sqrt{5})c^{1/5}+2c^{2/5}\right)\\
&(1+\sqrt{5})\log\left(2-(1+\sqrt{5})c^{1/5}+2c^{2/5}\right)\Big)+(-1+P_{active})\,(P_{active})^2\,\Gamma\left(\frac{3}{5}\right)^3\Big(\mathrm{i}\sqrt{2(5+\sqrt{5})}\\
&\log\left(1+\frac{\mathrm{i}(-1+\sqrt{5}+4\mathrm{c}^{1/5})}{\sqrt{2(5+\sqrt{5})}}\right)-4\log\left(1+c^{1/5}\right)+(-1+\sqrt{5})\log\left(2+(-1+\sqrt{5})c^{1/5}+2c^{2/5}\right)\\
&+(1+\sqrt{5})\log\left(2-(1+\sqrt{5})c^{1/5}+2c^{2/5}\right)\Big)-2\,(-2+P_{active})\,(2+P_{active}\,(-2+P_{active}))\\
&\left(2\log(1+c)+5\log\left(P_{active}\Gamma\left(\frac{3}{5}\right)\right)-5\log\left(1-P_{active}+P_{active}c^{2/5}\Gamma\left(\frac{3}{5}\right)\right)\right)\Big]\\
&+10\log\left(1-P_{active}+P_{active}c^{2/5}\Gamma\left(\frac{3}{5}\right)\right)\Big]\Big/\left(-4\,(-1+P_{active})^5+4\,(P_{active})^5\,\Gamma\left(\frac{3}{5}\right)^5\right),\\
&where\ b=2\sqrt{\frac{16}{9}+\frac{2}{P_{active}}},\ c=1.3099
\end{aligned}
\tag{3.35}
$$

5

Chapter 4

Generalized Analysis of Poisson Cellular Networks

Having derived closed form expressions for the ergodic rate in the interference limited case, we can proceed with the extension of the analysis to the general case, that is, in a scenario limited simultaneously by noise and interference. In this direction, the present analysis derives a tight approximation in closed form for the DL ergodic rate for a setup of BSs coordinating with their immediate neighbors (with the objective of counteracting any emerging LOS interference). The derived closed form expressions quantify the performance of the network under the examined coordination scheme. Moreover, the tractability of the expressions makes them suitable for revealing trends in complex optimization problems, related to BS coordination.

4.1 The Wireless Cellular Network Architecture and the Ergodic rate Approximation

4.1.1 The Wireless Cellular Network Scenario

A wireless cellular system is considered, comprising a set of BSs BS_i, whose positions follow a spatial distribution given by a homogeneous Poisson point process (PPP) Ψ of density λ (BSs/m^2), similar to the network architecture of section 3.1. However in the present analysis, the network is assumed to comprise always significantly more users than BSs and every BS is active and transmitting, acting as an interferer in the DL. Moreover, a predefined number of BSs adjacent to BS_0 are assumed to coordinate and not to create any interference. The number of coordinating BSs in the following analysis is defined by an elementary property of stochastic geometry. In particular, the mean degree in the Poisson-Delaunay tessellation is 6 [35], hence in the Poisson-Delaunay tessellation of Ψ, the average number of adjacent cells to the cell comprising BS_0 is 6 (similar to

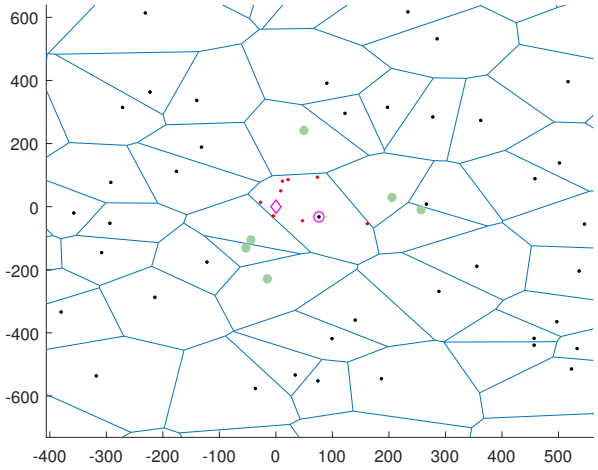

Figure 4.1: The Considered Network Scenario

hexagonal grids). Hence, the 6 BSs closest to BS_0 are assumed to coordinate. However, the subsequent analysis can be extended to any number of coordinating BSs.

The considered scenario is depicted in Figure 4.1, where BS_0 is marked by the magenta circle, the reference UE by the magenta diamond and the intra cell users are depicted in red. In this setup the interfering BSs are depicted in black and the 6 coordinated BSs in green.

As already stressed in Chapter 1, the investigated coordination scheme can be implemented in practice since BSs are aware of the topology of their immediate neighbors to facilitate the handover process. Moreover, such a scheme can counteract effectively the LOS interference which is the most detrimental in UDNs. Hence, LOS interference is assumed to be counteracted in this setup and single-slope path loss models are considered henceforth. For high network densities, where LOS interferers reside also after the 6th closest BSs, the analysis could be extended accordingly.

4.1.2 The Ergodic Rate Bound

The ergodic rate of a UE placed at distance d from BS_0 resulting from the average over fast fading, if no additional BSs are overlaid, is given by

$$\mathbb{E}[R] = \mathbb{E}_h \left\{ \log \left(1 + d^{-\beta} |h|^2 \gamma \right) \right\}, \tag{4.1}$$

where the expectation is with respect to the fading coefficient h, $\log(\cdot)$ in all the expressions henceforth represents the natural logarithm, β is the path-loss exponent, and γ is

the SNR at the reference distance with

$$\gamma = \frac{P_{BS}}{\sigma^2 L_{ref}}. \tag{4.2}$$

In (4.2) P_{BS} is the transmission power of the BS.

Assuming that the BSs BS_i are placed at distance d_i from the UE and every BS_i is acting as an interferer (for simplicity in this section's notation, although this is not the case in coming sections due to the coordination of the 6 closest BSs) the expectation of the rate must be calculated with respect to the fading coefficient h, the distances d and d_i and the fading coefficient h_i of all interferers. However, as already stressed in Chapter 3 the incorporation of h_i in the calculation would imply perfect knowledge of the channel of all interferers, which is not available in practice. Hence, the expectation with respect to h_i is omitted and the lower bound for the rate is calculated as follows:

$$\mathbb{E}[R] \geq \mathbb{E}_{h,d,d_i} \left\{ \log \left(1 + \frac{\gamma |h|^2 d^{-\beta}}{\sum_{i=1}^{\infty} \gamma d_i^{-\beta} + 1} \right) \right\}. \tag{4.3}$$

4.1.3 Taylor Approximation

Following a similar approach to that of Chapter 2, a mathematical manipulation is introduced and the convex function $f(x) = \log(1 + \exp(x))$ is employed, revising (4.3) as follows:

$$\mathbb{E}[R] \geq \mathbb{E}_{h,d,d_i} \left\{ f \left(\log \left(\frac{\gamma |h|^2 d^{-\beta}}{\sum_{i=1}^{\infty} \gamma d_i^{-\beta} + 1} \right) \right) \right\}. \tag{4.4}$$

The right-hand side of (4.4) can be approximated by an N-order Taylor expansion, as follows:

$$\mathbb{E}\{f(y)\} \approx f(\mathbb{E}\{y\}) + \sum_{n=2}^{N} \frac{\mathbb{E}\{y - \mathbb{E}\{y\}\}^n}{n!} f^{(n)}(E\{y\}) + R_N. \tag{4.5}$$

where, $y = \log \left(\frac{\gamma |h|^2 d^{-\beta}}{\sum_{i=1}^{\infty} \gamma d_i^{-\beta} + 1} \right)$ and R_N is the error after N terms (Lagrange Remainder) and is given by:

$$R_N = \mathbb{E} \left\{ \frac{(y - y_0)^{N+1}}{(N+1)!} f^{(n)}(\zeta(y, y_0)) \right\} \tag{4.6}$$

for some $\zeta(y, y_0) \in [y, y_0]$.

The proposed framework allows for a twofold approach. On the one hand, an infinitely large number of Taylor terms can be analytically defined, thus, allowing the analytical computation of (4.4) at the expense of computational time. On the other hand, a tight approximation of (4.4) can be provided by employing the first two terms of (4.5) as follows:

$$\mathbb{E}\{f(y)\} \approx f(\mathbb{E}\{y\}) + \left(\mathbb{E}\{y - \mathbb{E}\{y\}\}^2 \right) f''(E\{y\}). \tag{4.7}$$

Further to the approximation of (4.7), the employment of Jensen's inequality for the convex function $f(x)$ provides the following lower bound:

$$\mathbb{E}\{f(y)\} \geq f(\mathbb{E}\{y\}). \tag{4.8}$$

In addition, in the case of a second order expansion, there exists an $\alpha \in [0,1]$ such that [43]:

$$\mathbb{E}\{f(y)\} = f(\mathbb{E}\{y\}) + \frac{1}{2}\left(\mathbb{E}\{y - \mathbb{E}\{y\}\}^2\right)\mathbb{E}\{f''(\alpha y + E\{y\}(1-\alpha))\}. \tag{4.9}$$

Hence, employing the descent lemma [43], and since function $f''(y)$ attains its maximum value $f''(0) = \frac{1}{4}$ at $y = 0$ for $\alpha = 1$, an upper bound can be defined as follows:

$$\mathbb{E}\{f(y)\} \leq f(\mathbb{E}\{y\}) + \frac{1}{8}\left(\mathbb{E}\{y - \mathbb{E}\{y\}\}^2\right). \tag{4.10}$$

Having defined the bounds of (4.8) and (4.10) that provide a guideline regarding the validity of the obtained expressions, a correction factor $c(\mathbb{E}\{y\})$ is introduced to fine tune (4.7). The correction factor $c(\mathbb{E}\{y\})$ is a polynomial function of $\mathbb{E}\{y\}$ that is obtained numerically from the Lagrange remainder of (4.5) as detailed in the Appendix of the chapter. Thus, (4.7) is redefined as follows:

$$\mathbb{E}\{f(y)\} \approx f(\mathbb{E}\{y\}) + c(\mathbb{E}\{y\})\left(\mathbb{E}\{y - \mathbb{E}\{y\}\}^2\right)f''(E\{y\}). \tag{4.11}$$

In order to employ (4.7)-(4.11) for the computation of (4.4), $\mathbb{E}\{y\}$ needs to be defined. Since the expectations over the fading and the distances are independent, $\mathbb{E}\{y\}$ is obtained as follows:

$$\mathbb{E}\{y\} = \mathbb{E}_{h,d,d_i}\left\{\log\left(\frac{\gamma|h|^2 d^{-\beta}}{\sum_{i=1}^{\infty}\gamma d_i^{-\beta}+1}\right)\right\} \tag{4.12}$$

$$= \log(\gamma) + \mathbb{E}_h\left\{2\log(|h|)\right\} - \mathbb{E}_d\left\{\beta\log(d)\right\} - \mathbb{E}_{d_i}\left\{\log\left(\sum_{i=1}^{\infty}\gamma d_i^{-\beta}+1\right)\right\}. \tag{4.13}$$

Assuming a Rayleigh fading where h follows a zero-mean circularly symmetric Gaussian distribution with variance equal to 1, then the pdf of the fast fading is given by $f_H(|h|) = 2\,|h|\,e^{-|h|^2}$. Moreover, the pdf of the distance d between a reference user and its closest BS is given by [26]

$$f_D(d) = 2\pi d\lambda e^{-\lambda\pi d^2}, d \geq 0. \tag{4.14}$$

Since the pdf of a Rayleigh distribution is given by:

$$f_Y(y) = \frac{y}{\sigma_y^2}e^{\frac{-y^2}{2\sigma_y^2}}, \tag{4.15}$$

both random variables $|h|$ and d follow a Rayleigh distribution with $\sigma_d^2 = \frac{1}{2\pi\lambda}$ and $\sigma_h^2 = \frac{1}{2}$. Hence, the random variables of the second and third term of (4.13) follow a log-Rayleigh distribution.

The mean of a log-Rayleigh distributed variable μ is given by [44]

$$\mathbb{E}\{\mu\} = \log\sigma + \frac{\log 2}{2} - \frac{\psi}{2}. \tag{4.16}$$

where ψ is the Euler−Mascheroni constant defined as $\psi = -\int_0^\infty \log(x)\exp(-x)dx \approx 0.577$. The variance of the log-Rayleigh distributed variable μ is given by [44]

$$\mathbb{E}\{\mu - \mathbb{E}\{\mu\}\}^2 = \frac{\pi^2}{24}. \tag{4.17}$$

Since $\log d$ and $\log|h|$ are log-Rayleigh distributed random variables of variance σ_d^2 and σ_h^2, by employing (4.13) and (4.16) it follows that

$$\mathbb{E}\{y\} = \log(\gamma) + \frac{\beta}{2}(\psi + \log(\pi\lambda)) - \psi - \mathbb{E}_{d_i}\left\{ \log\left(\sum_{i=1}^{\infty} \gamma d_i^{-\beta} + 1\right)\right\} \tag{4.18}$$

and by (4.13) and (4.17):

$$\mathbb{E}\{y - \mathbb{E}\{y\}\}^2 = (\beta^2+4)\frac{\pi^2}{24} - \mathrm{var}\left\{ \log\left(\sum_{\mathrm{i}=1}^{\infty} \gamma {d_i}^{-\beta} + 1\right)\right\}. \tag{4.19}$$

In order to compute (4.18) and (4.19), the expectation and the variance of the log of the aggregate interference needs to be computed. In this course, it is known that the expectation and the variance of the aggregate interference can be computed in an exact manner by Campbell's theorem as follows [45]:

$$\mathbb{E}_{d_i}\left\{\sum_{i\in\Psi} d_i^{-\beta}\right\} = \lambda\int_{\mathbb{R}^+} d_i^{-\beta}\, 2\pi d_i dd_i, \tag{4.20}$$

$$\mathrm{var}_{d_i}\left\{\sum_{\mathrm{i}\in\Psi} \mathrm{d_i}^{-\beta}\right\} = \lambda\int_{\mathbb{R}^+} \left(d_i^{-\beta}\right)^2 2\pi d_i dd_i. \tag{4.21}$$

Employing the results of (4.20) and (4.21), the expectation and variance of the log of the aggregate interference can be approximated by the Taylor expansion of (4.5) as follows:

$$\mathbb{E}_{d_i}\left\{ \log\left(\sum_{i=1}^{\infty} \gamma d_i^{-\beta} + 1\right)\right\} \approx \tag{4.22}$$

$$\log\left(\mathbb{E}_{d_i}\left\{\sum_{i=1}^{\infty} \gamma d_i^{-\beta}\right\} + 1\right) - \frac{\mathrm{var}_{d_i}\left\{\sum_{\mathrm{i}=1}^{\infty} \gamma\, {d_i}^{-\beta}\right\}}{2\left(\mathbb{E}_{d_i}\left\{\sum_{i=1}^{\infty} \gamma d_i^{-\beta}\right\} + 1\right)^2}$$

and

$$\mathrm{var}_{d_i}\left\{\log\left(\sum_{\mathrm{i}=1}^{\infty}\gamma \mathrm{d_i}^{-\beta}+1\right)\right\}\approx\frac{\mathrm{var}_{d_i}\left\{\sum_{\mathrm{i}=1}^{\infty}\gamma {d_i}^{-\beta}\right\}}{\left(\mathbb{E}_{\mathrm{d_i}}\left\{\sum_{\mathrm{i}=1}^{\infty}\gamma \mathrm{d_i}^{-\beta}\right\}+1\right)^2}. \tag{4.23}$$

By plugging (4.20) and (4.21) into (4.22) and (4.23), the expectation and variance of (4.18) and (4.19) are defined.

4.1.4 The Correction Factor $c(\mathbb{E}\{y\})$

For the Log-Rayleigh random variables of (4.18), an infinitely large number of moments can be computed analytically [46]. In addition, the moment generating function (MGF) of the mean interference appearing in (4.18) is also known [4]. Hence, after obtaining the cumulants from the respective moments, an infinitely large number of Taylor terms of (4.5) can be computed analytically for the exact calculation of the bound of (4.4).

However, in the present analysis, the employment of the function $f(y)$ allows for the introduction of a correction factor $c(\mathbb{E}\{y\})$ into the first two terms of the Taylor expansion. This correction by a polynomial function provides extremely accurate results. The correction factor $c(\mathbb{E}\{y\})$ needs to be computed numerically for different values of the path-loss exponent. This computation is performed offline for different path-loss exponents and the obtained results are tabulated in Table 4.1. The derivation of $c(\mathbb{E}\{y\})$ is presented in the Appendix of the chapter.

Table 4.1: The correction factor $c(\mathbb{E}\{y\})$

β	$c(\mathbb{E}\{y\})$
3	-0.0001$(\mathbb{E}\{y\})^5$ + 0.0006$(\mathbb{E}\{y\})^4$ - 0.0044$(\mathbb{E}\{y\})^3$ + 0.0918$(\mathbb{E}\{y\})^2$ - 0.0199$(\mathbb{E}\{y\})$ + 0.6730
4	-0.0002$(\mathbb{E}\{y\})^5$ + 0.0016$(\mathbb{E}\{y\})^4$ - 0.0052$(\mathbb{E}\{y\})^3$ + 0.0937$(\mathbb{E}\{y\})^2$ - 0.0254$(\mathbb{E}\{y\})$ + 0.6059
5	-0.0004$(\mathbb{E}\{y\})^5$ + 0.0023$(\mathbb{E}\{y\})^4$ - 0.0036$(\mathbb{E}\{y\})^3$ + 0.0926$(\mathbb{E}\{y\})^2$ - 0.0293$(\mathbb{E}\{y\})$ + 0.5465

4.1.5 Coordination of Immediate Neighbors

For the particular scenario considered herein, where the first interfering BS is in fact the 7th closest BS to BS_0, the first interferer is not in the vicinity of the UE. As a result of this large value of d_i, (4.23) and the last term of (4.22) tend to zero and (4.18) and

(4.19) are defined as follows:

$$\mathbb{E}\{y\} = \log(\gamma) + \frac{\beta}{2}(\psi + \log(\pi\lambda)) - \psi - \log\left(\lambda \int_{\mathbb{R}^+} \gamma d_i^{-\beta}\, 2\pi d_i dd_i + 1\right), \tag{4.24}$$

and by (4.13) and (4.17) we have:

$$\mathbb{E}\{y - \mathbb{E}\{y\}\}^2 = (\beta^2 + 4)\frac{\pi^2}{24}. \tag{4.25}$$

However, the integration limits of the last term of (4.24) needs to be defined accordingly, taking into account only the interference from BSs farther than the 6th closest BSs to BS_0. By assuming that the UE and the BS_0 are relatively close compared to the distance to the first interferer (which for the considered scenario is actually the case), it can be assumed that the 6th closest BS to BS_0 is in fact the 7th closest BS to the UE (the closest BS to the UE is BS_0). Hence, in order to define the distance between the UE and the first interferer, the distance between the UE and the 7th BS must be defined.

In this direction, the pdf of the distance to the n-th neighbor in a $2-$dimensional PPP is employed, which is given by [47]

$$f_{R_n}(r) = \exp(-\pi\lambda r^2)\frac{2(\lambda\pi r^2)^n}{r\Gamma(n)} \tag{4.26}$$

Hence, the expected distance between the UE and its 7th closest BS is given by

$$\mathbb{E}\{d_7\} = \int_0^\infty d\exp(-\pi\lambda d^2)\frac{2(\lambda\pi d^2)^7}{\Gamma(7)d}dd = \frac{3003}{2048\sqrt{\lambda}}. \tag{4.27}$$

The result of (4.27) can be employed for the lower integration limit of the last term of (4.24). Moreover, since BS_0 coordinates with its 6 closest BSs, this implies that the whole network also coordinates in a similar fashion. Hence, out of the BSs acting as interferers, only one out of seven BSs transmits at any given resource block. Thus, the density of the interferers is in fact $\lambda_I = \frac{\lambda}{7}$ and the last term of (4.24) is given by

$$\mathbb{E}\{\sum_{i\in\Psi} d_i^{-\beta}\mathbf{1}\{d_i \geq \mathbb{E}\{d_7\}\}\} = \int_{\frac{3003}{2048\sqrt{\lambda}}}^\infty d^{-\beta+1}\lambda_I 2\pi dr \overset{\beta>2}{=} \frac{2\pi\lambda}{7(\beta-2)}(\frac{2048\sqrt{\lambda}}{3003})^{\beta-2}. \tag{4.28}$$

Hence, by plugging (4.28) into (4.24), the following holds:

$$\mathbb{E}\{y\} = \log(\gamma) + \frac{\beta}{2}(\psi + \log(\pi\lambda)) - \psi - \log\left(\frac{2\gamma\pi\lambda}{7(\beta-2)}\left(\frac{2048\sqrt{\lambda}}{3003}\right)^{\beta-2} + 1\right). \tag{4.29}$$

The expectation of (4.29) along with the variance of (4.25) can be employed for the computation of the DL ergodic rate by the approximations and bounds of (4.7)-(4.11). For the sake of completeness in the expressions, the approximation of (4.7) is given by:

$$\mathbb{E}\{R\} \approx \log(1 + \exp(E\{y\})) + \left(\mathbb{E}\{y - \mathbb{E}\{y\}\}^2\right)\frac{\exp(E\{y\})}{(1+\exp(E\{y\}))^2}. \tag{4.30}$$

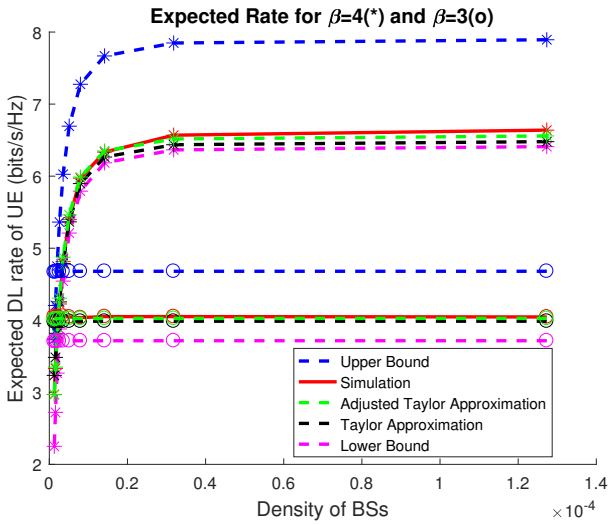

Figure 4.2: Expected DL rate vs density of BSs for different path loss exponents: $\beta = 4$ and $\beta = 3$

4.2 Simulations

In order to demonstrate the tight performance of the extremely tractable approximation of (4.30) and of all bounds and approximations defined in (4.7)-(4.11), the wireless network of Section 4.1.1 has been simulated, encompassing BSs positioned according to a homogeneous PPP of spatial density λ and a reference UE. The 6 closest BSs to BS_0 which serves the UE do not produce any interference. As opposed to those BSs that do not transmit, one in every seven of the remaining BSs is selected randomly and acts as an interferer in the DL. The parameters employed for the calculation of the link budget are tabulated in Table 4.2.

The tight relationship between the obtained analytical expression of (4.7)-(4.11) and the simulated results is manifested in Fig. 4.2, where the ergodic DL rate of the reference UE is plotted for different BS densities and for two different path loss exponents. The tight performance of the expressions verifies the reliability of the preceding analysis and its utility toward devising efficient coordination strategies.

Furthermore, the behavior of the network, demonstrated in Fig. 4.2, corroborates the analyses of Chapters 2 and 3 and the fundamental conclusions of stochastic geometry presented in section 1.1. In particular, for small BS densities, the network operates in the noise limited regime and the expected DL rate increases linearly with the BS density, as suggested by the analysis of Chapter 2 and Fig. 2.4. Subsequently, the network enters the fully loaded interference limited regime and the DL ergodic rate reaches a plateau, being invariant with the BS density, as suggested by the findings of Chapter 3 and Fig.

3.6, as well as the theoretical conclusions of section 1.1 for the fully loaded case.

This consistency of all analyses across all three chapters verifies the validity of the analyses for the noise limited, the interference limited and the general case. Furthermore, the tractability of the derived expressions that quantify the ergodic rate in closed form gives rise to a simple stochastic geometry framework that was not available hitherto. The latter can be employed to reveal trends in the behavior of UDNs and, more importantly, to allow for the resolution of complex optimization problems in UDNs realizing the envisaged rate objectives of UDNs. The work presented in this chapter has been published in [48].

Table 4.2: Link Budget Parameters

Parameter	**Value**
BS Transmit Power P_{BS}	33 dBm
Bandwidth	10 MHz
Noise Power Spectral Density	-174 dBm/Hz
Noise Power σ^2	-104 dBm
Path Loss at Reference Distance L_{ref} (Including Antenna Gains)	25.6 dB
Path Loss Exponent	3 & 4

4.3 Appendix

Langrange Remainder

Following the definition of (4.5) and (4.6), the funcion $f(x) = \log(1 + \exp(x))$ can be expanded around x_0 as follows:

$$f(x) = f(x_0) + f'(x_0)(x - x_0) + R_1(x, x_0), \tag{4.31}$$

where

$$R_1(x, x_0) = \frac{(x - x_0)^2}{2} f''(\zeta(x, x_0)) \tag{4.32}$$

is the Langrange remainder for some $\zeta(x, x_0) \in [x, x_0]$.

Note, that the function $f''(x) = \frac{e^x}{(1+e^x)^2}$ tends to zero for values outside the interval (-6,6). Therefore, the remainder needs to be defined only within this interval. By employing (4.31), $\mathbb{E}\{R_1(x, x_0)\}$ can be computed numerically in this particular interval. That is, by assuming that x follows a log−Rayleigh distribution, which is the case if the interference is disregarded. The analysis can be repeated taking also the statistics of the interference into account. However, in this case the accuracy gain is minimal and by far outweighed by the complexity introduced in the analysis.

Adjusting correction factor $c(\mathbb{E}\{y\})$

In order to compute $\mathbb{E}\{f(\cdot)\} = \mathbb{E}\{\log(1+\exp(\cdot))\}$, the series is expanded around $\mathbb{E}\{y\}$, and ,by employing (4.31), (4.11) and (4.25), we obtain:

$$\mathbb{E}\{f(y)\} = f(E\{y\}) + \mathbb{E}\{R_1(x, E\{y\})\} = f(E\{y\}) + c(E\{y\})f''(E\{y\})(\beta^2+4)\frac{\pi^2}{24}. \tag{4.33}$$

Having defined $\mathbb{E}\{R_1(x, x_0)\}$ numerically, $c(\mathbb{E}\{y\})$ can be expressed employing (4.33) for different values of β. The numerically obtained correction factor $c(\mathbb{E}\{y\})$ is then approximated by a polynomial approximation and the results are tabulated in Table 4.1 for different values of β.

Chapter 5

Revisiting the Entrenched Stochastic Geometry Framework

Having derived closed form expressions for the ergodic rate in the noise limited, the interference limited, and the general case in the previous chapters, we have already given rise to a closed-form stochastic geometry framework that can simplify relevant analyses to a great extent. Thus, giving rise to a framework that can reveal trends in the behavior of UDNs and, more importantly, allow for the resolution of complex optimization problems toward achieving the envisaged rate objectives of UDNs.

However, even though the ergodic rate (quantified in a closed form above) is the most sensible figure of merit for evaluating and optimizing the performance of the network, the aforementioned analysis cannot be easily extended to different figures of merit, if the latter is of interest. Moreover, the emerging stochastic geometry approaches consider more complex scenarios giving rise to expressions characterized by significant intractability. Therefore, even though the derivation of tractable approximations for these expressions (with approaches similar to those of Chapters 2-4) could allow for the resolution of the emerging complex problems, the unabated increase of the intractability of the stochastic geometry frameworks makes this a challenging task. Hence, if stochastic geometry is to be used in practice for the design and modeling of UDNs, a novel approach needs to be developed able to transform the entrenched intractable frameworks.

In this course, the present analysis diverges from the entrenched approach that focuses on the MGF of the interference and the coverage probability, and attempts to revisit the stochastic geometry framework by addressing one of the fundamental problems that remains open since the introduction of stochastic geometry in wireless networks. This problem is the development of an accurate approximation for the PDF of the inter-cell interference in the DL. The PDF of the interference would characterize the random variable of the interference explicitly, giving rise to a innovative approach for the analysis of UDNs. In this course, the present chapter introduces an accurate approximation for

the PDF of the interference for a particular path loss exponent value.

5.1 Approximate PDF of the Aggregate Other-cell Interference

The wireless cellular network considered in the present chapter is the same as that of section 3.1 and the aggregate other-cell interference g (or inter-cell interference for brevity) is the one mathematically formulated in (3.1). Once again the inter-cell interference is defined without taking into account the fast fading of the interferers. However, since the objective of the present chapter is the development of an analytical expression for the PDF of the aggregate interference, this will allow for averaging over the inter-cell interference and over the fast fading of the interferers successively, if the latter is of interest. Having defined the considered network scenario and the inter-cell interference in the DL, we can proceed with the mathematical formulation of an approximation of the characteristic function (CF) of g following an approach similar to that of Chapter 3. Since the CF constitutes the Fourier transform of the PDF, the inverse Fourier transform of the CF approximation will allow for the computation of an approximation of the PDF of the inter-cell interference at the end of the present section.

5.1.1 Derivation of the CF

The CF of the inter-cell interference g is obtained as follows:

$$\begin{aligned}
\phi_g\left(t; L^{(0)}\right) =& \mathbb{E}_\Psi\left\{\exp\left(-jtg\right)\right\} \\
=& \mathbb{E}_\Psi\left\{\exp\left(-jt\sum_{x\in\Psi}\frac{P_{\text{tx}}}{L^{(x)}}\,\mathbf{1}\left(L^{(x)} > L^{(0)}\right)\right)\right\} \\
=& \mathbb{E}_\Psi\left\{\prod_{x\in\Psi}\exp\left(-jt\frac{P_{\text{tx}}}{L^{(x)}}\,\mathbf{1}\left(L^{(x)} > L^{(0)}\right)\right)\right\} \\
\overset{(a)}{=}& \exp\left(\int_{L^{(0)}}^{\infty}\left(\exp\left(-jt\frac{P_{\text{tx}}}{y}\right)-1\right)\left(\frac{2\pi\lambda}{\beta}\left(\frac{1}{\kappa}\right)^{\frac{2}{\beta}}y^{\frac{2}{\beta}-1}\right)dy\right) \\
\overset{(b)}{=}& \exp\left(\pi\lambda\left(\frac{L^{(0)}}{\kappa}\right)^{\frac{2}{\beta}}\left(1-{}_1F_1\left(-\frac{2}{\beta},1-\frac{2}{\beta},\frac{-jtP_{\text{tx}}}{L^{(0)}}\right)\right)\right), t\in\mathbb{R},
\end{aligned} \tag{5.1}$$

where j denotes the imaginary unit, and all steps of (5.1) hold by following the derivations of (3.4), with (a) holding by employing (3.3c), and (b) being attained by using the result of (3.5) which also holds for imaginary arguments.

Having derived the CF of g, an accurate approximation of (5.1) can be derived following an approach similar to that of (3.8), but tailored to the imaginary argument of the CF. Hence, the CF of (5.1a) can be revised as follows:

$$
\begin{aligned}
&\phi_g\left(t; L^{(0)}\right) \\
&\overset{(a)}{=} \exp\left(\int_{L^{(0)}}^{\infty}\left(\exp\left(-jt\frac{P_{\text{tx}}}{y}\right)-1\right)\left(\frac{2\pi\lambda}{\beta}\left(\frac{1}{\kappa}\right)^{\frac{2}{\beta}} y^{\frac{2}{\beta}-1}\right)dy\right) \\
&\overset{(b)}{=} \exp\left(\int_{L^{(0)}}^{\infty}\left(\sum_{n=1}^{\infty}\frac{1}{n!}\left(-jt\frac{P_{\text{tx}}}{y}\right)^{n}\right)\left(\frac{2\pi\lambda}{\beta}\left(\frac{1}{\kappa}\right)^{\frac{2}{\beta}} y^{\frac{2}{\beta}-1}\right)dy\right) \\
&\overset{(c)}{=} \exp\left(\frac{2\pi\lambda}{\beta}\left(\frac{L^{(0)}}{\kappa}\right)^{\frac{2}{\beta}}\left(\sum_{n=1}^{\infty}\frac{(-1)^{n+1}(jtP_{\text{tx}})^{n}}{\left(L^{(0)}\right)^{n} n!(\frac{2}{\beta}-n)}\right)\right) \\
&\overset{(d)}{=} \exp\left(-\pi\lambda\left(\frac{L^{(0)}}{\kappa}\right)^{\frac{2}{\beta}}\left(\exp\left(\frac{-jtP_{\text{tx}}}{L^{(0)}}\right)-1+\left(\frac{jtP_{\text{tx}}}{L^{(0)}}\right)^{\frac{2}{\beta}}\Gamma\left(1-\frac{2}{\beta},0,\frac{jtP_{\text{tx}}}{L^{(0)}}\right)\right)\right) \\
&\overset{(e)}{=} \exp\left(-\pi\lambda\left(\frac{L^{(0)}}{\kappa}\right)^{\frac{2}{\beta}}\left(\exp\left(\frac{-jtP_{\text{tx}}}{L^{(0)}}\right)-1+\left(\frac{jtP_{\text{tx}}}{L^{(0)}}\right)^{\frac{2}{\beta}}\int_{0}^{\frac{jtP_{\text{tx}}}{L^{(0)}}} t^{-\frac{2}{\beta}}\exp(-t)dt\right)\right), \\
&t\in\mathbb{R},
\end{aligned}
\tag{5.2}
$$

where (b) holds by employing the Taylor expansion of the exponential term, (c) holds by a simple calculation of the integral, and (d) and (e) are obtained from the definition of the generalized incomplete gamma function $\Gamma(\cdot,\cdot,\cdot)$.

In order to derive a tractable approximation of the CFwe need to approximate the term $\Gamma\left(1-\frac{2}{\beta},0,\frac{jtP_{\text{tx}}}{L^{(0)}}\right)$ of (5.2d), which it should be noted that is a complex function. Hence, the piecewise approximation of (3.9) involving a constant value when $\exp(\frac{tP_{\text{tx}}}{L^{(0)}}) \approx 0$ cannot be employed. In the complex domain, $\Gamma\left(1-\frac{2}{\beta},0,\frac{jtP_{\text{tx}}}{L^{(0)}}\right)$ does not converge to a constant value, but oscillates in the form of a sinusoid around this constant value. Hence, $\Gamma\left(1-\frac{2}{\beta},0,\frac{jtP_{\text{tx}}}{L^{(0)}}\right)$ can be approximated in the complex domain by a piecewise function involving for the first piece the Taylor expansion around 0 and for the second piece a damped sinusoid around a constant value, as follows:

$$
\Gamma\left(1-\frac{2}{\beta},0,jx\right) \overset{(a)}{\approx} \begin{cases} -(jx)^{-\frac{2}{\beta}}\sum_{n=1}^{\infty}\frac{\beta(-jx)^{n}}{(n-1)!(n\beta-2)}, & x<c, \\ -e^{-jx}(jx)^{-\frac{2}{\beta}}+\Gamma\left(1-\frac{2}{\beta}\right), & x>c \end{cases}
$$

$$\overset{(b)}{\approx} \begin{cases} -(jx)^{-\frac{2}{\beta}} \sum_{n=1}^{\infty} \frac{\beta(-jx)^n}{(n-1)!(n\beta-2)}, & x < c, \\ -e^{-jx}e^{-j\pi/\beta}(x)^{-\frac{2}{\beta}} + \Gamma\left(1-\frac{2}{\beta}\right), & x > c \end{cases} \tag{5.3}$$

where $x \in \mathbb{R}$.

Thus, by introducing (5.3) into (5.2d) and by keeping only the first two Taylor terms of (5.3) the following holds:

$$\begin{aligned}
&\phi_g\left(t; L^{(0)}\right) \\
&\overset{(a)}{=} \exp\left(\left[\pi\lambda\left(\frac{L^{(0)}}{\kappa}\right)^{\frac{2}{\beta}}\left(1 - {}_1F_1\left(-\frac{2}{\beta}, 1-\frac{2}{\beta}, \frac{-jtP_{\text{tx}}}{L^{(0)}}\right)\right)\right]\right) \\
&\overset{(b)}{\approx} \Re\left\{\exp\left(-\pi\lambda\left(\frac{L^{(0)}}{\kappa}\right)^{\frac{2}{\beta}}\left(\frac{2\left(\frac{jtP_{\text{tx}}}{L^{(0)}}\right)}{(\beta-2)} + \frac{\left(\frac{tP_{\text{tx}}}{L^{(0)}}\right)^2}{(2\beta-2)}\right)\right)\right\}\mathbf{1}\left(\frac{tP_{\text{tx}}}{L^{(0)}} \le c\right) \\
&\quad + \Re\left\{\exp\left(\pi\lambda\left(\frac{L^{(0)}}{\kappa}\right)^{\frac{2}{\beta}}\left(1 - \left(\frac{jtP_{\text{tx}}}{L^{(0)}}\right)^{\frac{2}{\beta}}\Gamma\left(1-\frac{2}{\beta}\right)\right)\right)\right\}\mathbf{1}\left(\frac{tP_{\text{tx}}}{L^{(0)}} > c\right) \\
&\quad + j\Im\left\{\exp\left(-\pi\lambda\left(\frac{L^{(0)}}{\kappa}\right)^{\frac{2}{\beta}}\left(\frac{2\left(\frac{jtP_{\text{tx}}}{L^{(0)}}\right)}{(\beta-2)} + \frac{\left(\frac{tP_{\text{tx}}}{L^{(0)}}\right)^2}{(2\beta-2)}\right)\right)\right\}\mathbf{1}\left(\frac{tP_{\text{tx}}}{L^{(0)}} \le d\right) \\
&\quad + j\Im\left\{\exp\left(\pi\lambda\left(\frac{L^{(0)}}{\kappa}\right)^{\frac{2}{\beta}}\left(1 - \left(\frac{jtP_{\text{tx}}}{L^{(0)}}\right)^{\frac{2}{\beta}}\Gamma\left(1-\frac{2}{\beta}\right)\right)\right)\right\}\mathbf{1}\left(\frac{tP_{\text{tx}}}{L^{(0)}} > d\right), \\
&t \in \mathbb{R},
\end{aligned} \tag{5.4}$$

where (a) is given by (5.1b) and is provided for the sake of completeness, and (b) is obtained from the introduction of (5.3) into (5.2d). In (b), the symbol $\Re\{\cdot\}$ denotes the real part, and the symbol $\Im\{\cdot\}$ the imaginary part. Moreover, c denotes the point of intersection of the two functions comprising the CF in the real domain and d the point of intersection of the two functions in the imaginary domain.

In order to derive the PDF of g the inverse Fourier transform of the CF of g needs to be computed. The inverse Fourier of (5.4a) cannot be computed, hence the PDF of the interference had not been analytically formulated hitherto. However, the inverse Fourier of (5.4b) can be computed analytically for $\beta = 4$, allowing for the analytical formulation of the PDF of the inter-cell interference g. (For $\beta \neq 4$ the inverse Fourier of the CF cannot be computed. However, the analysis can be extended employing the expressions derived herein and this will be done in future work.)

For $\beta = 4$, the following holds $\sqrt{j} = (1+j)/\sqrt{2}$ and the CF of (5.4b) is given by:

$$\begin{aligned}\phi_g\left(t;a\right) \approx & \exp\left(\frac{a\left(\frac{tP_{\mathrm{tx}}}{L^{(0)}}\right)^2}{6}\right)\cos\left(a\frac{tP_{\mathrm{tx}}}{L^{(0)}}\right)\mathbf{1}\left(\frac{tP_{\mathrm{tx}}}{L^{(0)}}\leq c\right)\\ & + \exp\left(a\left(\sqrt{\pi\frac{tP_{\mathrm{tx}}}{L^{(0)}}}-1\right)\right)\cos\left(a\sqrt{\pi\frac{tP_{\mathrm{tx}}}{L^{(0)}}}\right)\mathbf{1}\left(c<\frac{tP_{\mathrm{tx}}}{L^{(0)}}\right)\\ & + j\exp\left(\frac{a\left(\frac{tP_{\mathrm{tx}}}{L^{(0)}}\right)^2}{6}\right)\sin\left(a\frac{tP_{\mathrm{tx}}}{L^{(0)}}\right)\mathbf{1}\left(\frac{tP_{\mathrm{tx}}}{L^{(0)}}\leq d\right)\\ & + j\exp\left(a\left(\sqrt{\pi\frac{tP_{\mathrm{tx}}}{L^{(0)}}}-1\right)\right)\sin\left(a\sqrt{\pi\frac{tP_{\mathrm{tx}}}{L^{(0)}}}\right)\mathbf{1}\left(d<\frac{tP_{\mathrm{tx}}}{L^{(0)}}\right),\quad t\in\mathbb{R},\end{aligned}\tag{5.5}$$

where $a=-\pi\lambda\sqrt{\frac{L^{(0)}}{\kappa}}$. Moreover, c is the point of intersection of the two functions comprising the real part of (5.5) and can be obtained by solving the following equation:

$$\exp\left(\frac{ac^2}{6}\right)\cos\left(ac\right)=\exp\left(a\left(\sqrt{\frac{\pi c}{2}}-1\right)\right)\cos\left(a\sqrt{\frac{\pi c}{2}}\right).\tag{5.6}$$

Respectively, d is the point of intersection of the two functions comprising the imaginary part of (5.5) and can be obtained by solving the following equation:

$$\exp\left(\frac{ac^2}{6}\right)\sin\left(ac\right)=\exp\left(a\left(\sqrt{\frac{\pi c}{2}}-1\right)\right)\sin\left(a\sqrt{\frac{\pi c}{2}}\right).\tag{5.7}$$

Note that (5.6) and (5.7) are transcendental equations that cannot be solved analytically. However, c and d can be approximated through the graphical representation of the implicit curves of (5.6) and (5.7). This graphical approach is a widely used method for solving transcendental equations. Moreover, given the plethora of the solutions satisfying (5.6) and (5.7), the graphical approach allows for selecting the ones providing the best approximation of (5.1a). Thus, after selecting the solutions of the implicit curves of (5.6) and (5.7) that provide the best matching of (5.4a), c and d can be approximated by piecewise functions as follows:

$$c=\begin{cases}0.47a+0.75 & -0.4\leq a\leq 0\\ 0.42a+2.03 & -2.4\leq a<-0.4\\ 0.28a+2.43 & -4.4\leq a<-2.4\\ 0.53a+4.7 & -5\leq a<-4.4\\ 2 & a<-5\end{cases}\tag{5.8}$$

$$d = \begin{cases} 1.37 & -0.4 \leq a \leq 0 \\ 1.9a + 4.06 & -1.1 \leq a < -0.4 \\ 0.41a + 2.42 & -2.4 \leq a < -1.1 \\ 0.33a + 2.89 & -4.4 \leq a < -2.4 \\ 2.8 & a < -4.4 \end{cases} \tag{5.9}$$

where $c < d$ for all values of a.

5.1.2 Derivation of the Approximate PDF

Having defined the previous approximation of the CF of the aggregate interference for $\beta = 4$, an approximation of the PDF of the aggregate inter-cell interference can be derived by the inverse Fourier transform of (5.5). The formulation of an approximate PDF will provide valuable insight into the behavior of the PDF which will be subsequently exploited to provide a rigorous formulation of the PDF employing known probability distributions. The approximate PDF $f_g(g)$ can be derived by the inverse Fourier transform of the CF as follows:

$$f_g(g) = \frac{1}{2\pi} \int_{\mathbb{R}} \exp(jtg)\, \phi_g(t) dt. \tag{5.10}$$

Employing (5.5), the argument of the integral of (5.10), for $c \leq d$ is given by:

$$\begin{aligned} &\exp(jtg)\, \phi_g(t) = \\ &\exp\left(\frac{ax^2}{6}\right) \left(\cos(x(b+a))\, \mathbf{1}_{(x \leq c)} - \sin(ax) \sin(bx) \mathbf{1}_{(c < x \leq d)}\right) \\ &+ \exp\left(a\left(\sqrt{\frac{\pi x}{2}} - 1\right)\right) \left(\cos\left(xb + a\sqrt{\frac{\pi x}{2}}\right) \mathbf{1}_{(d < x)} + \cos\left(a\sqrt{\frac{\pi x}{2}}\right) \cos(bx) \mathbf{1}_{(c < x \leq d)}\right) \\ &+ j \exp\left(\frac{ax^2}{6}\right) \left(\sin(x(a+b))\, \mathbf{1}_{(x \leq c)} + \sin(ax) \cos(bx) \mathbf{1}_{(c < x \leq d)}\right) \\ &+ j \exp\left(a\left(\sqrt{\frac{\pi x}{2}} - 1\right)\right) \left(\sin\left(a\sqrt{\frac{\pi x}{2}} + bx\right) \mathbf{1}_{(d < x)} + \cos\left(a\sqrt{\frac{\pi x}{2}}\right) \sin(bx) \mathbf{1}_{(c < x \leq d)}\right), \end{aligned} \tag{5.11}$$

where $x = \frac{tP_{\text{tx}}}{L^{(0)}}$, $b = \frac{gL^{(0)}}{P_{\text{tx}}}$ and, as already mentioned, $a = -\pi\lambda\sqrt{\frac{L^{(0)}}{\kappa}}$.

Employing (5.10) and (5.11), and since (5.11) is Hermitian, the PDF $f_g(g)$ is given by:

$$
\begin{aligned}
f_g(g) &= \frac{1}{\pi}\int_0^{\infty} \Re\{\exp(jtg)\,\phi_g(t)\}dt \\
&= \frac{L^{(0)}}{\pi P_{\text{tx}}}\Bigg(\int_0^{c}\exp\left(\frac{ax^2}{6}\right)\cos\left(x(b+a)\right)dx - \int_c^{d}\exp\left(\frac{ax^2}{6}\right)\sin(ax)\sin(bx)dx \\
&\quad + \int_c^{d}\exp\left(a\left(\sqrt{\frac{\pi x}{2}}-1\right)\right)\cos\left(a\sqrt{\frac{\pi x}{2}}\right)\cos(bx)dx \\
&\quad + \int_d^{\infty}\exp\left(a\left(\sqrt{\frac{\pi x}{2}}-1\right)\right)\cos\left(xb+a\sqrt{\frac{\pi x}{2}}\right)dx\Bigg).
\end{aligned} \tag{5.12}
$$

The constituent integrals of (5.12) can be computed in closed form as detailed in the Appendix of the chapter. Hence, combining (5.12), (5.36), (5.37), (5.38), and (5.41), the PDF of the inter-cell interference is given by:

$$
\begin{aligned}
&f_g(g) = \\
&\frac{-w\pi a e^{\frac{\pi a^2}{4gw}-a}}{\pi 4(gw)^{3/2}}\left(\Im\left(\text{erf}\left(\frac{-\sqrt{\pi}a+\sqrt{2}(1+j)\sqrt{c}gw}{2\sqrt{gw}}\right)\right)-\Im\left(\text{erf}\left(\frac{-\sqrt{\pi}a+\sqrt{2}(1+j)\sqrt{d}gw}{2\sqrt{gw}}\right)\right)\right) \\
&+\frac{w\pi a e^{-\frac{\pi a^2}{4gw}-a}}{\pi 4(gw)^{3/2}}\left(\Re\left(\text{erf}\left(\frac{j\sqrt{\pi}a+\sqrt{2}(1+j)\sqrt{c}gw}{2\sqrt{gw}}\right)\right)+\Re\left(\text{erf}\left(\frac{j\sqrt{\pi}a+\sqrt{2}(1+j)\sqrt{d}gw}{2\sqrt{gw}}\right)\right)\right) \\
&-\frac{w}{\pi 2\sqrt{-a}}\sqrt{\frac{3\pi}{2}}e^{\frac{3(a+gw)^2}{2a}}\left(\Re\left(\text{erf}\left(\frac{ac+3j(a+gw)}{\sqrt{6}\sqrt{-a}}\right)\right)+\Re\left(\text{erf}\left(\frac{ad+3j(a+gw)}{\sqrt{6}\sqrt{-a}}\right)\right)\right) \\
&-\frac{w}{\pi 2\sqrt{-a}}\sqrt{\frac{3\pi}{2}}e^{\frac{3(a-gw)^2}{2a}}\left(\Re\left(\text{erf}\left(\frac{ac+3j(a-gw)}{\sqrt{6}\sqrt{-a}}\right)\right)-\Re\left(\text{erf}\left(\frac{ad+3j(a-gw)}{\sqrt{6}\sqrt{-a}}\right)\right)\right) \\
&-\frac{we^{-a}}{gw\pi 2\sqrt{-a}}\left(e^{\sqrt{\frac{\pi}{2}}a\sqrt{c}}\cos\left(\sqrt{\frac{\pi}{2}}a\sqrt{c}\right)\sin(cgw)+e^{\sqrt{\frac{\pi}{2}}a\sqrt{d}}\sin\left(\sqrt{\frac{\pi}{2}}a\sqrt{d}\right)\cos(dgw)\right) \\
&-\frac{ae^{-\frac{\pi a^2}{4wg}-a}}{2\sqrt{w}g^{3/2}},
\end{aligned} \tag{5.13}
$$

where $w = \frac{L^{(0)}}{P_{\text{tx}}}$, $a = -\pi\lambda\sqrt{\frac{L^{(0)}}{\kappa}}$, c is a function of a given by (5.8) and d is also a function of a given by (5.9).

5.1.3 PDF and Moments of the Aggregate Other-cell Interference

The PDF of (5.13) allows us to formulate the PDF of the inter-cell interference in closed form and to study its behavior. The parameters a and w that govern the behavior of the PDF of (5.13) also govern the behavior of the MGF which is defined in (3.4a) and (3.4b) and repeated here to facilitate the perusal of the present analysis:

$$M_g\left(s;L^{(0)}\right) \overset{(a)}{=} \exp\left(\int_{L^{(0)}}^{\infty}\left(\exp\left(-s\frac{P_{\text{tx}}}{y}\right)-1\right)\frac{2\pi\lambda}{\beta}\left(\frac{1}{\kappa}\right)^{\frac{2}{\beta}} y^{\frac{2}{\beta}-1}dy\right)$$
$$\overset{(b)}{=} \exp\left(\pi\lambda\left(\frac{L^{(0)}}{\kappa}\right)^{\frac{2}{\beta}}\left(1-{}_1F_1\left(-\frac{2}{\beta},1-\frac{2}{\beta},\frac{-sP_{\text{tx}}}{L^{(0)}}\right)\right)\right),$$
$$s\in\mathbb{R}. \tag{5.14}$$

Employing (5.14b) and the parameters a and w the cumulant generating function (CGF) for $\beta = 4$ is defined as follows:

$$K_g(s;a) = a\left({}_1F_1\left(-\frac{1}{2},\frac{1}{2},\frac{-s}{w}\right)-1\right), s\in\mathbb{R}. \tag{5.15}$$

Differentiating $K_g(s;a)$ n times with respect to s and setting $s = 0$, we obtain the respective n_{th} cumulant. After differentiating (5.15) the n_{th} cumulant, for $n \leq 5$, is given by:

$$k_n = -\frac{aw^{-n}}{2n-1}. \tag{5.16}$$

Hence, the mean of the inter-cell interference is given by:

$$\mu = k_1 = -\frac{a}{w}, \tag{5.17}$$

and the variance of the inter-cell interference is given by:

$$\sigma^2 = k_2 = -\frac{a}{3w^2}. \tag{5.18}$$

Having defined the cumulants and, implicitly, the moments of the inter-cell interference, we can verify the validity of the approximate PDF of (5.13) with respect to its moments and, subsequently, study its behavior. In this course, the PDF is plotted for three different sets of the parameters a and w. The selected parameters give rise to three PDFs of different mean values μ that demonstrate the three different behaviors of Fig. 5.1-5.3. In particular, Fig. 5.1 demonstrates the behavior of the PDF for $a = -0.1$, $w = 1$ and $\mu = 0.1$, with every PDF of smaller mean interference retaining the same shape. Fig. 5.2 demonstrates the behavior of the PDF for $a = -1$, $w = 1$ and $\mu = 1$ and Fig. 5.3 demonstrates the behavior of the PDF for $a = -5$, $w = 1$ and $\mu = 5$ with every PDF of higher mean interference retaining the same shape.

The area of all PDFs of Fig. 5.1- 5.3 is equal to 1 and the mean and variance is equal to the mean and variance given by (5.17) and (5.18). However, Fig. 5.1- 5.3 demonstrate that the derived approximate PDF is not always positive, oscillating around 0. This oscillation is a corollary of the fact that (5.13) is an approximation of the actual PDF.

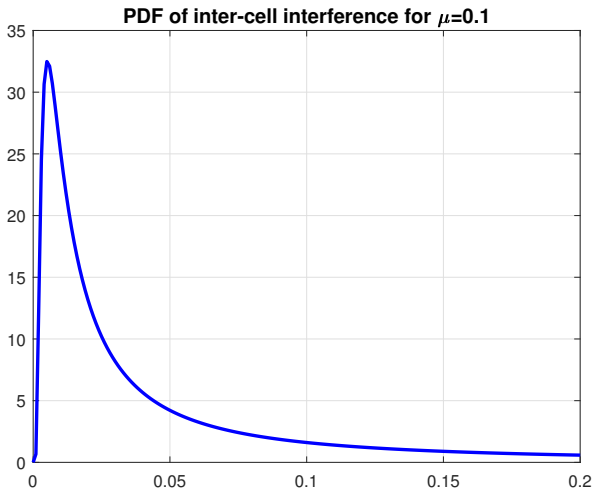

Figure 5.1: PDF of inter-cell interference of (5.13) for $a = -0.1$, $w = 1$, and $\mu = 0.1$.

However, because of these negative values, the expression defined in (5.13), cannot be employed as a PDF per se, but it can be proven to be a significant tool in defining the PDF based on well-known probability distributions as will be demonstrated in the following section.

5.2 Defining the PDF of the Aggregate Other-cell Interference: a Pearson Moment Matching Approach

5.2.1 The Pearson System of Distributions

The formulation of the cumulants in (5.16) that define the moments of the PDF and the derivation of (5.13), which defines the shape of the PDF, provide all necessary pieces to define explicitly the PDF based on known probability distributions. In this course, the Pearson system of distributions is employed [49], [50]. A Pearson density function $y_X(x)$ is defined to be any valid solution to the differential equation:

$$\frac{dy}{dx} = \frac{y(m-x)}{p_1 + p_2 x + p_3 x^2}. \tag{5.19}$$

The Pearson system of distributions comprises a wide range of known distributions such as the normal, the beta, the gamma, etc. with each one corresponding to a different type of Pearson distribution. Moreover, it provides an extremely tractable framework for moment matching, allowing for defining the parameters p_1, p_2, p_3 and m as functions of the moments of the distribution in hand. Further to that, the approximate PDF of (5.13) can be used as a guideline, to ensure that the derived Pearson distribution also

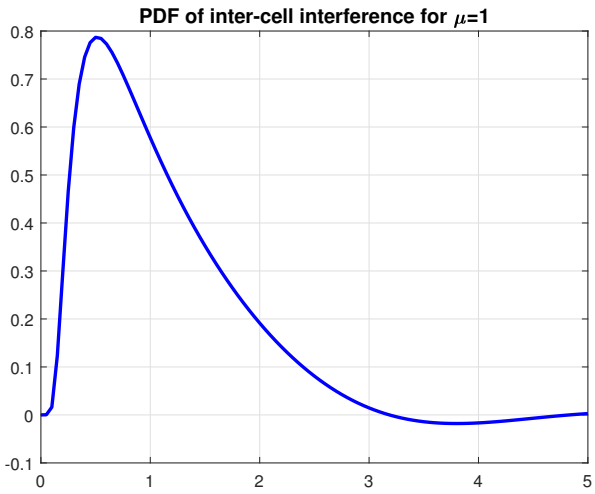

Figure 5.2: PDF of inter-cell interference of (5.13) for $a = -1$, $w = 1$, and $\mu = 1$.

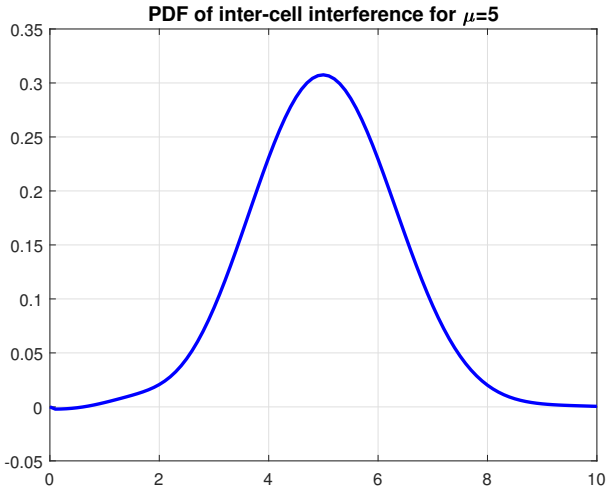

Figure 5.3: PDF of inter-cell interference of (5.13) for $a = -5$, $w = 1$, and $\mu = 5$.

matches the shape of the probability in hand. Hence, the Pearson system of distributions constitutes an ideal framework for matching the PDF of the inter-cell interference defined by (5.16) and (5.13) to a known probability distribution.

In order to map the PDF of the aggregate interference to the right type of Pearson distribution based on the moments of the former, the K-criterion is employed [51], where K is given by:

$$K = \frac{\beta_1(\beta_2+3)^2}{4(4\beta_2-3\beta_1)(-3\beta_1+2\beta_2-6)}, \tag{5.20}$$

where, $\beta_1 = \frac{k_3^2}{k_2^3}$ denotes the skewness, $\beta_2 = \frac{k_4+3k_2^2}{k_2^2}$ the kurtosis and k_n the n_{th} cumulant. Employing (5.16) we obtain:

$$K = -\frac{27\left(\frac{9w^4\left(\frac{a^2}{3w^4}-\frac{a}{7w^4}\right)}{a^2}+3\right)^2}{100a\left(\frac{18w^4\left(\frac{a^2}{3w^4}-\frac{a}{7w^4}\right)}{a^2}+\frac{81}{25a}-6\right)\left(\frac{36w^4\left(\frac{a^2}{3w^4}-\frac{a}{7w^4}\right)}{a^2}+\frac{81}{25a}\right)}, \tag{5.21}$$

and since $a<0$ and $w\in\mathbb{R}$, it holds that $K<0$. Since $K<0$ the PDF is given by the Pearson distribution type I [51], which is given by:

$$y_X(x) = \frac{2^{\frac{1}{p_3}-1}\left(\frac{p_2^2}{4p_3^2}-\frac{p_1}{p_3}\right)^{\frac{1}{2}\left(\frac{1}{p_3}-1\right)}\left(\sqrt{\frac{p_2^2}{4p_3^2}-\frac{p_1}{p_3}}-\frac{p_2}{2p_3}-x\right)^{-\frac{-m+\sqrt{\frac{p_2^2}{4p_3^2}-\frac{p_1}{p_3}}-\frac{p_2}{2p_3}}{2p_3\sqrt{\frac{p_2^2}{4p_3^2}-\frac{p_1}{p_3}}}}\left(\sqrt{\frac{p_2^2}{4p_3^2}-\frac{p_1}{p_3}}+\frac{p_2}{2p_3}+x\right)^{\frac{-m-\sqrt{\frac{p_2^2}{4p_3^2}-\frac{p_1}{p_3}}-\frac{p_2}{2p_3}}{2p_3\sqrt{\frac{p_2^2}{4p_3^2}-\frac{p_1}{p_3}}}}}{B\left(\frac{-m-\sqrt{\frac{p_2^2}{4p_3^2}-\frac{p_1}{p_3}}-\frac{p_2}{2p_3}}{2\sqrt{\frac{p_2^2}{4p_3^2}-\frac{p_1}{p_3}}p_3}+1,1-\frac{-m+\sqrt{\frac{p_2^2}{4p_3^2}-\frac{p_1}{p_3}}-\frac{p_2}{2p_3}}{2\sqrt{\frac{p_2^2}{4p_3^2}-\frac{p_1}{p_3}}p_3}\right)}, \tag{5.22}$$

for $-\sqrt{\frac{p_2^2}{4p_3^2}-\frac{p_1}{p_3}}-\frac{p_2}{2p_3} < x < \sqrt{\frac{p_2^2}{4p_3^2}-\frac{p_1}{p_3}}-\frac{p_2}{2p_3}$

5.2.2 Pearson Moment Matching

Having defined the type of Pearson distribution that matches the PDF in hand, the parameters p_1, p_2, p_3 and m of (5.22) need to be defined based on the moments given by the cumulants of (5.16). In this direction, the Pearson recursive relationship can be employed, associating the Pearson parameters to the raw moments of the distribution. This recursive relationship is defined as follows [50]:

$$p_1\cdot n\cdot r_{n-1} + p_2\cdot(n+1)\cdot r_n + p_3\cdot(n+2)\cdot r_{n+1} = -m\cdot r_n + r_{n+1}, \tag{5.23}$$

where r_n denotes the n_{th} raw moment.

Since $r_0 = 1$, four independent equations can emerge from (5.23) for $0 \leq n \leq 3$ allowing us to define the parameters p_1, p_2, p_3 and m as follows:

$$\begin{aligned}
p_1 &= -\frac{-r_0r_1r_3r_4 + 4r_0r_2^2r_4 - 3r_0r_2r_3^2 - 3r_1^2r_2r_4 + 4r_1^2r_3^2 - r_1r_2^2r_3}{2\left(-5r_0^2r_2r_4 + 6r_0^2r_3^2 + 5r_0r_1^2r_4 - 16r_0r_1r_2r_3 + 9r_0r_2^3 + 4r_1^3r_3 - 3r_1^2r_2^2\right)},\\
p_2 &= -\frac{r_0^2r_3r_4 - 7r_0r_1r_2r_4 + 2r_0r_1r_3^2 + 3r_0r_2^2r_3 + 6r_1^3r_4 - 8r_1^2r_2r_3 + 3r_1r_2^3}{2\left(-5r_0^2r_2r_4 + 6r_0^2r_3^2 + 5r_0r_1^2r_4 - 16r_0r_1r_2r_3 + 9r_0r_2^3 + 4r_1^3r_3 - 3r_1^2r_2^2\right)},\\
p_3 &= -\frac{2r_0^2r_2r_4 - 3r_0^2r_3^2 - 2r_0r_1^2r_4 + 10r_0r_1r_2r_3 - 6r_0r_2^3 - 4r_1^3r_3 + 3r_1^2r_2^2}{2\left(-5r_0^2r_2r_4 + 6r_0^2r_3^2 + 5r_0r_1^2r_4 - 16r_0r_1r_2r_3 + 9r_0r_2^3 + 4r_1^3r_3 - 3r_1^2r_2^2\right)},\\
m &= -\frac{-r_0^2r_3r_4 + 13r_0r_1r_2r_4 - 8r_0r_1r_3^2 - 3r_0r_2^2r_3 - 12r_1^3r_4 + 20r_1^2r_2r_3 - 9r_1r_2^3}{2\left(-5r_0^2r_2r_4 + 6r_0^2r_3^2 + 5r_0r_1^2r_4 - 16r_0r_1r_2r_3 + 9r_0r_2^3 + 4r_1^3r_3 - 3r_1^2r_2^2\right)}.
\end{aligned} \tag{5.24}$$

The raw moments can be derived directly from the cumulants as follows:

$$r_0 = 1; r_1 = k_1; r_2 = k_1^2 + k_2; r_3 = k_1^3 + 3k_1k_2 + k_3; r_4 = k_1^4 + 6k_1^2k_2 + 4k_1k_3 + 3k_2^2 + k_4; \tag{5.25}$$

Hence, employing (5.16), (5.25) and (5.24), the parameters p_1, p_2, p_3 and m are given by:

$$p_1 = \frac{a(47a - 24)}{6(350a + 3)w^2}, \tag{5.26}$$

$$p_2 = -\frac{45 - 288a}{700aw + 6w}, \tag{5.27}$$

$$p_3 = \frac{39}{6 + 700a}, \tag{5.28}$$

$$m = \frac{-700a^2 - 216a + 45}{700aw + 6w}. \tag{5.29}$$

The distribution of (5.22) and the parameters (5.26)-(5.29) give rise to a PDF that has the first four moments equal to the first four moments of the MGF of (5.14b). However, apart from the moments of the distribution, the shape of the distribution must also coincide with the shape of the approximate PDF of (5.13).

In this course, it should be noted that the approximate PDF is unimodal and the derived PDF must exhibit the same behavior. If a Pearson distribution $y_X(x)$ is unimodal, the location of its mode is at $x = m$ [50]. Hence, since the PDF in hand is always unimodal, m is always equal to the mode, i.e. equal to the value of the interference that has the maximum likelihood. However, the value of the interference can only be positive, therefore m must always be positive as well. In a different case the shape of the Pearson distribution does not coincide with the shape of the distribution in hand. Therefore, the Pearson distribution of (5.22) characterizes the PDF in hand accurately only for $m > 0$.

Employing (5.29) and since $w > 0$, the expression $m > 0$ holds (and, therefore, the Pearson type I, with parameters (5.26)-(5.29), characterizes the PDF in hand accurately) only for $-a \geq -\frac{1}{350}\left(-54 - 3\sqrt{1199}\right) \approx 0.45$. Equivalently, employing the definition of $a = -\pi\lambda\sqrt{\frac{L^{(0)}}{\kappa}}$, and since $\lambda, \kappa > 0$, the Pearson type I is accurate for $L^{(0)} \geq \frac{0.45^2\kappa}{\pi^2\lambda^2}$. However, the PDF must be defined over the whole range of $L^{(0)}$, and, therefore, also in the range of $0 \leq -a < 0.45$ and $L^{(0)} < \frac{0.45^2\kappa}{\pi^2\lambda^2}$.

5.2.3 PDF for $L^{(0)} < \frac{0.45^2\kappa}{\pi^2\lambda^2}$

In order to derive a PDF for the inter-cell interference in the $0 \leq -a < 0.45$ range, the approximate PDF of (5.13) can be employed. In particular, for $0 \leq -a < 0.45$ the last term of (5.13) is sufficient to provide an accurate approximation of the PDF. This is due to the fact that the last term of (5.13) constitutes an upper bound of the PDF and, therefore, never takes negative values like the approximate PDF. For $0 \leq -a < 0.45$ this upper bound is extremely tight and the remaining terms have practically no impact on the behavior of the PDF. As the value of $-a$ increases (note that $0 \leq -a$), the upper bound becomes loose and the remaining terms play an important role. However, for $0 \leq -a < 0.45$, the last term of (5.13) constitutes a very tight approximation of the PDF, taking only positive values and being extremely tractable. Hence, this term can approximate the PDF accurately, provided that the proper support of the PDF is defined for the area to be equal to 1. In this course, the support of the PDF is defined from 0 to u (i.e. $supp(f_g(g)) = [0, u]$) and u can be derived by the last term of (5.13) as follows:

$$\int_0^u -\frac{ae^{-\frac{\pi a^2}{4wg}-a}}{2\sqrt{w}g^{3/2}}\,dg = 1 \Rightarrow u = \frac{\pi a^2}{4w\left(\mathrm{erfc}^{-1}\left(e^a\right)\right)^2}. \tag{5.30}$$

5.2.4 General Expression of the PDF

After combining (5.22), the last term of (5.13), and (5.30), the PDF of the aggregate other-cell interference is given by:

$$f_g(g) = \begin{cases} \dfrac{2^{\frac{1}{p_3}-1}\left(\frac{p_2^2}{4p_3^2}-\frac{p_1}{p_3}\right)^{\frac{1}{2}\left(\frac{1}{p_3}-1\right)}\left(\sqrt{\frac{p_2^2}{4p_3^2}-\frac{p_1}{p_3}}-\frac{p_2}{2p_3}-g\right)^{-\frac{-m+\sqrt{\frac{p_2^2}{4p_3^2}-\frac{p_1}{p_3}}-\frac{p_2}{2p_3}}{2p_3\sqrt{\frac{p_2^2}{4p_3^2}-\frac{p_1}{p_3}}}}\left(\sqrt{\frac{p_2^2}{4p_3^2}-\frac{p_1}{p_3}}+\frac{p_2}{2p_3}+g\right)^{\frac{-m-\sqrt{\frac{p_2^2}{4p_3^2}-\frac{p_1}{p_3}}-\frac{p_2}{2p_3}}{2p_3\sqrt{\frac{p_2^2}{4p_3^2}-\frac{p_1}{p_3}}}}}{B\left(\frac{-m-\sqrt{\frac{p_2^2}{4p_3^2}-\frac{p_1}{p_3}}-\frac{p_2}{2p_3}}{2\sqrt{\frac{p_2^2}{4p_3^2}-\frac{p_1}{p_3}}p_3}+1,1-\frac{-m+\sqrt{\frac{p_2^2}{4p_3^2}-\frac{p_1}{p_3}}-\frac{p_2}{2p_3}}{2\sqrt{\frac{p_2^2}{4p_3^2}-\frac{p_1}{p_3}}p_3}\right)}, \\ \qquad \text{for } -\sqrt{\frac{p_2^2}{4p_3^2}-\frac{p_1}{p_3}}-\frac{p_2}{2p_3} < g < \sqrt{\frac{p_2^2}{4p_3^2}-\frac{p_1}{p_3}}-\frac{p_2}{2p_3} \text{ and } -a \geq 0.45 \\ -ae^{-\frac{\pi a^2}{4wg}-a}/(2\sqrt{w}g^{3/2}), \qquad \text{for } 0 \leq g \leq \pi a^2/(4w\left(\mathrm{erfc}^{-1}\left(e^a\right)\right)^2) \text{ and } 0 \leq -a < 0.45, \end{cases} \tag{5.31}$$

with p_1, p_2, p_3 and m being given by (5.26)-(5.29).

For the sake of completeness, the Pearson parameters defined in (5.26)-(5.29) are defined also hereafter employing the definitions of $w = \frac{L^{(0)}}{P_{\mathrm{tx}}}$, and $a = -\pi\lambda\sqrt{\frac{L^{(0)}}{\kappa}}$. Hence, the Pearson parameters are given by:

$$p_1 = -\frac{\pi\lambda P_{\text{tx}}^2\left(24\kappa\sqrt{\frac{L^{(0)}}{\kappa}} + 47\pi L^{(0)}\lambda\right)}{6\kappa {L^{(0)}}^2\left(350\pi\lambda\sqrt{\frac{L^{(0)}}{\kappa}} - 3\right)}, \tag{5.32}$$

$$p_2 = \frac{9P_{\text{tx}}\left(32\pi\lambda\sqrt{\frac{L^{(0)}}{\kappa}} + 5\right)}{2L^{(0)}\left(350\pi\lambda\sqrt{\frac{L^{(0)}}{\kappa}} - 3\right)}, \tag{5.33}$$

$$p_3 = \frac{39}{6 - 700\pi\lambda\sqrt{\frac{L^{(0)}}{\kappa}}}, \tag{5.34}$$

$$m = \frac{216\pi\kappa\lambda P_{\text{tx}}\sqrt{\frac{L^{(0)}}{\kappa}} + 45\kappa P_{\text{tx}} - 700\pi^2 L^{(0)}\lambda^2 P_{\text{tx}}}{6\kappa L^{(0)} - 700\pi\kappa L^{(0)}\lambda\sqrt{\frac{L^{(0)}}{\kappa}}}. \tag{5.35}$$

In order to demonstrate the accuracy of the PDF derived in (5.31), the PDF is plotted against the numerical PDF obtained by the numerical evaluation of the inverse Fourier transform. To elaborate, employing the exact CF of (5.4a) the inverse Fourier transform of (5.10) is computed numerically and the numerical results are compared against those of expression (5.31) for different values of a in Fig. 5.4-5.6. Fig. 5.4-5.6 demonstrate that the derived analytical PDF is extremely accurate with respect to the shape of the PDF, whereas the moments of (5.31) are also equal to the moments calculated by (5.16) and (5.25).

5.3 Appendix

Derivation of the approximate PDF and the constituent integrals of (5.12)

The constituent integrals of (5.12) can be computed in closed form as follows:

Integral 1

$$\int_0^c \exp\left(\frac{ax^2}{6}\right)\cos(x(a+b))\,dx = \\ \frac{1}{2\sqrt{a}}\sqrt{\frac{3\pi}{2}}e^{\frac{3(a+b)^2}{2a}}\left(\text{erfi}\left(\frac{a(c-3i)-3ib}{\sqrt{6}\sqrt{a}}\right) + \text{erfi}\left(\frac{a(c+3i)+3ib}{\sqrt{6}\sqrt{a}}\right)\right) \tag{5.36}$$

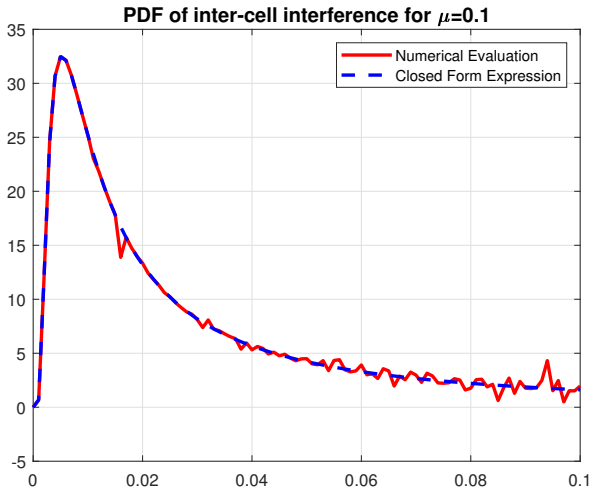

Figure 5.4: PDF of inter-cell interference. Closed form expression of (5.31) vs Numerical Evaluation for $a = -0.1$, $w = 1$, and $\mu = 0.1$.

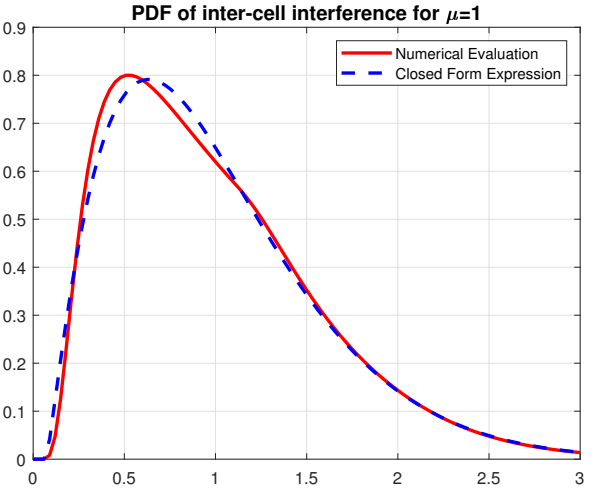

Figure 5.5: PDF of inter-cell interference. Closed form expression of (5.31) vs Numerical Evaluation for $a = -1$, $w = 1$, and $\mu = 1$.

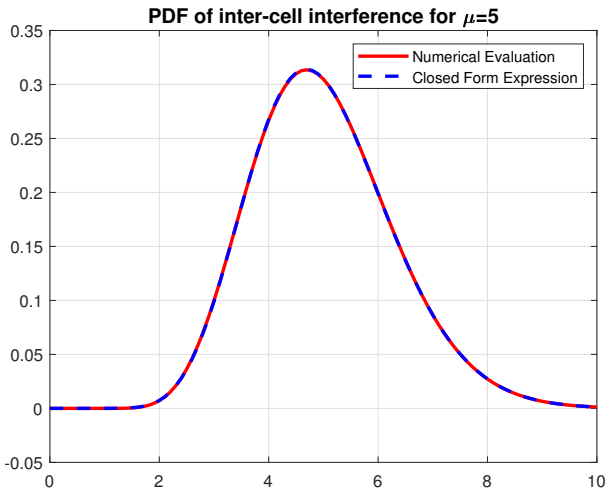

Figure 5.6: PDF of inter-cell interference. Closed form expression of (5.31) vs Numerical Evaluation for $a = -5$, $w = 1$, and $\mu = 5$.

Integral 2

$$\begin{aligned}
&\int_c^d -\exp\left(\frac{ax^2}{6}\right)\sin(ax)\sin(bx)dx = \\
&\frac{1}{2}\sqrt{\frac{3\pi}{8a}}\left(e^{\frac{3(a+b)^2}{2a}}\left(\operatorname{erfi}\left(\frac{ac-3j(a+b)}{\sqrt{6}\sqrt{a}}\right)+\operatorname{erfi}\left(\frac{ac+3j(a+b)}{\sqrt{6}\sqrt{a}}\right)\right.\right. \\
&\left.-\operatorname{erfi}\left(\frac{ad-3j(a+b)}{\sqrt{6}\sqrt{a}}\right)-\operatorname{erfi}\left(\frac{ad+3j(a+b)}{\sqrt{6}\sqrt{a}}\right)\right) \\
&+e^{\frac{3(a-b)^2}{2a}}\left(-\operatorname{erfi}\left(\frac{a(c-3j)+3jb}{\sqrt{6}\sqrt{a}}\right)-\operatorname{erfi}\left(\frac{a(c+3j)-3jb}{\sqrt{6}\sqrt{a}}\right)\right. \\
&\left.\left.+\operatorname{erfi}\left(\frac{a(d-3j)+3jb}{\sqrt{6}\sqrt{a}}\right)+\operatorname{erfi}\left(\frac{a(d+3j)-3jb}{\sqrt{6}\sqrt{a}}\right)\right)\right)
\end{aligned} \tag{5.37}$$

Integral 3

$$\begin{aligned}
&\int_c^d \exp\left(a\left(\sqrt{\frac{\pi x}{2}}-1\right)\right)\cos\left(a\sqrt{\frac{\pi x}{2}}\right)\cos(bx)dx = \\
&\frac{1}{8b^{3/2}}\exp\left(-\frac{a\left(\pi a+b\left(4+2j\sqrt{2\pi}\left(\sqrt{c}+\sqrt{d}\right)\right)\right)}{4b}-jb(c+d)\right) \\
&\left(\exp\left(\frac{1}{2}j\left(\sqrt{2\pi}a\left(\sqrt{c}+\sqrt{d}\right)+2b(c+d)\right)\right)\left(8\sqrt{b}e^{\frac{a\left(\pi a+2\sqrt{2\pi}b\sqrt{d}\right)}{4b}}\cos\left(\sqrt{\frac{\pi}{2}}a\sqrt{d}\right)\sin(bd)\right.\right.
\end{aligned}$$

$$
\begin{aligned}
&+\pi a\Big(je^{\frac{\pi a^2}{2b}}\Big(\operatorname{erf}\left(\frac{\sqrt{\pi}a+2(-1)^{3/4}b\sqrt{c}}{2\sqrt{b}}\right)+\operatorname{erf}\left(\frac{2\sqrt[4]{-1}b\sqrt{c}-\sqrt{\pi}a}{2\sqrt{b}}\right)\\
&+\operatorname{erfc}\left(\frac{\sqrt{\pi}a+2(-1)^{3/4}b\sqrt{d}}{2\sqrt{b}}\right)+\operatorname{erfc}\left(\frac{2\sqrt[4]{-1}b\sqrt{d}-\sqrt{\pi}a}{2\sqrt{b}}\right)-2\Big)\\
&+\operatorname{erf}\left(\frac{2\sqrt[4]{-1}b\sqrt{c}+j\sqrt{\pi}a}{2\sqrt{b}}\right)-j\operatorname{erfi}\left(\frac{\sqrt{\pi}a+2\sqrt[4]{-1}b\sqrt{c}}{2\sqrt{b}}\right)\\
&-\operatorname{erf}\left(\frac{2\sqrt[4]{-1}b\sqrt{d}+j\sqrt{\pi}a}{2\sqrt{b}}\right)+\operatorname{erf}\left(\frac{2(-1)^{3/4}b\sqrt{d}+j\sqrt{\pi}a}{2\sqrt{b}}\right)\Big)\Big)\\
&+2j\sqrt{b}\left(1+e^{j\sqrt{2\pi}a\sqrt{c}}\right)\left(-1+e^{2jbc}\right)\exp\left(\frac{1}{4}a\left(\frac{\pi a}{b}+2\sqrt{2\pi}\left(\sqrt{c}+j\sqrt{d}\right)\right)+jbd\right)\Big)
\end{aligned}
\tag{5.38}
$$

Integral 4

$$
\begin{aligned}
&\int_d^t \exp\left(a\left(\sqrt{\frac{\pi x}{2}}-1\right)\right)\cos\left(xb+a\sqrt{\frac{\pi x}{2}}\right)dx=\\
&\frac{e^{-a}}{4b^{3/2}}\Bigg(\pi a e^{-\frac{\pi a^2}{4b}}\Bigg(\operatorname{erf}\left(\frac{2\sqrt[4]{-1}b\sqrt{d}+j\sqrt{\pi}a}{2\sqrt{b}}\right)-j\Bigg(\operatorname{erfi}\left(\frac{\sqrt{\pi}a+2\sqrt[4]{-1}b\sqrt{d}}{2\sqrt{b}}\right)\\
&-\operatorname{erfi}\left(\frac{\sqrt{\pi}a+2\sqrt[4]{-1}b\sqrt{t}}{2\sqrt{b}}\right)+\operatorname{erfi}\left(\frac{\sqrt{\pi}a-2(-1)^{3/4}b\sqrt{t}}{2\sqrt{b}}\right)\Bigg)\Bigg)\\
&-2j\sqrt{b}\Bigg(e^{(1-j)\sqrt{\frac{\pi}{2}}a\sqrt{d}-jbd}-e^{(1+j)\sqrt{\frac{\pi}{2}}a\sqrt{d}+jbd}-e^{(1-j)\sqrt{\frac{\pi}{2}}a\sqrt{t}-jbt}+e^{\sqrt{\frac{\pi}{2}}(1+j)a\sqrt{t}+jbt}\Bigg)\Bigg).
\end{aligned}
\tag{5.39}
$$

In order to compute the upper limit of the integration of (5.39) at $\lim_{t\to\infty}$, the following approximation for the error function is employed [52]:

$$
\operatorname{erf}(x)=\sqrt{1-\exp\left(-\frac{x^2\left(0.14x^2+\frac{4}{\pi}\right)}{0.14x^2+1}\right)},
\tag{5.40}
$$

and the integral of (5.39) is given by:

$$
\begin{aligned}
&\int_d^\infty \exp\left(a\left(\sqrt{\frac{\pi x}{2}}-1\right)\right)\cos\left(xb+a\sqrt{\frac{\pi x}{2}}\right)dx=\\
&-\frac{je^{-a}}{4b^{3/2}}\Bigg(-\pi ja e^{-\frac{\pi a^2}{4b}}\operatorname{erf}\left(\frac{(-2-2j)b\sqrt{d}-\sqrt{2\pi}ja}{2\sqrt{2}\sqrt{b}}\right)\\
&+j\pi a e^{-\frac{\pi a^2}{4b}}\operatorname{erf}\left(\frac{(2-2j)b\sqrt{d}-\sqrt{2\pi}ja}{2\sqrt{2}\sqrt{b}}\right)\\
&-2\sqrt{b}e^{(1-j)\sqrt{\frac{\pi}{2}}a\sqrt{d}-jbd}\left(-1+e^{j\left(\sqrt{2\pi}a\sqrt{d}+2bd\right)}\right)\Bigg)-\frac{\pi a e^{-\frac{\pi a^2}{4b}-a}}{2b^{3/2}}.
\end{aligned}
\tag{5.41}
$$

Chapter 6

Conclusions

6.1 Conclusions

Summing up, the present thesis has demonstrated how stochastic geometry tools can be exploited to derive not just exact but cumbersome expressions, but also simple, albeit extremely accurate closed form expressions that allow for the investigation of complex optimization problems. These problems could pertain to the optimization of the network connectivity as demonstrated in Chapter 2, or to the optimization of the network's mode of operation through the clustering of users under active BSs as highlighted in Chapter 3. Additionally, appropriate coordination schemes could be investigated for the mitigation of the aggregate interference as highlighted in Chapter 4. The resolution of such problems is essential in order to reap the rate benefits of UDNs, and achieve the envisaged linear capacity increase with the network density. However, the resolution of these problems is preconditioned on the existence of closed-form figures of merit, which hindered the resolution of relevant optimization problems hitherto.

In this direction, the present thesis has demonstrated the feasibility of a closed-form analysis of UDNs, providing closed form expressions for the ergodic rate for a noise limited, an interference limited and a general scenario. The accuracy of the derived expressions has been verified by extensive Monte Carlo simulation, whereas the consistency of the results, across all respective chapters further verifies the validity of the analyses for all different scenarios.

Moreover, the obtained expressions provided a practical guide associating the network performance to the degree of densification of the network. The latter can facilitate the design and management of efficient cellular networks, where the QoS objectives can be guaranteed a priori based on the spatial density of the network. Thus, this may provide an important leeway to the network operators to capitalize on the advantages of cellular dense networks. Furthermore, the expressions of Chapter 3 and the respective figures quantify effectively the densification threshold between the fully loaded and the non-fully

loaded operation, whereas the expressions and respective figure of Chapter 4 quantify the densification threshold between the noise limited and the interference limited operation. Both of them being metrics of extreme value for the network design and planning.

Furthermore, the present thesis has proposed a flexible DUDe framework that allows for the incorporation of the DUDe connectivity benefits in 5G and B5G networks, accounting for the detrimental effect of the ACK synchronization in different 5G services. Moreover, the proposed framework allows for the integration of Wi-Fi into the 5G ecosystem through DUDe connectivity schemes and for strong backhaul support through the exploitation of dark fiber.

Last but not least, the present thesis provided two powerful tools that can be of actual merit for researchers in the field. Firstly, the derivation of an accurate and simple approximation for the MGF of the aggregate other-cell interference. Given the pivotal role of the MGF in stochastic geometry analyses, the derived approximation can be employed by a multitude of applications to simplify the analysis and facilitate the derivation of closed form expressions. Secondly, an accurate approximation for the PDF of the inter-cell interference in Poisson cellular networks. This PDF paves the way for revisiting the stochastic geometry frameworks employed hitherto, in the direction of weaning off the employment of the MGF. This will allow for the derivation of much simpler frameworks allowing for the efficient design and optimization of wireless systems in practice.

6.2 Future Work

The derivation of a tractable stochastic geometry framework, for the analyses of Poisson cellular networks, gives rise to a number of research problems to which the present work can be extended. In particular, the derived expressions can be used as part of the objective functions of complex optimization problems like the ones mentioned in the previous section, among others. Thus, allowing for the resolution of complex optimization problems related to UDN operation.

Furthermore, the analysis should also be extended to non-homogeneous Poisson cellular networks. This could allow for deriving figures of merit that would fully characterize the performance of the system. Indicatively, let us mention that the extension to the non-homogeneous Poisson case would allow for the characterization of the system performance in the UL, where the interferers follow a non-homogeneous PPP [18].

Furthermore, an extension further from the homogeneous PPP case could allow for examining the "typical cell" case instead of the "typical user" case. To elaborate, the random selection of a user from a pool of users that follow a homogeneous PPP and are served by BSs that also follow a homogeneous PPP, results in a setup where the spatial distribution of the BSs around the user follows the homogeneous PPP. This is known a the "typical user" case or the Crofton cell [41]. However, the random selection of a BS

in the same setup gives rise to the "typical cell" case and the BSs around a randomly selected user in that cell do not follow the homogeneous PPP. The "typical cell" case however, is much more interesting to network designers that are interested in the average ergodic rate provided in a "typical cell" and do not examine the network from a user perspective. Hence, the extension of the analysis to the "typical cell" case can be of actual merit to network operators and designers.

In addition, the analysis of the PDF of the inter-cell interference, needs to be extended to different pathloss exponent values. Subsequently, this powerful tool needs to be exploited for the resolution of complex optimization problems. Indicatively, a PDF of the interference defined in closed form can be exploited for efficient receiver design, adjusted to the distribution of the power of the interference.

Last but not least, the tractable closed-form framework developed herein, paves the way for the incorporation of stochastic geometry and random spatial processes to the analysis of B5G and 6G networks. In particular, 6G smart radio ecosystems are expected to customize even the propagation of the radio waves through the employment of meta-surfaces [55]. Hence, meta-surfaces are expected to be attached to environmental objects and distributed in the network according to very complex spatial patterns. Hence, the existing frameworks for the analysis of random spatial processes are too intractable to be employed effectively for the analysis of problems related to the distribution of deployed meta-surfaces in large-scale wireless networks, or related to the wave manipulations applied by the meta-surfaces on the radio waves impinging upon them. Hence, the advent of 6G networks imposes the development of simple and accurate frameworks for the analysis of random processes and the present thesis takes a step in this direction, that needs to be extended further in future works.

Bibliography

[1] J. Andrews, S. Buzzi, W. Choi, S. Hanly, A. Lozano, A. C. K. Soong, and J. C. Zhang, "What will 5g be?" *IEEE Journal on Selected Areas in Communications,*, vol. 32, no. 6, pp. 1065–1082, June 2014.

[2] V. Chandrasekhar, J. G. Andrews, and A. Gatherer, "Femtocell networks: a survey," *IEEE Communications Magazine*, vol. 46, no. 9, pp. 59–67, September 2008.

[3] F. Baccelli, B. Blaszczyszyn, and P. Muhlethaler, "An Aloha protocol for multihop mobile wireless networks," *IEEE Transactions on Information Theory*, vol. 52, pp. 421–436, February 2006.

[4] M. Haenggi, *Stochastic Geometry for Wireless Networks.* Cambridge University Press, 2013.

[5] J. G. Andrews, F. Baccelli, and R. K. Ganti, "A tractable approach to coverage and rate in cellular networks," *IEEE Transactions on Communications*, vol. 59, no. 11, pp. 3122–3134, November 2011.

[6] H. S. Dhillon, R. K. Ganti, F. Baccelli, and J. G. Andrews, "Modeling and analysis of k-tier downlink heterogeneous cellular networks," *IEEE Journal on Selected Areas in Communications*, vol. 30, no. 3, pp. 550–560, April 2012.

[7] S. Singh, X. Zhang, and J. G. Andrews, "Joint rate and SINR coverage analysis for decoupled uplink-downlink biased cell associations in HetNets," *IEEE Transactions on Wireless Communications*, vol. 14, no. 10, pp. 5360–5373, Oct. 2015.

[8] M. D. Renzo, W. Lu, and P. Guan, "The intensity matching approach: A tractable stochastic geometry approximation to system-level analysis of cellular networks," *IEEE Transactions on Wireless Communications*, vol. 15, no. 9, pp. 5963–5983, Sept 2016.

[9] M. Ding, P. Wang, D. Lopez-Perez, G. Mao, and Z. Lin, "Performance impact of los and nlos transmissions in dense cellular networks," *IEEE Transactions on Wireless Communications*, vol. 15, no. 3, pp. 2365–2380, March 2016.

[10] J. G. Andrews, "Seven ways that hetnets are a cellular paradigm shift," *IEEE Communications Magazine*, vol. 51, no. 3, pp. 136–144, March 2013.

[11] M. Ding, D. Lopez-Perez, G. Mao, and Z. Lin, "Performance impact of idle mode capability on dense small cell networks," *IEEE Transactions on Vehicular Technology*, vol. 66, no. 11, pp. 10 446–10 460, Nov 2017.

[12] H. Elshaer, M. N. Kulkarni, F. Boccardi, J. G. Andrews, and M. Dohler, "Downlink and uplink cell association with traditional macrocells and millimeter wave small cells," *IEEE Transactions on Wireless Communications*, vol. 15, no. 9, pp. 6244–6258, Sep. 2016.

[13] J. G. Andrews, "Seven ways that HetNets are a cellular paradigm shift," *IEEE Communications Magazine*, vol. 51, no. 3, pp. 136–144, March 2013.

[14] D. Astely, E. Dahlman, G. Fodor, S. Parkvall, and J. Sachs, "LTE release 12 and beyond [accepted from open call]," *IEEE Communications Magazine*, vol. 51, no. 7, pp. 154–160, July 2013.

[15] F. Boccardi, R. W. Heath, A. Lozano, T. L. Marzetta, and P. Popovski, "Five disruptive technology directions for 5G," *IEEE Communications Magazine*, vol. 52, no. 2, pp. 74–80, Febr. 2014.

[16] R. W. Heath, M. Kountouris, and T. Bai, "Modeling heterogeneous network interference using poisson point processes," *IEEE Transactions on Signal Processing*, vol. 61, no. 16, pp. 4114–4126, Aug 2013.

[17] G. Geordie, "Device-to-device communication and wearable networks: Harnessing spatial proximity," Ph.D. dissertation, Universitat Pompeu Fabra, 2017.

[18] Y. Wang, M. Haenggi, and Z. Tan, "The meta distribution of the sir for cellular networks with power control," *IEEE Transactions on Communications*, vol. 66, no. 4, pp. 1745–1757, April 2018.

[19] T. Bai, R. Vaze, and R. W. Heath, "Analysis of blockage effects on urban cellular networks," *IEEE Transactions on Wireless Communications*, vol. 13, no. 9, pp. 5070–5083, Sept. 2014.

[20] J. G. Andrews, F. Baccelli, and R. K. Ganti, "A tractable approach to coverage and rate in cellular networks," *IEEE Transactions on Communications*, vol. 59, no. 11, pp. 3122–3134, November 2011.

[21] A. Goldsmith, "Wireless communications." Cambridge University Press, 2005, ch. 2.

[22] E. Calvo, J. Vidal, and J. R. Fonollosa, "Optimal resource allocation in relay-assisted cellular networks with partial CSI," *IEEE Transactions on Signal Processing*, vol. 57, no. 7, pp. 2809–2823, July 2009.

[23] S. Boyd and L. Vandenberghe, *Convex Optimization*, 1st ed. Cambridge University Press, 2004.

[24] A. Lapidoth and S. M. Moser, "Capacity bounds via duality with applications to multiple-antenna systems on flat-fading channels," *IEEE Transactions on Information Theory*, vol. 49, no. 10, pp. 2426–2467, Oct. 2003.

[25] I. S. Gradshteyn and I. M. Ryzhik, "Table of integrals, series, and products." New York: Academic, 2000, ch. 4.352-1.

[26] S. Sadr and R. S. Adve, "Partially-distributed resource allocation in small-cell networks," *IEEE Transactions on Wireless Communications*, vol. 13, no. 12, pp. 6851–6862, Dec. 2014.

[27] H. Elshaer, F. Boccardi, M. Dohler, and R. Irmer, "Downlink and uplink decoupling: A disruptive architectural design for 5G networks," in *2014 IEEE Global Communications Conference*, Dec. 2014, pp. 1798–1803.

[28] P. Rost, A. Maeder, and X. Pérez-Costa, "Asymmetric uplink-downlink assignment for energy-efficient mobile communication systems," in *Vehicular Technology Conference (VTC Spring), 2012 IEEE 75th*, May 2012, pp. 1–5.

[29] K. Smiljkovikj, H. Elshaer, P. Popovski, F. Boccardi, M. Dohler, L. Gavrilovska, and R. Irmer, "Capacity analysis of decoupled downlink and uplink access in 5G heterogeneous systems," *CoRR*, vol. abs/1410.7270, 2014. [Online]. Available: http://arxiv.org/abs/1410.7270

[30] X. Ge, S. Tu, G. Mao, C. X. Wang, and T. Han, "5G ultra-dense cellular networks," *IEEE Wireless Communications*, vol. 23, no. 1, pp. 72–79, Febr. 2016.

[31] A. Papoulis and S. U. Pillai, *Probability, Random Variables and Stochastic Processes*, 4th ed. McGraw-Hill Europe, 2002.

[32] A. I. Aravanis, O. Munoz, A. Pascual-Iserte, and J. Vidal, "Analysis of downlink and uplink decoupling in dense cellular networks," in *2016 IEEE 21st International Workshop on Computer Aided Modelling and Design of Communication Links and Networks (CAMAD)*, Oct 2016, pp. 219–224.

[33] F. Boccardi, J. Andrews, H. Elshaer, M. Dohler, S. Parkvall, P. Popovski, and S. Singh, "Why to decouple the uplink and downlink in cellular networks and how to do it," *IEEE Communications Magazine*, vol. 54, no. 3, pp. 110–117, March 2016.

[34] A. Aravanis, A. Pascual-Iserte, and O. Munoz-Medina, "Closed-form capacity bounds for downlink and uplink decoupling," in *WSA 2018; 22nd International ITG Workshop on Smart Antennas*, March 2018, pp. 1–5.

[35] S. N. Chiu, D. Stoyan, W. Kendall, and J. Mecke, *Stochastic Geometry and its Applications*. John Wiley and Sons, 2013.

[36] T. Lam-Thanh, "New methods for the analysis and optimization of cellular networks by using stochastic geometry," Ph.D. dissertation, Universite Paris-Saclay, 2018.

[37] M. D. Renzo and W. Lu., "System-level analysis/optimization of cellular networks with simultaneous wireless information and power transfer: Stochastic geometry modeling," *IEEE Trans. Vehicular Technology*, vol. 66, p. 2251 –2275, Mar. 2017.

[38] J. Lee and F. Baccelli, "On the effect of shadowing correlation on wireless network performance," in *IEEE INFOCOM 2018 - IEEE Conference on Computer Communications*, April 2018, pp. 1601–1609.

[39] M. D. Renzo, A. Guidotti, and G. Corazza, "Average rate of downlink heterogeneous cellular networks over generalized fading channels: A stochastic geometry approach." *IEEE Transactions on Communications*, vol. 61, no. 7, pp. 3050–3071, 2013.

[40] G. Geordie, R. Mungara, A. Lozano, and M. Haenggi, "Ergodic spectral efficiency in MIMO cellular networks," *IEEE Transactions on Wireless Communications*, vol. 16, no. 5, May 2017.

[41] S. M. Yu and S. L. Kim, "Downlink capacity and base station density in cellular networks," in *2013 11th International Symposium and Workshops on Modeling and Optimization in Mobile, Ad Hoc and Wireless Networks (WiOpt)*, May 2013, pp. 119–124.

[42] A. I. Aravanis, T. T. Lam, O. Muñoz, A. Pascual-Iserte, and M. D. Renzo, "A tractable closed-form approximation of the ergodic rate in poisson cellular networks," *EURASIP Journal on Wireless Communications and Networking*, accepted for publication 2019.

[43] D. P. Bertsekas, *Nonlinear Programming*, 2nd ed. Athena Scientific, 1999.

[44] B. Rivet, L. Girin, and C. Jutten, "Log-rayleigh distribution: A simple and efficient statistical representation of log-spectral coefficients," *IEEE Transactions on Audio, Speech, and Language Processing*, vol. 15, no. 3, pp. 796–802, March 2007.

[45] M. Haenggi, J. G. Andrews, F. Baccelli, O. Dousse, and M. Franceschetti, "Stochastic geometry and random graphs for the analysis and design of wireless networks," *IEEE Journal on Selected Areas in Communications*, vol. 27, no. 7, pp. 1029–1046, September 2009.

[46] W. L. Shepherd and P. Milnarich, "Moments of log rayleigh distributions," *Proceedings of the IEEE*, vol. 62, no. 8, pp. 1168–1169, Aug 1974.

[47] M. Haenggi, "On distances in uniformly random networks," *IEEE Transactions on Information Theory*, vol. 51, no. 10, pp. 3584–3586, Oct 2005.

[48] A. I. Aravanis, O. Munoz, A. Pascual-Iserte, and M. Di-Renzo, "On the coordination of base stations in ultra dense cellular networks," in *2019 IEEE 88th Vehicular Technology Conference (VTC Spring)*, accepted for publication.

[49] K. Pearson, "Second supplement to a memoir on skew variation," *Phil. Trans.*, vol. A, no. 216, pp. 429–457, 1916.

[50] J. F. Kenney and E. S. Keeping, *Mathematics of Statistics Pt. 2.* 2nd ed. Princeton, NJ: Van Nostrand, 1951.

[51] W. Pan, X. An, Q. Y. D. University, and S. I. Inc., "Computing and graphing probability values of pearson distributions: A sas/iml macro," 2017.

[52] S. Winitzki, "A handy approximation for the error function and its inverse," *A lecture note obtained through private communication*, 2008.

[53] W. Webb, *The 5G Myth: And why consistent connectivity is a better future.* 1st ed. CreateSpace Independent Publishing Platform, 2016.

[54] Ericsson, Huawei, and Nokia, "5G Network Slicing for Vertical Industries," www.huawei.com/minisite/5g/img/gsa-5g-network-slicing-for-vertical-industries.pdf, September 2017, [Online;].

[55] M. D. Renzo, M. Debbah, D. Phan-Huy, A. Zappone, M. Alouini, C. Yuen, V. Sciancalepore, G. Alexandropoulos, J. Hoydis, H. Gacanin, J. D. Rosny, A. Bounceu, G. Lerosey, and M. Fink, "Smart radio environments empowered by ai reconfigurable meta-surfaces: An idea whose time has come," *EURASIP Journal on Wireless Communications and Networking*, 2019, accepted for publication.

[56] S. Kekki, W. Featherstone, Y. Fang, P. Kuure, A. Li, A. Ranjan, D. Purkayastha, F. Jiangping, D. Frydman, G. Verin, K. Wen, K. Kim, R. Arora, A. Odgers, L. Contreras, and S. Scarpina, "MEC in 5G networks," www.etsi.org/images/files/ETSIWhitePapers/etsi_wp28_mec_in_5G_FINAL.pdf, June 2018, eTSI White Paper No. 28. [Online].

[57] M. Ding, D. Lopez-Perez, G. Mao, and Z. Lin, "Performance impact of idle mode capability on dense small cell networks," *IEEE Transactions on Vehicular Technology*, vol. 66, no. 11, pp. 10 446–10 460, November 2017.

[58] Telus and Huawei, "Next generation SON for 5G," www-file.huawei.com/-/media/corporate/pdf/mbb/next-gene-ation-son-for-5g.pdf, 2016, white Paper, [Online].

[59] E. Dahlman, S. Parkvall, and J. Skold, *5G NR: The Next Generation Wireless Access Technology*. 1st ed. Academic Press, 2018.

[60] 5G-PPP, "5G EVE: 5G European validation platform for extensive trials," www.5g-eve.eu, 2018, (Project ID 815074). [Online].

[61] Fon.com, "Fon: The global WiFi network," fon.com, 2019, [Online].

[62] D. López-Pérez, J. Ling, B. H. Kim, V. Subramanian, S. Kanugovi, and M. Ding, "Boosted wifi through lte small cells: The solution for an all-wireless enterprise," in *2016 IEEE 27th Annual International Symposium on Personal, Indoor, and Mobile Radio Communications (PIMRC)*, 2016, pp. 1–6.

[63] M. Timmers, M. Guenach, C. Nuzman, and J. Maes, "G.fast: evolving the copper access network," *IEEE Communications Magazine*, vol. 51, no. 8, pp. 74–79, August 2013.